BI-RESAMPLED DATA STUDY

R. Benner
Advanced Image Processing Development Department
W. Young
Earth Resources Laboratory
International Business Machines Corporation
18100 Frederick Pike
Gaithersburg, MD 20760

(NASA-CR-156710) BI-RESAMPLED DATA STUDY N78-19530
Final Report, Oct. 1976 - Mar. 1977
(International Business Machines Corp.)
143 p HC A07/MF A01 CSCL 08B Unclas
G3/43 07355

March 1977
Final Report for Period October 1976 to March 1977

Prepared for

GODDARD SPACE FLIGHT CENTER

Greenbelt, Maryland 20771

BI-RESAMPLED DATA STUDY

R. Benner
Advanced Image Processing Development Department
W. Young
Earth Resources Laboratory
International Business Machines Corporation
18100 Frederick Pike
Gaithersburg, MD 20760

March 1977
Final Report for Period October, 1976 to March, 1977

Approved by: C. P. Colby, Jr.

R. Bernstein

Prepared for

NASA

GODDARD SPACE FLIGHT CENTER

Greenbelt, Maryland 20760

TECHNICAL REPORT STANDARD TITLE PAGE

1. Report No.	2. Government Accession No.	3. Recipient's Catalog No.
4. Title and Subtitle Bi-resampled Data Study		5. Report Date March, 1977 6. Performing Organization Code
7. Author(s) R. Benner, W. Young		8. Performing Organization Report No.
9. Performing Organization Name and Address International Business Machines Corporation 18100 Frederick Pike Gaithersburg, MD 20760		10. Work Unit No. 11. Contract or Grant No. NAS5-23708
12. Sponsoring Agency Name and Address NASA-GSFC Greenbelt, Maryland 20771 Bernard Peavey		13. Type of Report and Period Covered Final Report Oct. 1976 to Mar. 1977 14. Sponsoring Agency Code

15. Supplementary Notes

16. Abstract

This document reports on the results of an experimental study conducted to determine the geometric and radiometric effects of double resampling ("bi-resampling") performed on image data in the process of performing map projection transformations.

17. Key Words (Selected by Author(s))	18. Distribution Statement
Resampling Interpolation Digital Image Processing	

19. Security Classif. (of this report)	20. Security Classif. (of this page)	21. No. of Pages	22. Price*
Unclassified	Unclassified	128	

*For sale by the Clearinghouse for Federal Scientific and Technical Information, Springfield, Virginia 22151.

PREFACE

This document reports on the results of an experimental study conducted to determine the geometric and radiometric effects of double resampling ("bi-resampling") performed on digital images in the process of performing map projection transformations.

The technical support provided by Mr. Bernard Peavey of NASA-GSFC in the course of this study is gratefully acknowledged.

TABLE OF CONTENTS

LIST OF FIGURES

LIST OF TABLES

Section 1 Introduction and summary

This is the final report for the Experimental Bi-resampled Data Study performed by IBM for the Goddard Space Flight Center under contract NAS5-23708.

1.1 Overview

The purpose of this study is to determine the radiometric and geometric effects caused by the double resampling of an image. A double resampled (bi-resampled) image in this experiment is an image created by first resampling raw, uncorrected data into a Universal Transverse Mercator (UTM) projection, and then resampling this UTM image into a Lambert Conformal Conic projection. This image is then subjected to various comparative analyses with respect to singly resampled imagery which was created by resampling the raw data directly into the Lambert projection. The two scenes considered in this study are

1) band 5 of scene E-1080-15192 (a Chesapeake scene), and
2) bands 4 through 7 of a subimage of scene E-2183-16433 covering a LACIE intensive training site.

These scenes are designated as scene A and scene B, respectively, throughout this report.

The accuracy of the mapping functions used in the resampling process, for both the singly and doubly resampled imagery, is discussed in Section 2. Section 3 presents the results obtained in the measurements of the registration accuracy between the two versions of scene A. Various quantitative measures of the radiometric degradation due to the bi-resampling are discussed in Section 4. The final section discusses the results obtained for classification processing of the two versions of scene B.

1.2 Summary of Results

The results obtained in this study are summarized by the following items:

a) The misregistration of the two versions of scene A was found to be bounded by 0.29 pixels (the pixel spacing is 50.8 meters), and for the two versions of scene B the misregistration bound was 0.20 pixels. These are gross misregistration bounds.

b) IBM's correlation program was applied to 9 widely distributed features in scene A, and the maximum misregistration of any of these features was found to be less than 0.1 pixel. The program was also applied to 19 clustered features. The registration results obtained show random misregistration errors.

c) Radiometric differences on a pixel-by-pixel basis were found to be small. Difference imagery, radiometrically stretched for photographic recording, exhibits differences primarily along sharp edges, such as land-water interfaces and airport runways. Considering all bands of both scenes, roughly 97% of the pixel values in the bi-resampled imagery differed by less than 1 count from the corresponding values in the singly resampled imagery.

d) Edges were degraded slightly in the bi-resampling process. The bi-resampled data displayed "overshoot" on edges, similar to the Gibb's phenomenon of Fourier series at a discontinuity. No noticeable spreading of edges was observed.

e) The classification results obtained for the two versions of scene B were essentially the same. Classification accuracy,

with respect to ground truth data, is insensitive to the singly or doubly resampled nature of the data classified. The largest discrepancy observed in the areal proportion estimates obtained from the two data sets was 1.1%.

Section 2 Mapping Functions

IBM chose to resample, or project, the uncorrected scenes and the UTM scenes to the Lambert Conformal Conic (LCC) projection. The resampling task requires an inverse mapping function which maps pixels in the LCC image space to pixels in the input image space, which in this study was either the uncorrected image space or the UTM image space. These inverse mapping functions are denoted by G, which maps the LCC image space to the UTM image space, and H, which maps the LCC image space to the uncorrected data. The function G is the inverse mapping function for the bi-resampling process, and the function H is the mapping function for the single resampling process.

These functions were developed as a series of transformations and are illustrated in Figure 2-1. The function G is the mathematical composition of the following transformations:

a) T_1^{-1}, a rotation and scale change which transforms pixels in the LCC image space to (x,y) coordinates in LCC space,

b) ILAMBERT, which maps (x,y) coordinates in LCC space to geodetic latitude and longitude coordinates. Details of this transformation and its inverse transformation, LAMBERT, are provided in the appendix.

c) ULL, which maps geodetic latitude and longitude to the UTM coordinates of northing and easting. This transformation was provided by an APL version of the equations employed by IBM in correcting imagery to the UTM projection.

d) T_2, a translation, rotation and scale change which maps UTM northing and easting to UTM image coordinates.

The mapping function H is the composition of the above function G with F,

$$H = F \circ G$$

where F represents the inverse mapping function used in the original production of the UTM image. For scene 1080-15192, F is a pair of bivariate, fifth order polynomials. For the LACIE intensive training site, F is a pair of bivariate, second order polynomials. The UTM image of the LACIE site was not available, and so a region of the uncorrected image, consisting of approximately 400x400 samples, was resampled to create an UTM image of this area. The image size was chosen so that image edge effects would not be encountered in the subsequent resampling to LCC space. The explicit mapping function used in the original creation of the UTM image of scene B was not used to create this UTM subimage. Instead, a polynomial approximation to this explicit mapping function was developed by the method of least squares over a region containing Hand County and the LACIE site.

At this point it should be noted that if the functions G and H were used for mapping all image coordinates in the resampling program, there would be no registration error between the singly and doubly resampled images. However, it is impractical to specify G and H explicitly in the resampling program because of their computational complexity. Instead, the procedure used is to develop a pair of bivariate polynomials to approximate these mapping functions, and a regular grid as an interpolation net over the image. The resampling logic uses the polynomials to map the grid points and bilinear interpolation to map other image points. This introduces geometric errors which can be characterized as either errors due to the polynomial approximation (E) or errors due to the bilinear approximation of the polynomial at off-grid points (E_B). Bounds for these errors in the resampling performed in this study are presented in Table 2-1. The errors are expressed as a fraction of the 50.8 meter pixel spacing. For scene B,

which was small, polynomial approximations were not used. In this case the mapping was provided explicitly. In Table 2-1, the notation "LCC(UTM)" refers to the resampling to the LCC image from the UTM image and "LCC(II)" refers to resampling to the LCC image from the uncorrected image. Generally, the errors in the table are pessimistic, since the errors are probably not additive, and the bounds are only approached near the corners of the image.

	E(pixels)	E_B(pixels)	Grid Spacing
Scene A, UTM projection	0.01	0.06	100 pixels
LCC(UTM) projection	0.00	0.00	200 pixels
LCC(II) projection	0.01	0.19	200 pixels
Total misregistration bound	0.02	0.25	
Maximum Misregistration	0.27 pixel		
Scene B, UTM projection	NA	0.10	202 lines [illegible] samples
LCC(UTM) projection	NA	0.00	[illegible] pixels
LCC(II) projection	NA	0.10	[illegible] pixels
Total misregistration error	NA	0.20	
Maximum Misregistration	0.20 pixel		

Note: LCC(II) - Lambert derived directly from raw data.
LCC(UTM) - Lambert derived from UTM image.

Table 2-1. Registration Error Bounds

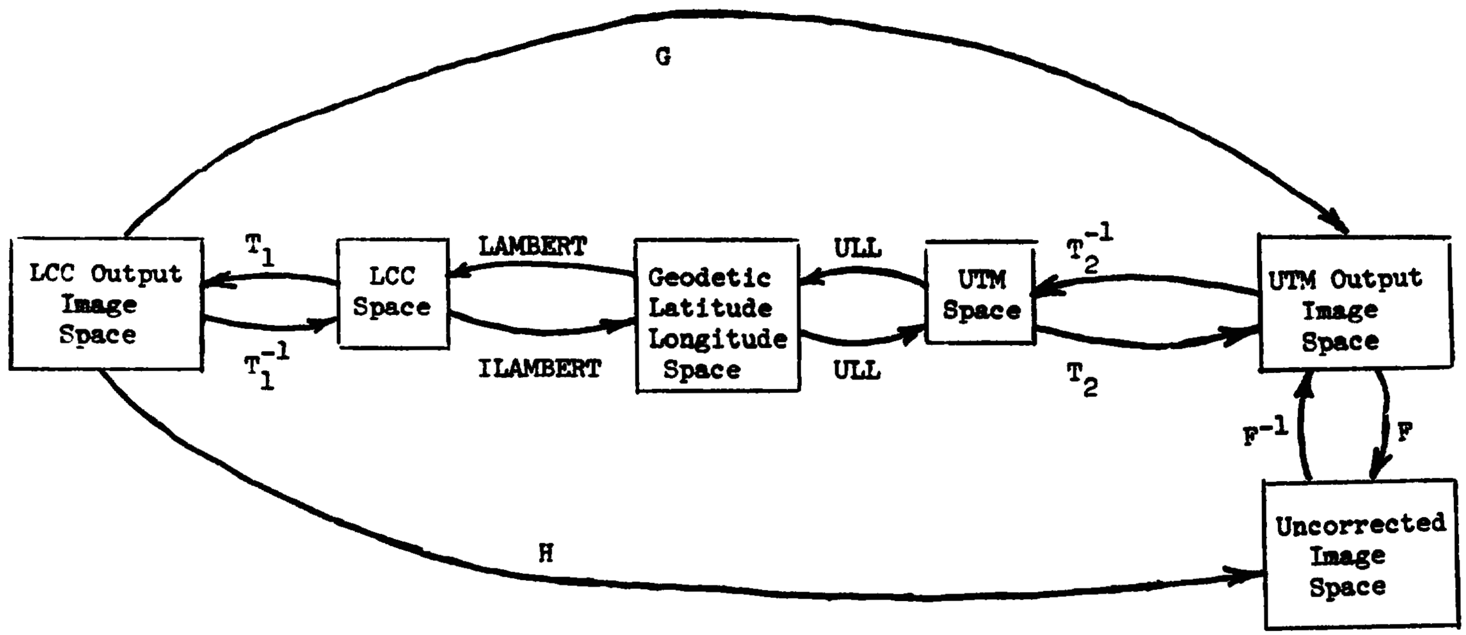

Figure 2-1. Inverse Mapping Function for the Singly and Doubly Resampled Imagery

Section 3 Measured Registration Error

Misregistration was investigated with IBM's control point correlation algorithm. Nine features widely distributed over scene A, and 19 closely clustered features in the Camp Hill region were chosen. The locations of these features are indicated in Figure 3-1, and the 9 widely distributed features from the singly and doubly resampled images are presented in Figures 3-2 and 3-3. In the latter figures, the features have been enlarged to a scale of approximately 1:50000. Shadeprints of the 9 features are provided in Figure 3-4.

The correlation program's registration results are given in Tables 3-1 and 3-2. In these tables, line and sample misregistration are given in units of the 50.8 meter output pixel spacing, and are designated as Ax and Ay, respectively. The worst case line and sample misregistration was found to be Ax = 0.07 and Ay = 0.07. The measured standard deviation of the misregistration in the cluster area suggest that the errors are random, assuming the error function to be slowly varying. Included in these misregistration errors are the estimation errors inherent in the correlation program. To estimate these errors, the algorithm was applied to the singly resampled scene alone. The resulting autocorrelation errors, which are purely algorithm estimation errors, are:

	Mean Ax	Mean Ay	Std Dev Ax	Std Dev Ay
Cluster Region (19 features)	0.002	-0.001	0.01	0.02
Distributed Features (9 features)	0.002	-0.003		

These results indicate that the misregistration results in Tables 3-1 and

3-2 are of the same order of magnitude as the correlation estimation errors. In both cases, the errors are negligably small. These control point results are well within the previously developed bounds on misregistration (Section 2).

Feature	Line Misregistration Δx (pixels)	Sample Misregistration Δy (pixels)
1	0.02	0.07
2	0.03	-0.03
3	0.03	0.04
4	-0.01	-0.05
5	-0.04	-0.05
6	0.00	0.01
7	-0.01	0.00
8	0.00	0.02
9	0.05	0.01
mean	0.008	0.002

Table 3-1. Measured Misregistration Errors for Nine Widely Distributed Features in Scene E-1080-15192

Cluster Feature	Line Misregistration Δx (pixels)	Sample Misregistration Δy (pixels)
1	0.00	0.01
2	-0.06	0.00
3	0.03	-0.02
4	0.05	0.02
5	0.07	-0.04
6	0.05	-0.03
7	-0.02	-0.01
8	-0.01	0.01
9	0.05	0.01
10	0.00	0.00
11	0.04	-0.05
12	-0.05	-0.03
13	0.01	0.02
14	-0.03	-0.04
15	-0.03	0.02
16	0.01	-0.03
17	-0.01	0.02
18	0.03	0.00
19	-0.02	0.06
mean	0.006	-0.004
std dev	0.04	0.03

Table 3-2. Measured Misregistration Errors for 19 Clustered Features in the Camp Hill Region of Scene E-1080-15192.

This figure is a photograph contained

in the pocket at the back of this report.

Figure 3-1. Feature Location, Cluster Region, and High, Medium and Low Frequency Regions of Scene E-1080-15192

This figure is a photograph contained

in the pocket at the back of this report.

Figure 3-2. Nine Features from the Singly Resampled Image of Scene E-1080-15192.

This figure is a photograph contained
in the pocket at the back of this report.

Figure 3-3. Nine Features from the Doubly Resampled Image of Scene E-1080-5192

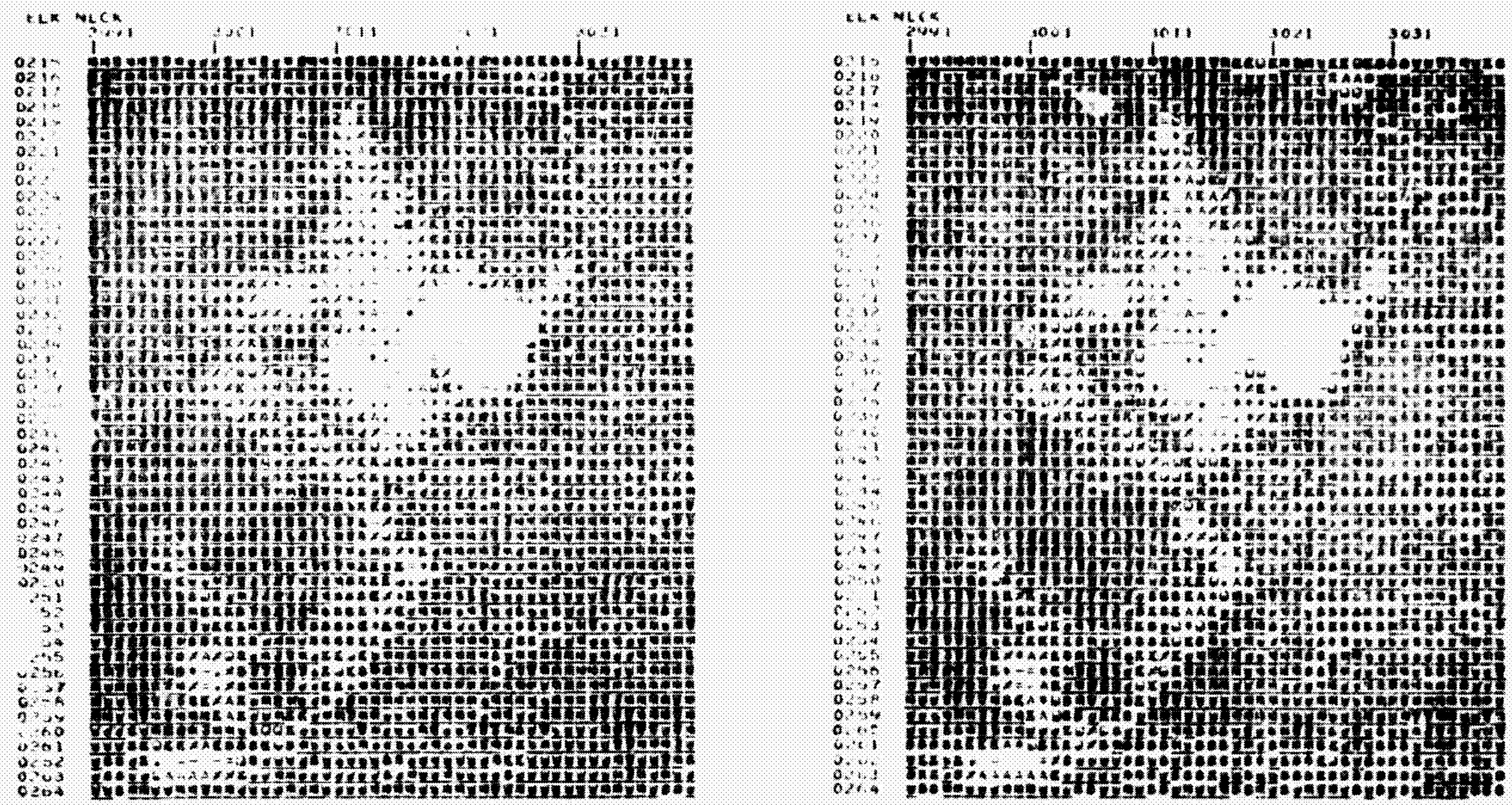

Figure 3-4 Shadeprints of the Nine Singly Resampled and Doubly Resampled Features in Scene E-1080-15192

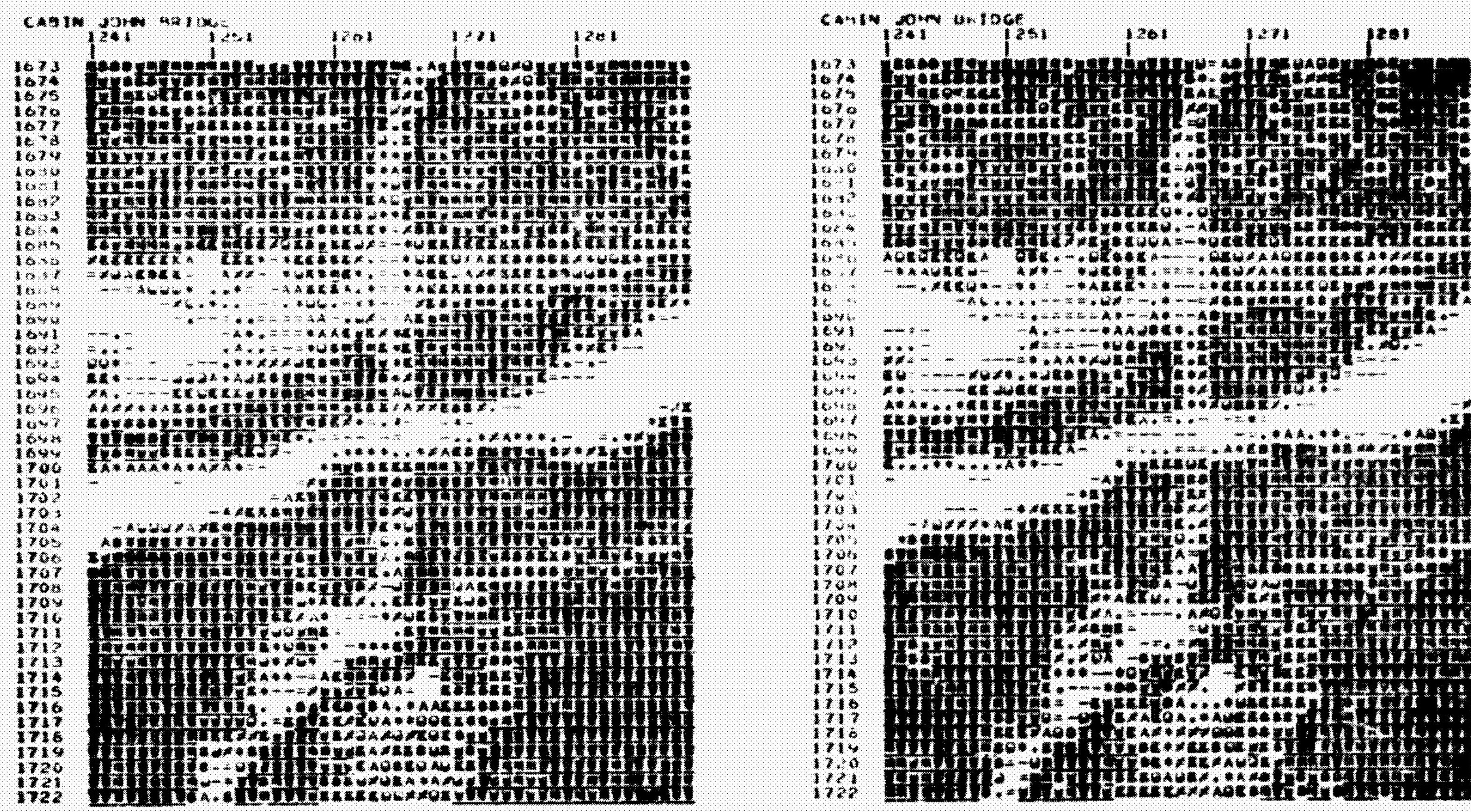

Figure 3-4 (cont'd) Shadeprints of the Nine Singly Resampled and Doubly Resampled Features in Scene E-1080-15192

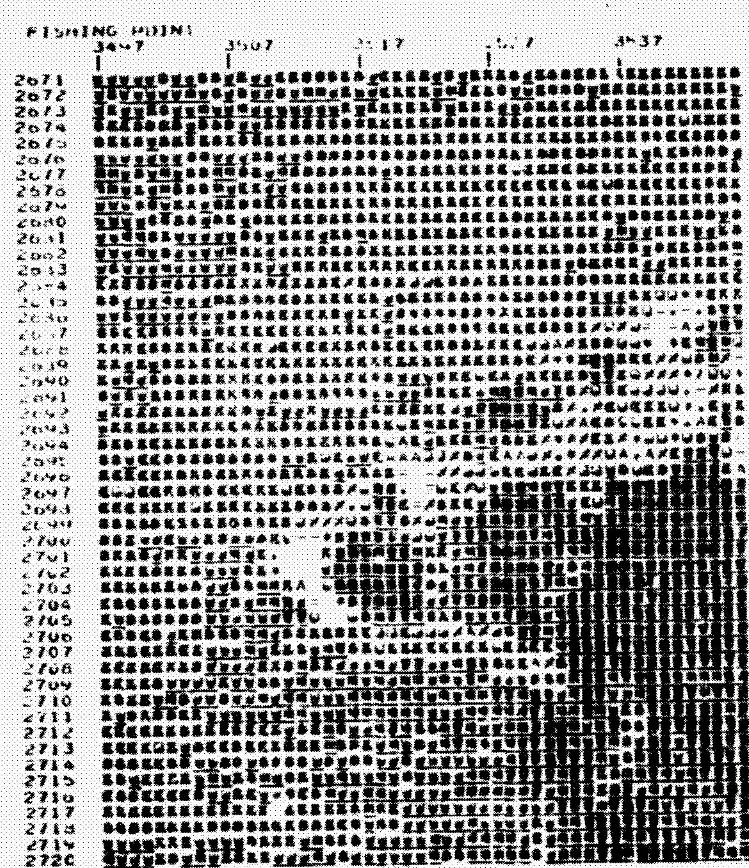

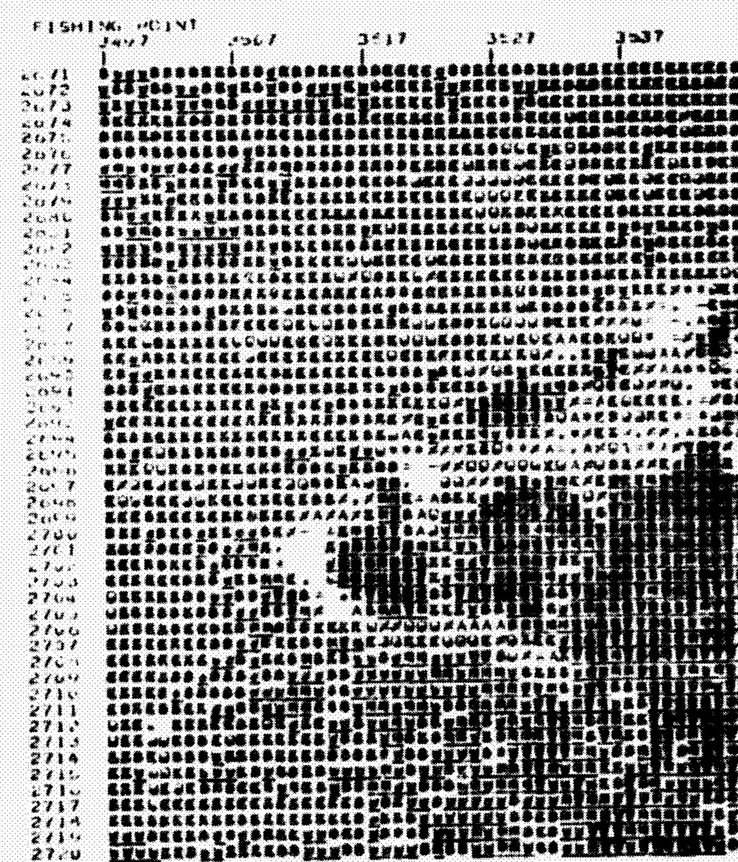

Figure 3-4 (cont'd) Shadeprints of the Nine Singly Resampled and Doubly Resampled Features in Scene E-1080-15192

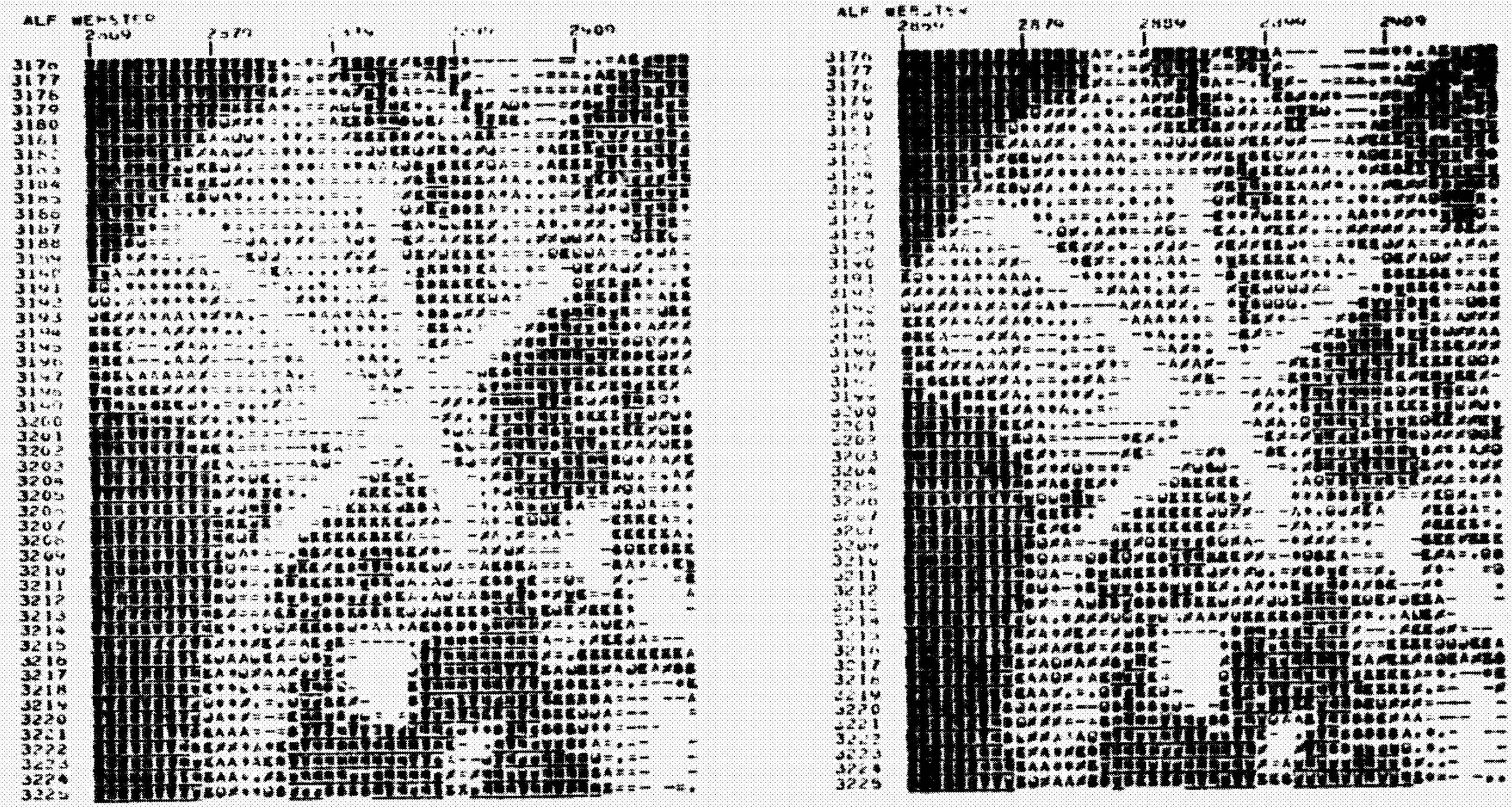

Figure 3-4 (cont'd) Shadeprints of the Nine Singly Resampled and Doubly Resampled Features in Scene E-1080-15192

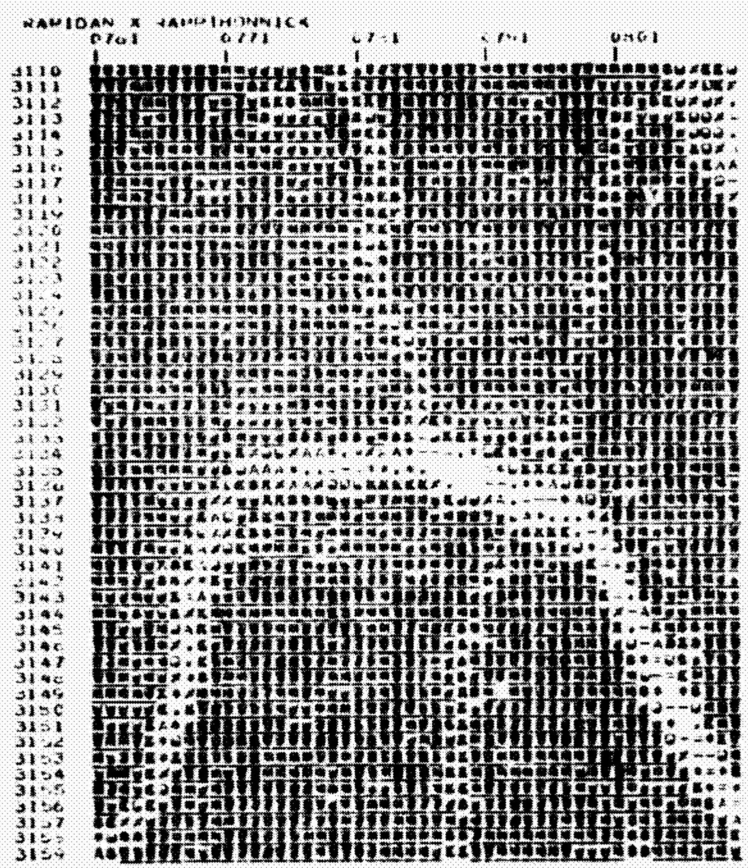

Figure 3-4 (cont'd) Shadeprints of the Nine Singly Resampled and Doubly Resampled Features in Scene E-1080-15192

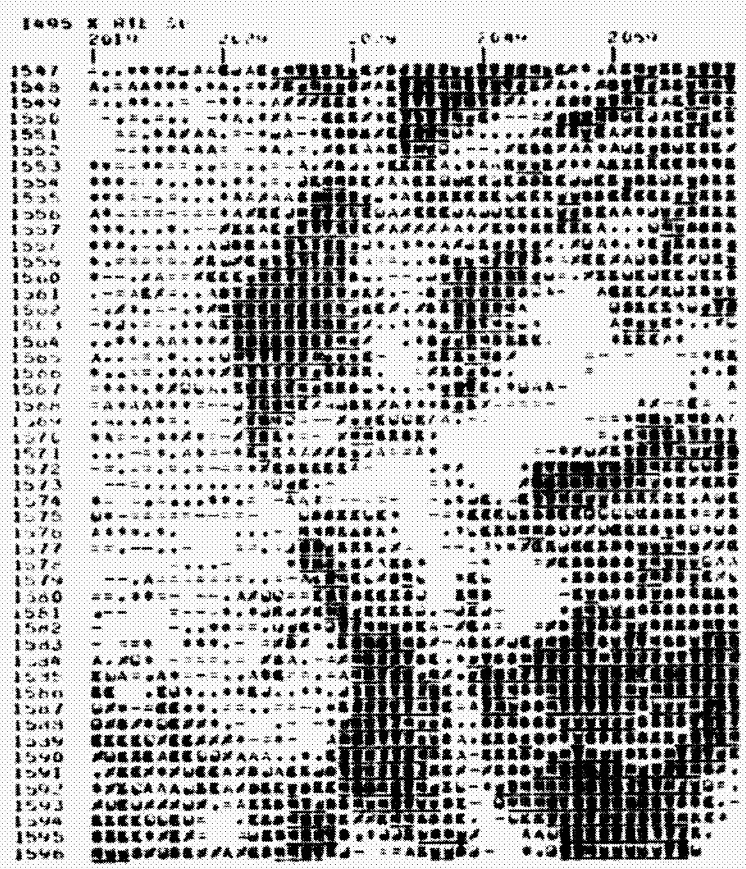


Figure 3-4 (cont'd) Shadeprints of the Nine Singly Resampled and Doubly Resampled Features in Scene E-1080-15192

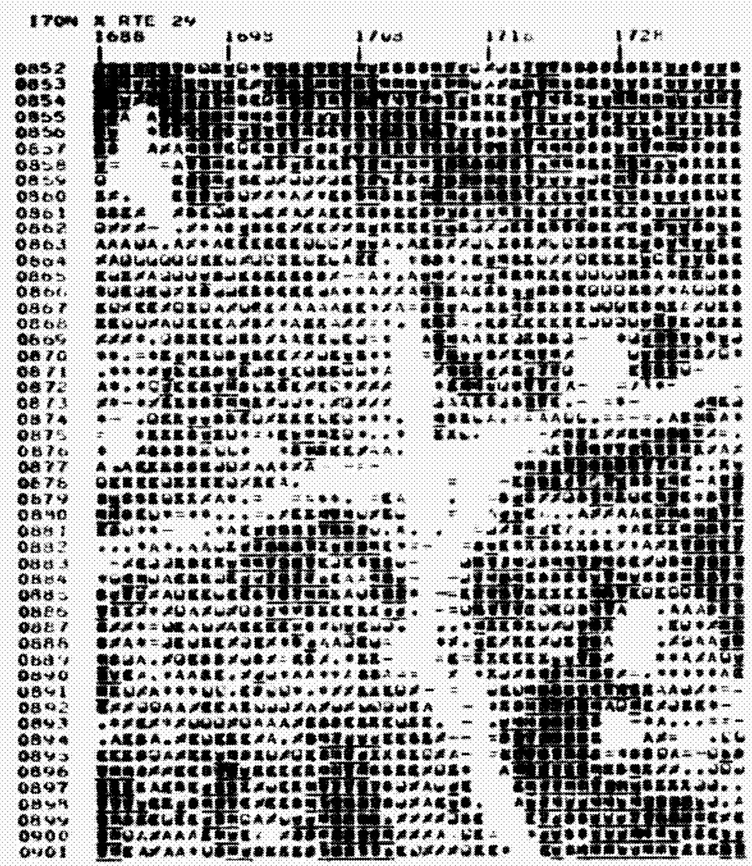

Figure 3-4 (cont'd) Shadeprints of the Nine Singly Resampled and Doubly Resampled Features in Scene E-1080-15192

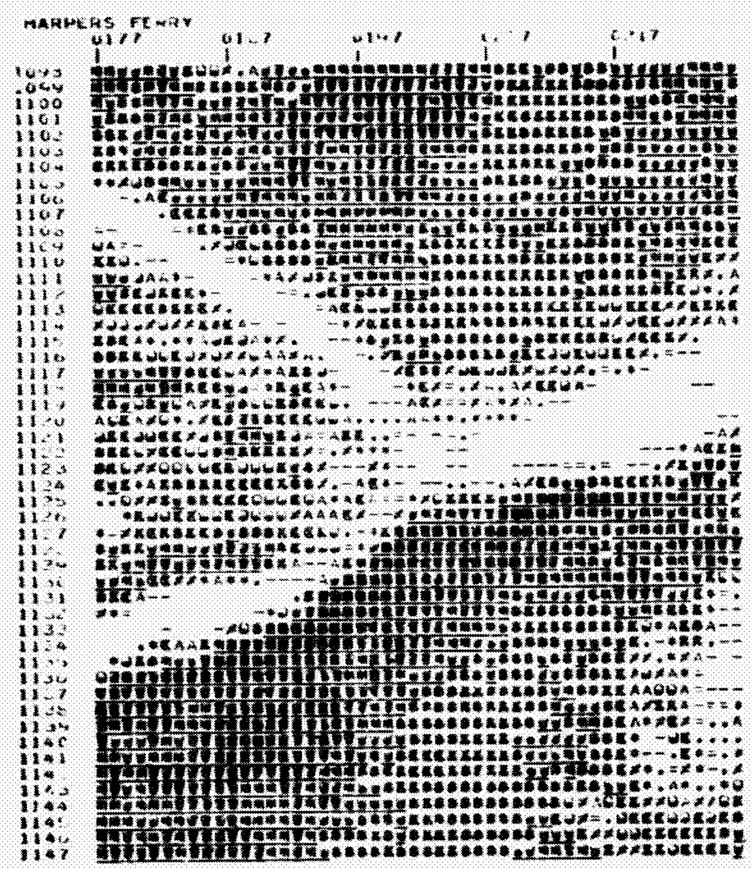

Figure 3-4 (cont'd) Shadeprints of the Nine Singly Resampled and Doubly Resampled Features in Scene E-1080-15192

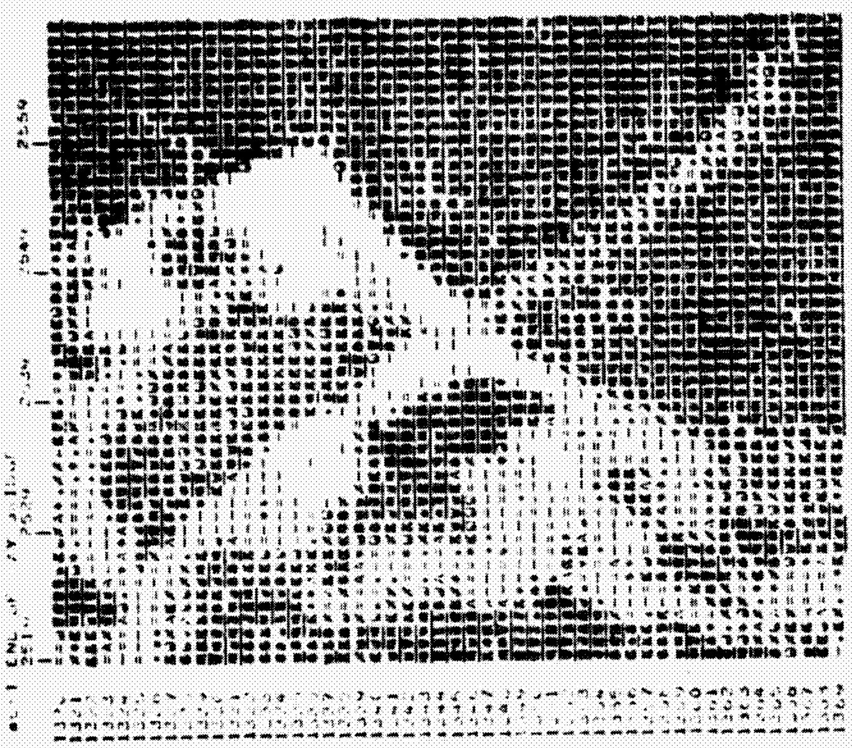

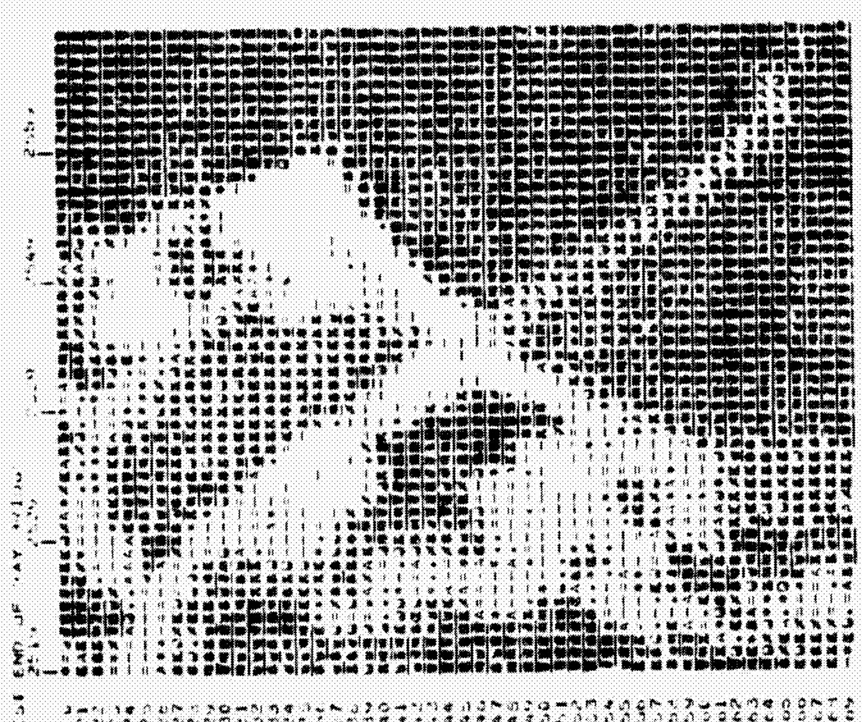

Figure 3-4 (cont'd) Shadeprints of the Nine Singly Resampled and Doubly Resampled Features in Scene E-1080-15192

Section 4. Radiometric Degradation

Visually, there appears to be little degradation of the bi-resampled image of scene A. The singly resampled image and the doubly resampled image are shown in Figures 4-1 and 4-2, respectively. A visual image of the radiometric differences was produced by subtracting the bi-resampled image from the singly resampled image, adding a bias, and exaggerating the radiometric scale. This difference image is shown in Figure 4-3. Keeping in mind the fact that these differences are slight, several comments can be made regarding the difference image. First, one can see in the difference image the land outlines and features with sharp edges, such as · rports. Second, the overall image tends to a uniform gray, indicating that there are no gross geometric distortions in the registration of the two images. Sharp edges stand out in the difference image due to the "overshoot" of the cubic convolution algorithm employed in the resampling process. This characteristic of the cubic convolution algorithm is discussed in more detail later in this section.

Quantitative measures of the effects of double resampling were obtained through histograms of the difference image, histograms and statistical evaluation of corresponding subimages from each of the resampled images, and power spectra analyses of these corresponding subimages.

a) A quantitative measure of the radiometric differences is provided in the histograms of the difference images and the two

images each of scenes A and B, Figures 4-4 through 4-9. In Figure 4-9, the histogram of the difference image of the interior region of scene A, 97% of all pixels have count differences of at most one count.

Two comments need to be made at this point regarding the UTM image of scene A, from which the bi-resampled image was created. First, the cubic convolution algorithm had a round-off error at the time the UTM image was produced. The effect of this problem is that the average count in the UTM image is 0.5 count lower than the average count in the raw, uncorrected data. This is supported by the histogram (Figure 4-6) which shows the average count of the difference image to be 140.5. Since the bias added to the difference image was 140, this implies that the singly resampled image has an average count 0.5 greater than the bi-resampled image, the count loss in the UTM image having been carried over to the bi-resampled image. Second, the UTM image did not have a sufficiently large border to eliminate "edge problems" when resampling to produce the bi-resampled image. The edge problem has the effect of spreading the histogram of the difference image. To eliminate the edge problem effect on the histogram, the interior region of the difference image was histogrammed, and is shown in Figure 4-9. This figure shows the elimination of the tails of the histogram in Figure 4-6. Neither of the above two problems apply to scene B.

b) Three regions of each scene were selected on the basis

of their relatively high, medium, and low spatial frequency characteristics. Areas selected in scene A are boxed in Figure 3-1, and histograms of each area for the singly and doubly resampled images are provided in Figures 4-10 and 4-11. A shadeprint of band 5 of scene B is given in Figure 4-12, and the areas selected in this scene are shown in Figure 4-13.

Radiometric averages and standard deviations were computed and plotted as a function of area size for the three regions from the singly and doubly resampled images. The various areas used in the computation are centered in their respective regions. Plots of these for scene A and the four bands of scene B are presented in Figures 4-14 through 4-18. In general the differences tend to be fractions of a count and are greater in the small areas (e.g. 2x2) where the calculations are more sensitive to individual pixel differences. One exception is in the high frequency region of scene B, band 5. This plot shows a higher standard deviation in the bi-resampled image. The nested square areas for which the mean and standard deviation are computed are centered on a sharp edge in the high frequency region. The greater standard deviation of the bi-resampled image is a manifestation of the overshoot of the cubic convolution algorithm when processing across an edge. An evaluation of this edge overshoot problem is presented in paragraph d) below.

c) One-dimensional power spectra of scene A were computed for the three regions, both in the vertical and the horizontal directions. An 128-point Discrete Fourier Transform (DFT) was employed in the calculation of the spectrum of each line. Spectra

of 50 contiguous lines were averaged by frequency in each of the regions. These averaged, or smoothed, spectra for the singly and doubly resampled images in all three regions, plus the absolute difference of the singly and doubly resampled image spectra are presented in Figures 4-19 through 4-36. In the computation of the spectra, the DC term was removed prior to the transform computation.

The power spectrum response of the single and double resampling process is shown in Figure 4-37. The frequency response of the bi-resampling is simply the convolution of the single resampling response with itself. These curves suggest that, relative to the single resampling process, bi-resampling boosts the lower frequencies and attenuates the higher frequencies, with a crossover point of 0.29 cycles/sample. (In the Figure 4-19 through 4-36, this crossover frequency corresponds to I = 37.) For the high and medium frequency regions, and for both the horizontal and vertical spectra, the power spectra curves show this behavior. Crossover frequencies for these four cases are:

Region	Crossover
high frequency,horizontal	37
high frequency,vertical	43
medium frequency,horizontal	41
medium frequency,vertical	45

The deviations of the actual crossover points from the theoretical crossover points can be attributed to errors in estimating and smoothing the frequency response of the digital data, plus discretization errors in the radiometric count computed for each pixel in the

single and double resampling process. The low frequency regions do not exhibit this general behavior. This is probably due to the computational errors, in the power spectrum estimation process, being larger than the actual energy present in the higher frequencies.

d) The process of bi-resampling primarily degrades edges. This is due to the suppression of the high frequency energy content in edges by the cubic convolution algorithm, as discussed above in c). This effect manifests itself as edge overshoot in the bi-resampled imagery. Several examples of this phenomenon are given in Figures 4-38 through 4-41. These figures compare the radiometric values of the singly resampled imagery with those of the bi-resampled imagery along either a vertical or a horizontal line which crosses a sharp edge. Also included in these figures is the "nearest neighbor" resampled raw data. (The raw data is not congruent to the resampled data and is provided only as a guide to the general shape of the uncorrupted data. However, in Figure 4-38, the raw data line deviates less than 0.04 pixel from the resampled lines.) The first three figures cross an edge in the high frequency region of Hand County. The last figure crosses an edge containing a bright spot of a runway of Dulles Airport. These figures also show that there is no noticeable spreading of the edges due to the high frequency energy loss in the bi-resampled data. It should be reemphasized here that the degradations, although measureable, are still slight and probably ignorable for most applications.

This figure is a photograph contained

in the pocket at the back of this report.

Figure 4-1. Scene E-1080-15192, Singly Resampled Image

This figure is a photograph contained

in the pocket at the back of this report.

Figure 4-2. Scene E-1080-15192, Doubly Resampled Image

This figure is a photograph contained
in the pocket at the back of this report.

Figure 4-3. Scene E-1080-15192, Difference Image

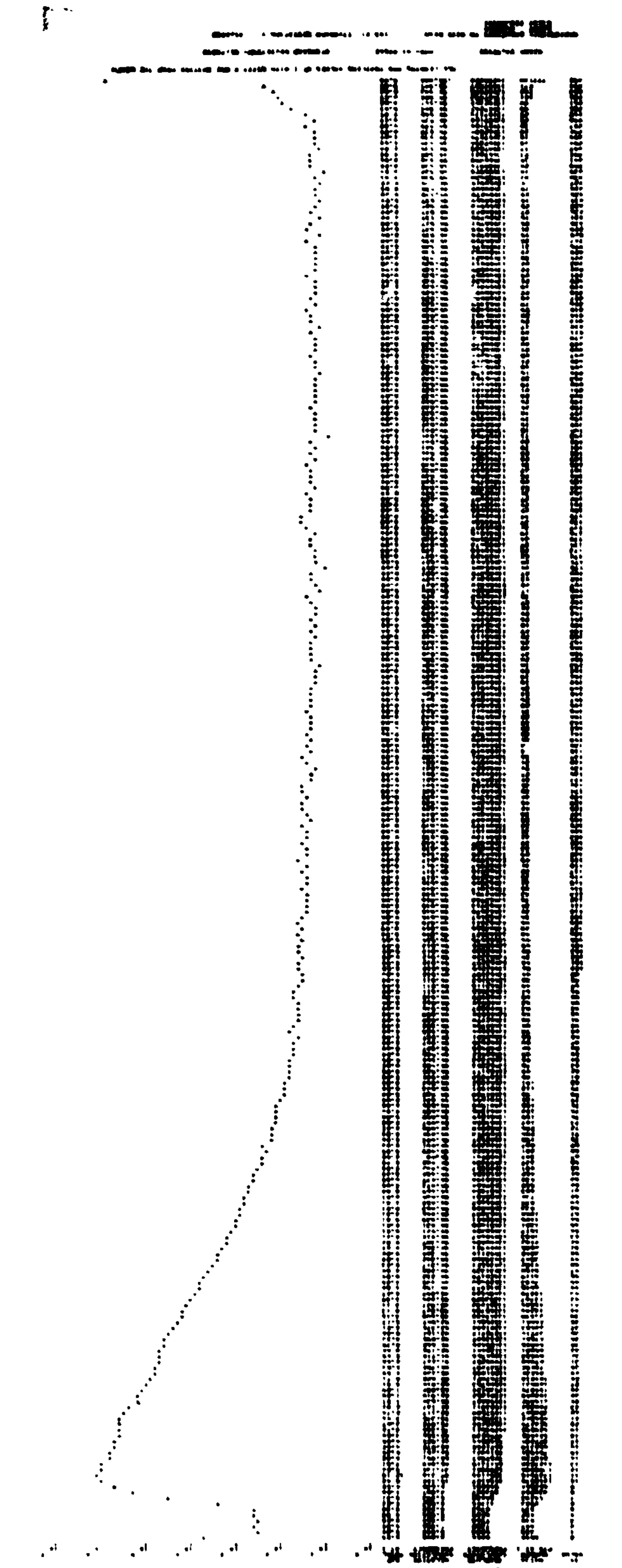

Figure 4-4 Scene E-1080-15192, Histogram of Singly Resampled Image

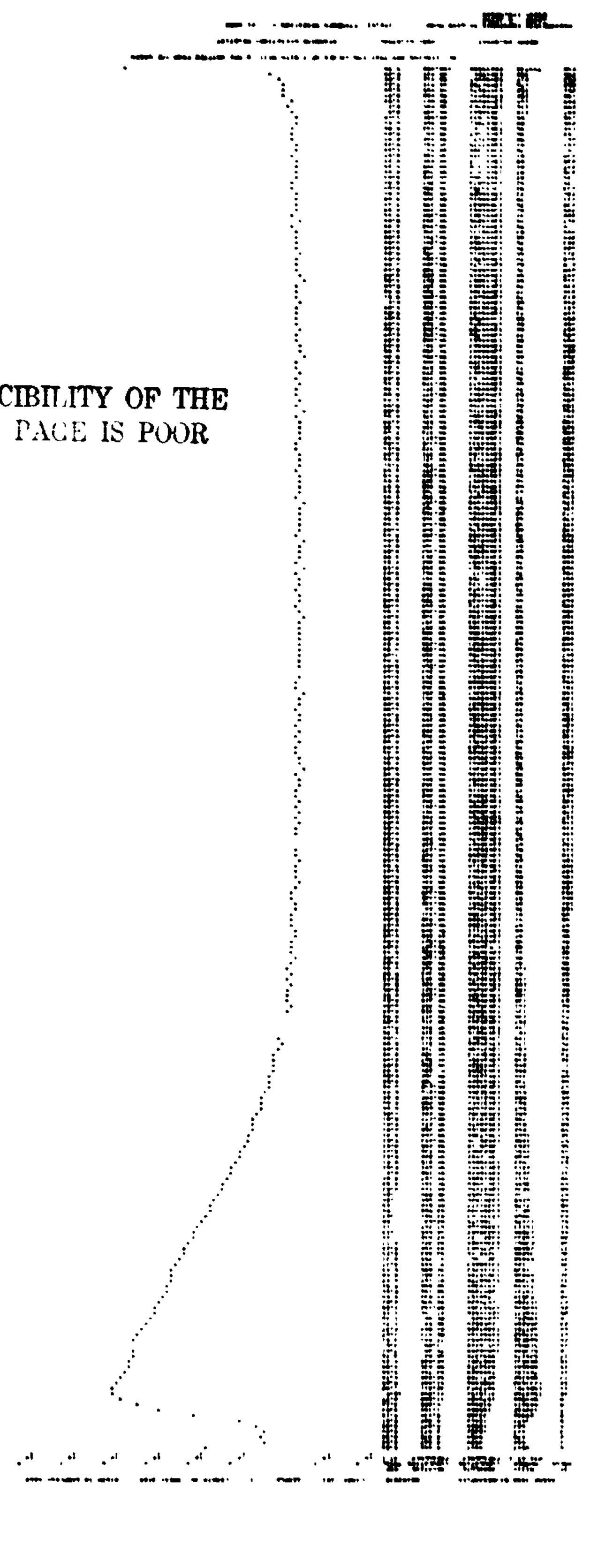

Figure 4-5   Scene E-1080-15192, Histogram of Doubly Resampled Image

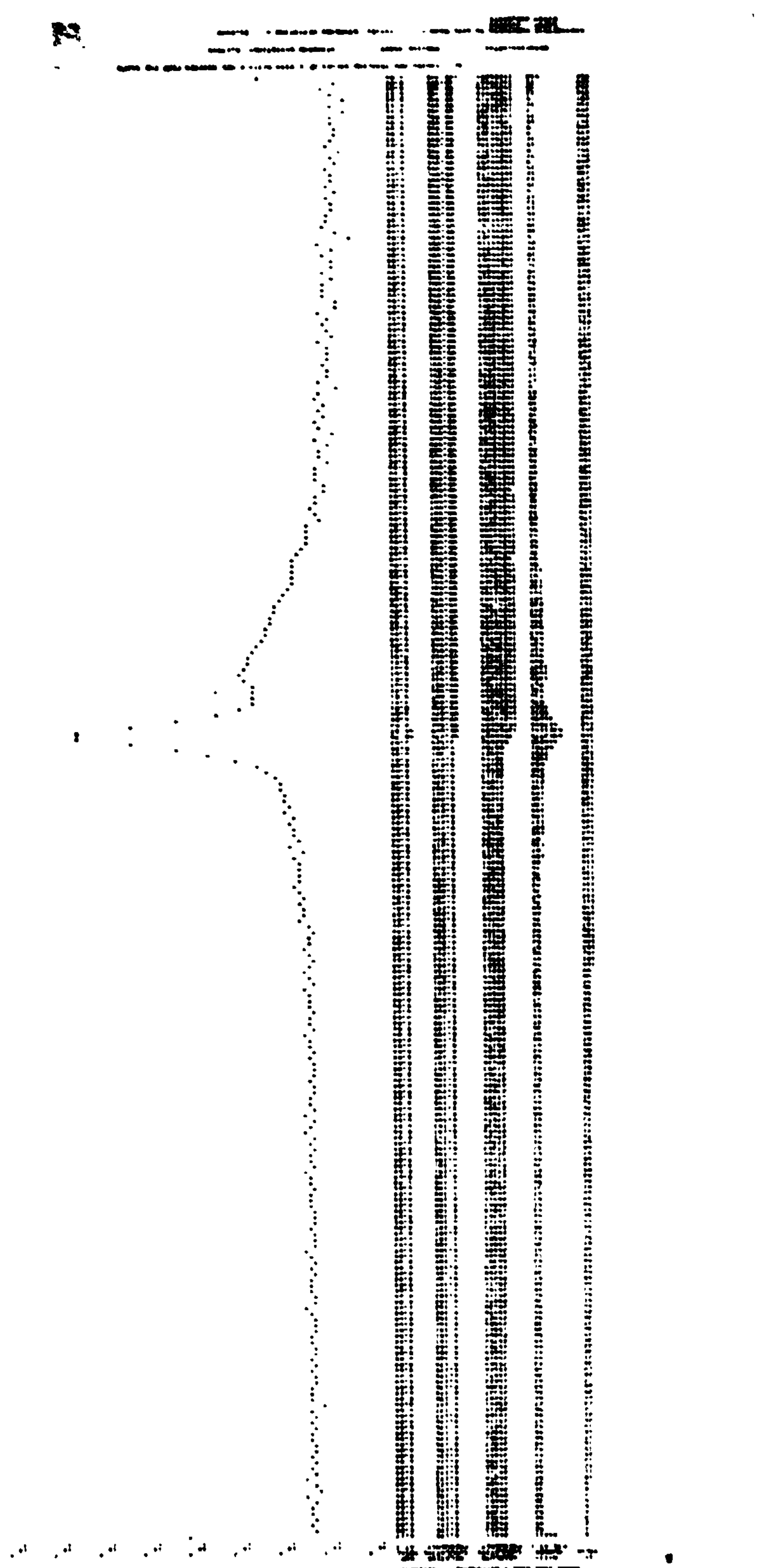

Figure 4-6 Scene E-1080-15192, Histogram of Difference Image

SCENE 2183 BAND 5 DIFFERENCE 00190010 LINE= 1 SAMPLE= 1 LENGTH IN LINES= 202 WIDTH IN SAMPLES= 235

I= VALUE	N(I)= NUMBER PTS AT I	ABSOLUTE CUMULATIVE FREQUENCY	RELATIVE CUMULATIVE FREQUENCY	%OF TOTAL AT I
135	3	3	0.006	0.01
136	30	33	0.070	0.06
137	101	134	0.282	0.21
138	670	804	1.694	1.41
139	8333	9137	19.248	17.55
140	28943	38080	80.219	60.97
141	8578	46658	98.289	18.07
142	688	47346	99.739	1.45
143	98	47444	99.945	0.21
144	24	47468	99.996	0.05
145	2	47470	100.000	0.00

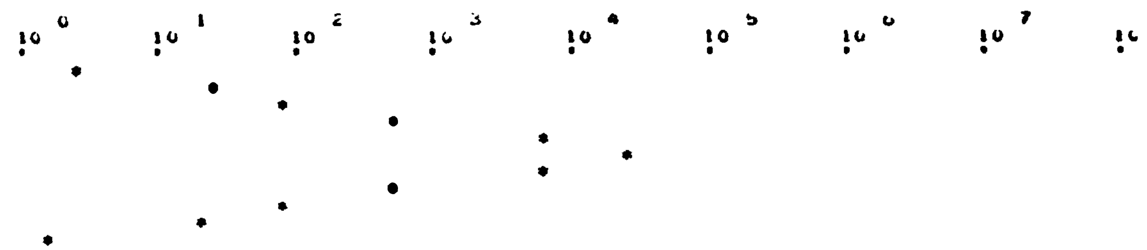

ALL LEADING AND TRAILING VALUES OF I WITH N(I)= 0 ARE OMITTED FROM THE GRAPH

MEAN=140.00511 RMS=140.00694 STANDARD DEVIATION= 0.71535

RADIOMETRIC CONSTANTS TO GIVE MEAN = 140.0; STANDARD DEVIATION = 21.0000
GAIN= 29.35645
BIAS=**********

SCENE 2183 BAND 4 DIFFERENCE 00160010 LINE= 1 SAMPLE= 1 LENGTH IN LINES= 202 WIDTH IN SAMPLES= 235

I= VALUE	N(I)= NUMBER PTS AT I	ABSOLUTE CUMULATIVE FREQUENCY	RELATIVE CUMULATIVE FREQUENCY	%OF TOTAL AT I
137	2	2	0.004	0.00
138	77	79	0.166	0.16
139	6186	6265	13.196	13.03
140	34915	41180	86.750	73.55
141	6219	47399	99.850	13.10
142	70	47469	99.998	0.15
143	1	47470	100.000	0.00

ALL LEADING AND TRAILING VALUES OF I WITH N(I)= 0 ARE OMITTED FROM THE GRAPH

MEAN=140.00034 RMS=140.00124 STANDARD DEVIATION= 0.50000

RADIOMETRIC CONSTANTS TO GIVE MEAN = 140.0; STANDARD DEVIATION = 21.0000
GAIN= 42.00000
BIAS=**********

Figure 4-7 Hand County, Bands 4 and 5, Histogram of Difference Image

SCENE 2183 BAND 6 DIFFERENCE 00160010 LINE= 1 SAMPLE= 1 LENGTH IN LINES= 202 WIDTH IN SAMPLES= 235

I= VALUE	N(I)= NUMBER PTS AT I	ABSOLUTE CUMULATIVE FREQUENCY	RELATIVE CUMULATIVE FREQUENCY	%OF TOTAL AT I
135	2	2	0.004	0.00
136	16	18	0.038	0.03
137	73	91	0.192	0.15
138	704	795	1.675	1.48
139	9107	9902	20.859	19.18
140	27562	37464	78.921	58.06
141	9127	46591	98.148	19.23
142	764	47355	99.758	1.61
143	96	47451	99.960	0.20
144	19	47470	100.000	0.04

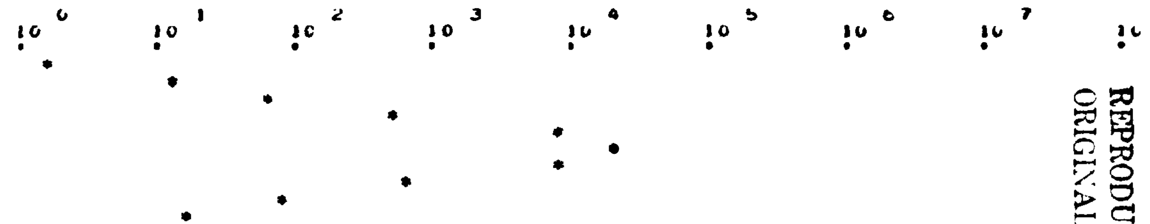

ALL LEADING AND TRAILING VALUES OF I WITH N(I)= 0 ARE OMITTED FROM THE GRAPH

MEAN=140.00444 RMS=140.00635 STANDARD DEVIATION= 0.73154

RADIOMETRIC CONSTANTS TO GIVE MEAN = 140.0; STANDARD DEVIATION = 21.0000
GAIN= 28.70641
BIAS=**********

REPRODUCIBILITY OF THE ORIGINAL PAGE IS POOR

SCENE 2183 BAND 7 DIFFERENCE 00190010 LINE= 1 SAMPLE= 1 LENGTH IN LINES= 202 WIDTH IN SAMPLES= 235

I= VALUE	N(I)= NUMBER PTS AT I	ABSOLUTE CUMULATIVE FREQUENCY	RELATIVE CUMULATIVE FREQUENCY	%OF TOTAL AT I
137	5	5	0.011	0.01
138	122	127	0.268	0.26
139	6620	6747	14.213	13.95
140	33832	40579	85.483	71.27
141	6764	47343	99.732	14.25
142	121	47464	99.987	0.25
143	6	47470	100.000	0.01

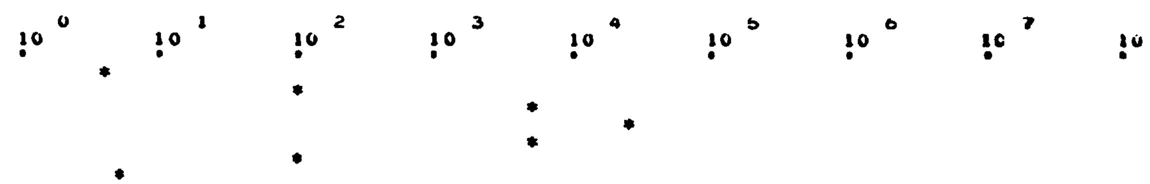

ALL LEADING AND TRAILING VALUES OF I WITH N(I)= 0 ARE OMITTED FROM THE GRAPH

MEAN=140.00305 RMS=140.00410 STANDARD DEVIATION= 0.54486

RADIOMETRIC CONSTANTS TO GIVE MEAN = 140.0; STANDARD DEVIATION = 21.0000
GAIN= 38.54184
BIAS=**********

Figure 4-8 Hand County, Bands 6 and 7, Histogram of Difference Image

SCENE 1080 DIFFERENCE (INTERIOR)00250010 LINE= 12 SAMPLE= 200 LENGTH IN LINES= 3661 WIDTH IN SAMPLES= 3448

I-VALUE	N(I)-NUMBER PTS AT I	ABSOLUTE CUMULATIVE FREQUENCY	RELATIVE CUMULATIVE FREQUENCY	%OF TOTAL AT I
127	1	1	0.000	0.00
128	2	3	0.000	0.00
129	2	5	0.000	0.00
130	6	11	0.000	0.00
131	8	19	0.000	0.00
132	28	47	0.000	0.00
133	48	95	0.001	0.00
134	131	226	0.002	0.00
135	374	600	0.005	0.00
136	1468	2068	0.016	0.01
137	6935	9003	0.071	0.05
138	40098	49101	0.387	0.32
139	393280	442381	3.485	3.10
140	5835917	6278298	49.466	45.98
141	5979029	12257327	96.575	47.11
142	395222	12652549	99.688	3.11
143	33783	12686332	99.955	0.27
144	4595	12690927	99.991	0.04
145	843	12691770	99.997	0.01
146	208	12691978	99.999	0.00
147	65	12692043	100.000	0.00
148	26	12692069	100.000	0.00
149	9	12692073	100.000	0.00
150	6	12692080	100.000	0.00
151	0	12692086	100.000	0.0
152	1	12692087	100.000	0.00
153	1	12692088	100.000	0.00

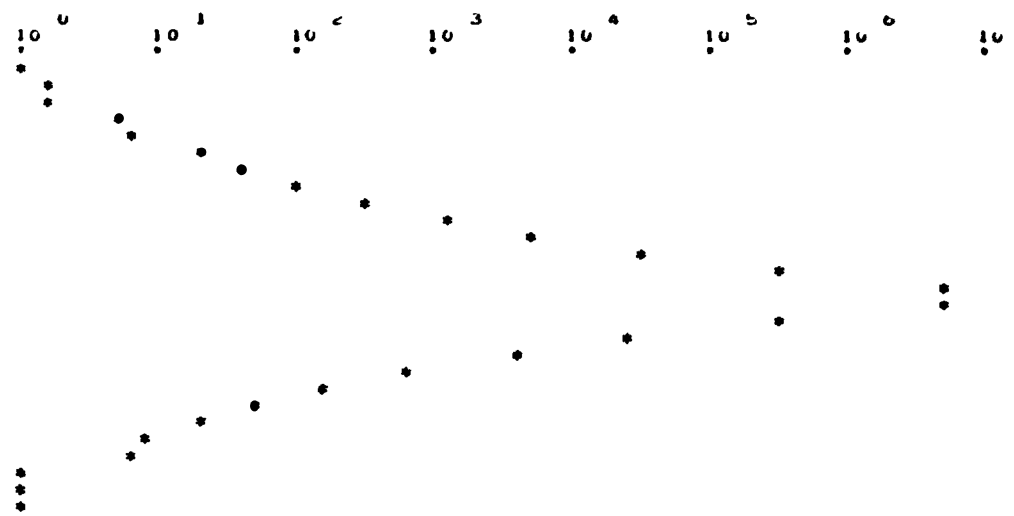

ALL LEADING AND TRAILING VALUES OF I WITH N(I)= 0 ARE OMITTED FROM THE GRAPH

MEAN=140.50348 RMS=140.50500 STANDARD DEVIATION= 0.65551

RADIOMETRIC CONSTANTS TO GIVE MEAN = 140.0; STANDARD DEVIATION = 21.0000
GAIN= 32.03633
BIAS=**********

Figure 4-9 Scene E-1080-15192, Histogram of Difference Image, Interior Region

SCENE 1080 LCC(II) HIGH FREQ   UG190010   LINE= 625   SAMPLE= 938   LENGTH IN LINES= 50   WIDTH IN SAMPLES= 128

I= VALUE	N(I)= NUMBER PTS AT I	ABSOLUTE CUMULATIVE FREQUENCY	RELATIVE CUMULATIVE FREQUENCY	%OF TOTAL AT I
5	1	1	0.016	0.02
6	0	1	0.016	0.0
7	1	2	0.031	0.02
8	0	2	0.031	0.0
9	5	7	0.109	0.08
10	23	30	0.469	0.36
11	62	92	1.437	0.97
12	82	174	2.719	1.28
13	110	284	4.437	1.72
14	123	407	6.359	1.92
15	179	586	9.156	2.80
16	314	900	14.063	4.91
17	342	1242	19.406	5.34
18	430	1672	26.125	6.72
19	542	2214	34.594	8.47
20	642	2856	44.625	10.03
21	635	3491	54.547	9.92
22	495	3986	62.281	7.73
23	357	4343	67.859	5.58
24	286	4629	72.328	4.47
25	243	4872	76.125	3.80
26	199	5071	79.234	3.11
27	174	5245	81.953	2.72
28	139	5384	84.125	2.17
29	144	5528	86.375	2.25
30	116	5644	88.187	1.81
31	105	5749	89.828	1.64
32	91	5840	91.250	1.42
33	88	5928	92.625	1.38
34	80	6008	93.875	1.25
35	55	6063	94.734	0.86
36	52	6115	95.547	0.81
37	43	6158	96.219	0.67
38	36	6194	96.781	0.56
39	29	6223	97.234	0.45
40	25	6248	97.625	0.39
41	35	6283	98.172	0.55
42	22	6305	98.516	0.34
43	16	6321	98.766	0.25
44	16	6337	99.016	0.25
45	13	6350	99.219	0.20
46	16	6366	99.469	0.25
47	9	6375	99.609	0.14
48	3	6378	99.656	0.05
49	5	6383	99.734	0.08
50	7	6390	99.844	0.11
51	2	6392	99.875	0.03
52	4	6396	99.937	0.06
53	0	6396	99.937	0.0
54	1	6397	99.953	0.02
55	2	6399	99.984	0.03
56	0	6399	99.984	0.0
57	1	6400	100.000	0.02

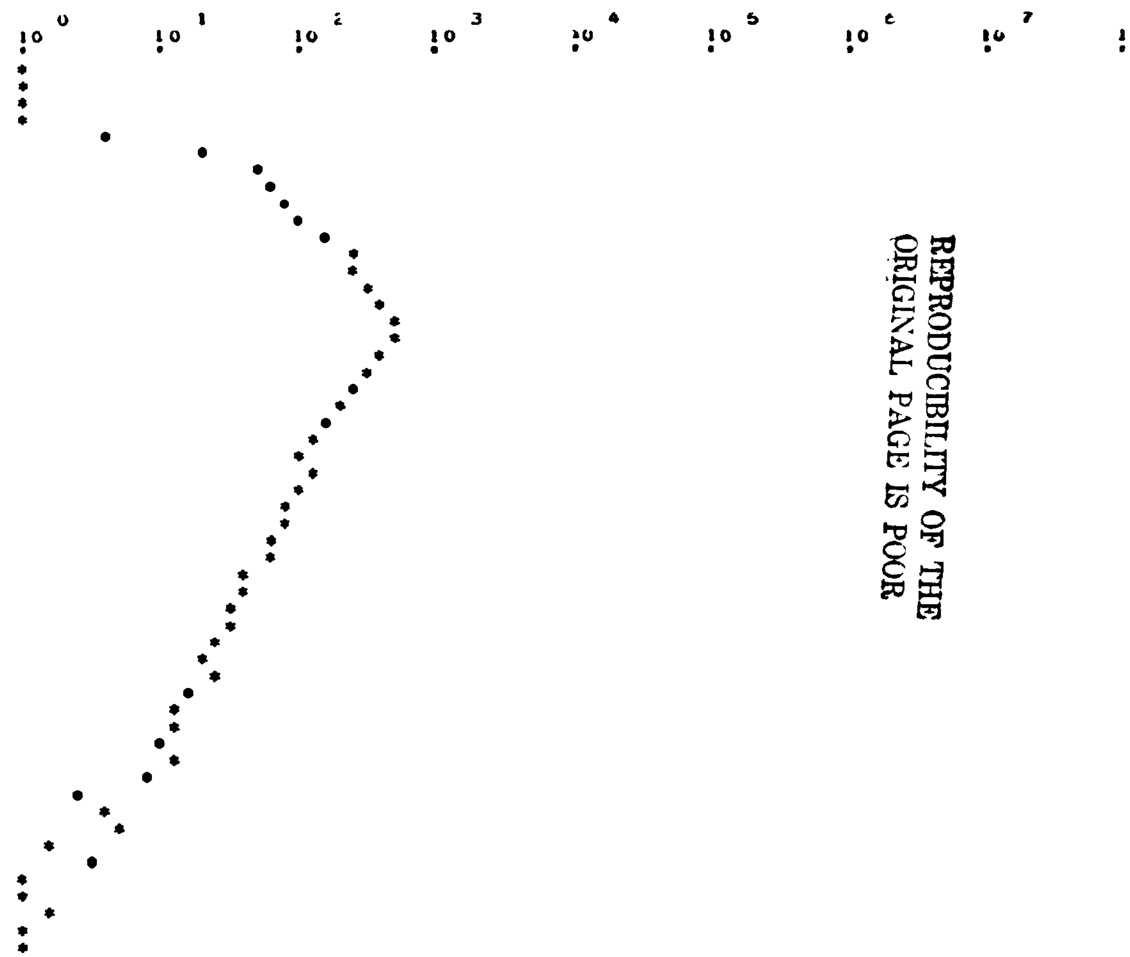

ALL LEADING AND TRAILING VALUES OF I WITH N(I)= 0 ARE OMITTED FROM THE GRAPH

MEAN= 22.45999   RMS= 23.42554   STANDARD DEVIATION= 6.65616

RADIOMETRIC CONSTANTS TO GIVE MEAN = 140.0; STANDARD DEVIATION = 21.0000
GAIN= 3.15497
BIAS= 69.13936

Figure 4-10(A) Scene E-1080-15192, Singly Resampled Image, Histogram of High Frequency Region

SCENE 1080 LCC(II) MEDIUM FREQ 00220010 LINE= 1[illegible]75 SAMPLE= 1625 LENGTH IN LINES= 50 WIDTH IN SAMPLES= 128

I= VALUE	N(I)= NUMBER PTS AT I	ABSOLUTE CUMULATIVE FREQUENCY	RELATIVE CUMULATIVE FREQUENCY	%OF TOTAL AT I
8	2	2	0.031	0.03
9	23	25	0.391	0.36
10	139	164	2.562	2.17
11	209	373	5.828	3.27
12	166	539	8.422	2.59
13	197	736	11.500	3.08
14	243	979	15.297	3.80
15	295	1274	19.906	4.61
16	280	1554	24.281	4.38
17	381	1935	30.234	5.95
18	412	2347	36.672	6.44
19	505	2852	44.562	7.89
20	584	3436	53.687	9.13
21	528	3964	61.937	8.25
22	429	4393	68.641	6.70
23	377	4770	74.531	5.89
24	275	5045	78.828	4.30
25	259	5304	82.875	4.05
26	215	5519	86.234	3.36
27	222	5741	89.703	3.47
28	159	5900	92.188	2.48
29	98	5998	93.719	1.53
30	106	6104	95.375	1.66
31	63	6167	96.359	0.98
32	59	6226	97.281	0.92
33	32	6258	97.781	0.50
34	23	6281	98.141	0.36
35	16	6297	98.391	0.25
36	31	6328	98.875	0.48
37	15	6343	99.109	0.23
38	5	6348	99.187	0.08
39	9	6357	99.328	0.14
40	10	6367	99.484	0.16
41	4	6371	99.547	0.06
42	6	6377	99.641	0.09
43	8	6385	99.766	0.13
44	2	6387	99.797	0.03
45	4	6391	99.859	0.06
46	1	6392	99.875	0.02
47	1	6393	99.891	0.02
48	1	6394	99.906	0.02
49	1	6395	99.922	0.02
50	1	6396	99.937	0.02
51	1	6397	99.953	0.02
52	2	6399	99.984	0.03
53	0	6399	99.984	0.0
54	0	6399	99.984	0.0
55	1	6400	100.000	0.02

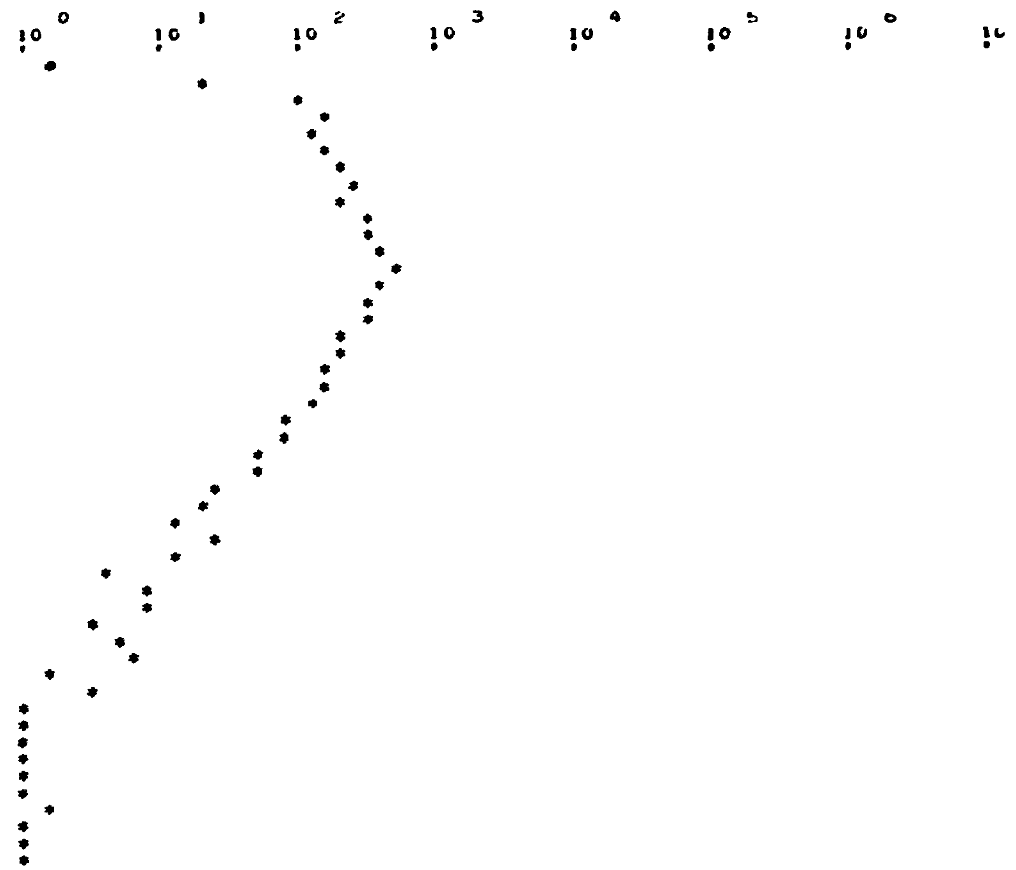

ALL LEADING AND TRAILING VALUES OF I WITH N(I)= 0 ARE OMITTED FROM THE GRAPH

MEAN= 20.40608 RMS= 21.21194 STANDARD DEVIATION= 5.79125

RADIOMETRIC CONSTANTS TO GIVE MEAN = 140.0; STANDARD DEVIATION = 21.0000
GAIN= 3.62616
BIAS= 66.00430

Figure 4-10(B) Scene E-1080-15192, Singly Resampled Image, Histogram of Medium Frequency Region

SCENE 1080 LCC(I) LOW FREQ 00250010 LINE= 2125 SAMPLE= 2625 LENGTH IN LINES= 50 WIDTH IN SAMPLES= 128

I= VALUE	N(I)= NUMBER PTS AT I	ABSOLUTE CUMULATIVE FREQUENCY	RELATIVE CUMULATIVE FREQUENCY	%OF TOTAL AT I
6	2	2	0.031	0.03
7	85	87	1.359	1.33
8	600	687	10.734	9.38
9	3439	4126	64.469	53.73
10	2098	6224	97.250	32.78
11	164	6388	99.812	2.56
12	12	6400	100.000	0.19

10^0 10^1 10^2 10^3 10^4 10^5 10^6 10^7

ALL LEADING AND TRAILING VALUES OF I WITH N(I)= 0 ARE OMITTED FROM THE GRAPH

MEAN= 9.26344 RMS= 9.29186 STANDARD DEVIATION= 0.72627

RADIOMETRIC CONSTANTS TO GIVE MEAN = 140.0; STANDARD DEVIATION = 21.0000
GAIN= 28.91492
BIAS=-127.65132

Figure 4-10(C) Scene E-1080-15192, Singly Resampled Image, Histogram of Low Frequency Region

SCENE 1080 LCC(UTM) HIGH FREQ   00190010   LINE= 625   SAMPLE= 938   LENGTH IN LINES= 50   WIDTH IN SAMPLES= 128

I-VALUE	N(I)= NUMBER PTS AT I	ABSOLUTE CUMULATIVE FREQUENCY	RELATIVE CUMULATIVE FREQUENCY	%OF TOTAL AT I
4	1	1	0.016	0.02
5	0	1	0.016	0.0
6	2	3	0.047	0.03
7	1	4	0.062	0.02
8	5	9	0.141	0.08
9	13	22	0.344	0.20
10	41	63	0.984	0.64
11	83	146	2.261	1.30
12	102	248	3.875	[illegible]59
13	112	360	5.625	[illegible]75
14	171	531	8.297	2.67
15	242	773	12.078	3.78
16	336	1109	17.328	5.25
17	383	1492	23.312	5.98
18	493	1985	31.016	7.70
19	588	2573	40.203	9.19
20	637	3210	50.156	9.95
21	580	3790	59.219	9.06
22	398	4188	65.437	6.22
23	295	4483	70.047	4.61
24	239	4722	73.781	3.73
25	244	4966	77.594	3.81
26	202	5168	80.750	3.16
27	149	5317	83.078	2.33
28	127	5444	85.062	1.98
29	123	5567	86.984	1.92
30	120	5687	88.859	1.88
31	97	5784	90.375	1.52
32	75	5859	91.547	1.17
33	94	5953	93.016	1.47
34	79	6032	94.250	1.23
35	36	6068	94.812	0.56
36	56	6124	95.687	0.88
37	45	6169	96.391	0.70
38	28	6197	96.828	0.44
39	26	6223	97.234	0.41
40	26	6249	97.641	0.41
41	30	6279	98.109	0.47
42	26	6305	98.516	0.41
43	16	6321	98.766	0.25
44	12	6333	98.953	0.19
45	16	6349	99.203	0.25
46	11	6360	99.375	0.17
47	6	6366	99.469	0.09
48	7	6373	99.578	0.11
49	8	6381	99.703	0.13
50	8	6389	99.828	0.13
51	3	6392	99.875	0.05
52	2	6394	99.906	0.03
53	2	6396	99.937	0.03
54	0	6396	99.937	0.0
55	2	6398	99.969	0.03
56	1	6399	99.984	0.02
57	1	6400	100.000	0.02

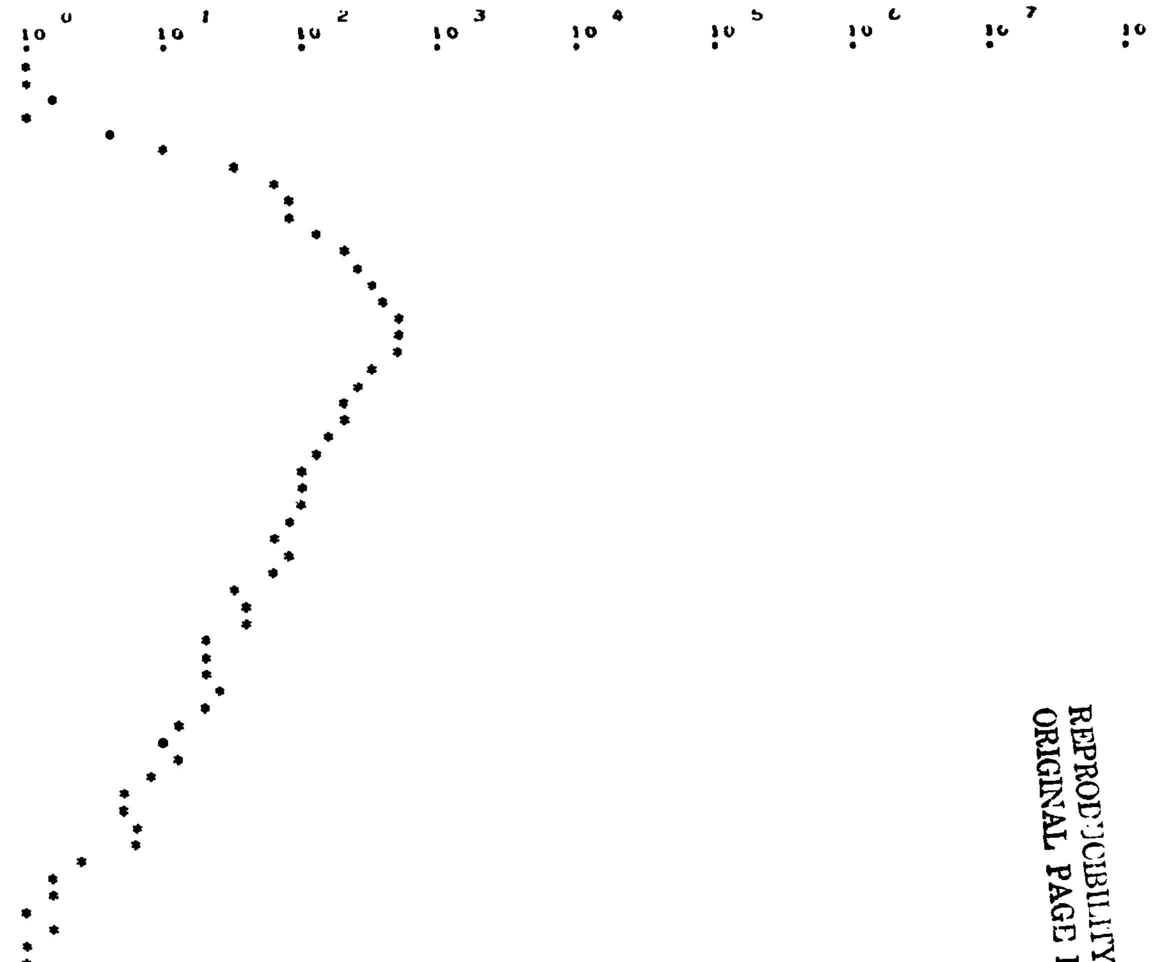

ALL LEADING AND TRAILING VALUES OF I WITH N(I)= 0 ARE OMITTED FROM THE GRAPH

MEAN= 21.94514   RMS= 22.98015   STANDARD DEVIATION= 6.81893

RADIOMETRIC CONSTANTS TO GIVE MEAN = 140.0; STANDARD DEVIATION = 21.0000
GAIN= 3.07966
BIAS= 72.41640

Figure 4-11(A) Scene E-1080-15192, Doubly Resampled Image, Histogram of High Frequency Region

SCENE 1080 LCC(UTM) MEDIUM FREQ 00220010   LINE= 1675   SAMPLE= 1625   LENGTH IN LINES= [illegible]   WIDTH IN SAMPLES= [illegible]

I= VALUE	N(I)= NUMBER PTS AT I	ABSOLUTE CUMULATIVE FREQUENCY	RELATIVE CUMULATIVE FREQUENCY	%OF TOTAL AT I
7	1	1	0.016	0.02
8	17	18	0.281	0.27
9	89	107	1.672	1.39
10	175	282	4.406	2.73
11	194	476	7.437	3.03
12	187	663	10.359	2.92
13	223	886	13.844	3.48
14	260	1146	17.906	4.06
15	288	1434	22.406	4.50
16	345	1779	27.797	5.39
17	391	2170	33.906	6.11
18	435	2605	40.703	6.80
19	534	3139	49.047	8.34
20	585	3724	58.187	9.14
21	482	4206	65.719	7.53
22	399	4605	71.953	6.23
23	286	4891	76.422	4.47
24	270	5161	80.641	4.22
25	222	5383	84.109	3.47
26	220	5603	87.547	3.44
27	204	5807	90.734	3.19
28	119	5926	92.594	1.86
29	98	6024	94.125	1.53
30	88	6112	95.500	1.38
31	64	6176	96.500	1.00
32	52	6228	97.312	0.81
33	36	6264	97.875	0.56
34	18	6282	98.156	0.28
35	22	6304	98.500	0.34
36	20	6324	98.812	0.31
37	14	6338	99.031	0.22
38	11	6349	99.203	0.17
39	9	6358	99.344	0.14
40	6	6364	99.437	0.09
41	9	6373	99.578	0.14
42	5	6378	99.656	0.08
43	4	6382	99.719	0.06
44	3	6385	99.766	0.05
45	5	6390	99.844	0.08
46	1	6391	99.859	0.02
47	1	6392	99.875	0.02
48	1	6393	99.891	0.02
49	0	6393	99.891	0.0
50	4	6397	99.953	0.06
51	1	6398	99.969	0.02
52	0	6398	99.969	0.0
53	0	6398	99.969	0.0
54	1	6399	99.984	0.02
55	1	6400	100.000	0.02

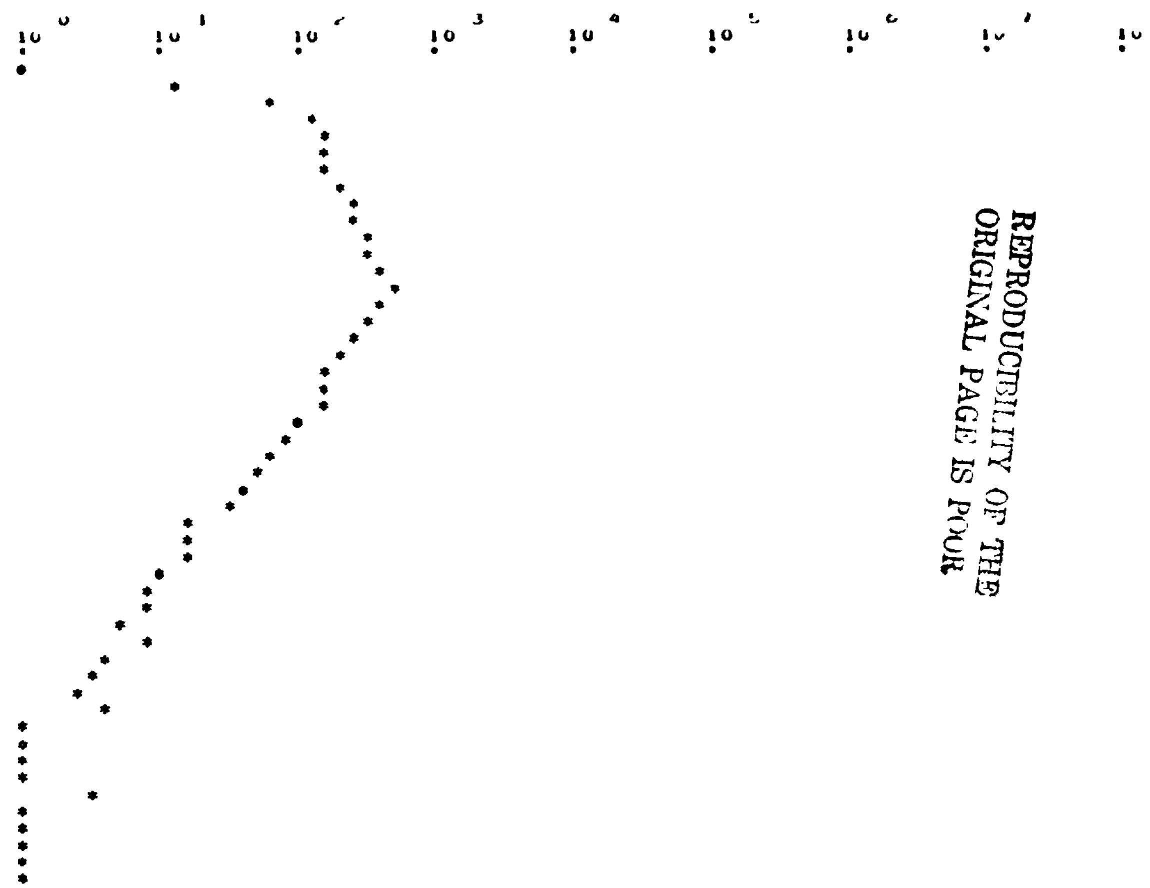

ALL LEADING AND TRAILING VALUES OF I WITH N(I)= 0 ARE OMITTED FROM THE GRAPH

MEAN= 19.90593   RMS= 20.76935   STANDARD DEVIATION= 5.92620

RADIOMETRIC CONSTANTS TO GIVE MEAN = 140.0; STANDARD DEVIATION = 21.0000
GAIN= 3.54358
BIAS= 69.46167

Figure 4-11(B) Scene E-1080-15192, Doubly Resampled Image, Histogram of Medium Frequency Region

SCENE 1080 LCC(UTM) LOW FREQ 00250010 LINE= 2125 SAMPLE= 2625 LENGTH IN LINES= 50 WIDTH IN SAMPLES= 1.0

I= VALUE	N(I)= NUMBER PTS AT I	ABSOLUTE CUMULATIVE FREQUENCY	RELATIVE CUMULATIVE FREQUENCY	XCF TOTAL AT I
6	25	25	0.391	0.39
7	241	266	4.156	3.77
8	2034	2300	35.938	31.78
9	3019	5319	83.109	47.17
10	1016	6335	98.984	15.88
11	59	6394	99.906	0.92
12	6	6400	100.000	0.09

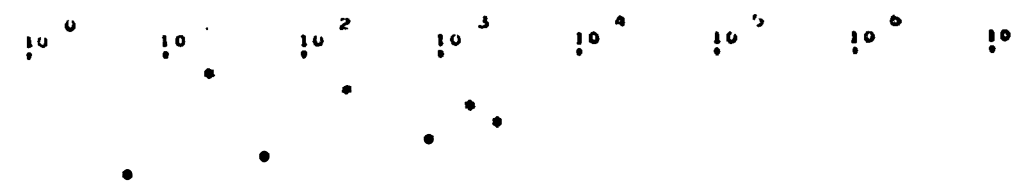

ALL LEADING AND TRAILING VALUES OF I WITH N(I)= 0 ARE OMITTED FROM THE GRAPH

MEAN= 8.77516 RMS= 8.81252 STANDARD DEVIATION= 0.81061

RADIOMETRIC CONSTANTS TO GIVE MEAN = 140.0; STANDARD DEVIATION = 21.0000
GAIN= 25.90640
BIAS= -87.33272

Figure 4-11(C) Scene E-1080-15192, Doubly Resampled Image, Histogram of Low Frequency Region

Figure 4-12 Hand County, Band 5, Singly Resampled Image

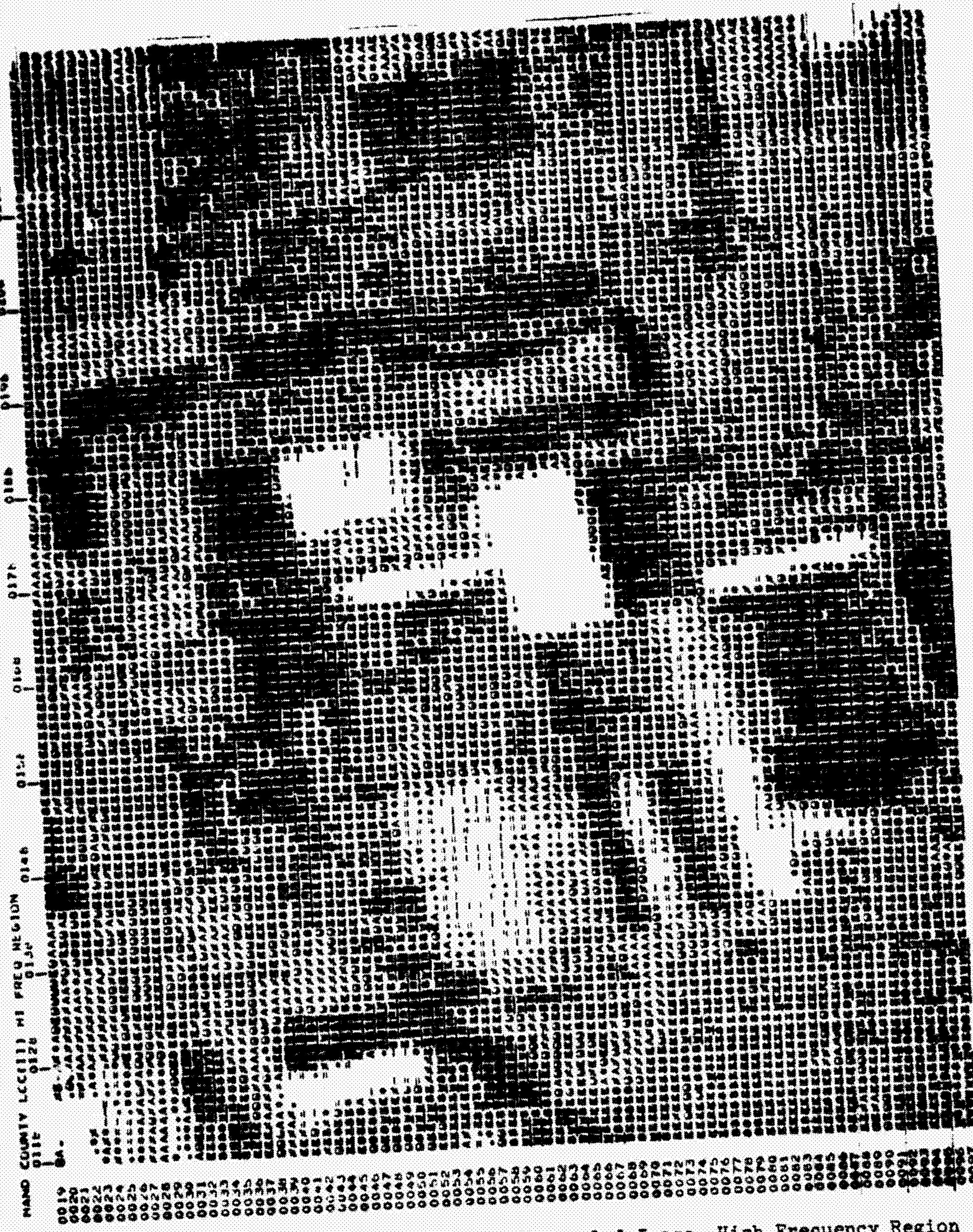

Figure 4-13(A) Hand County, Band 4, Singly Resampled Image, High Frequency Region

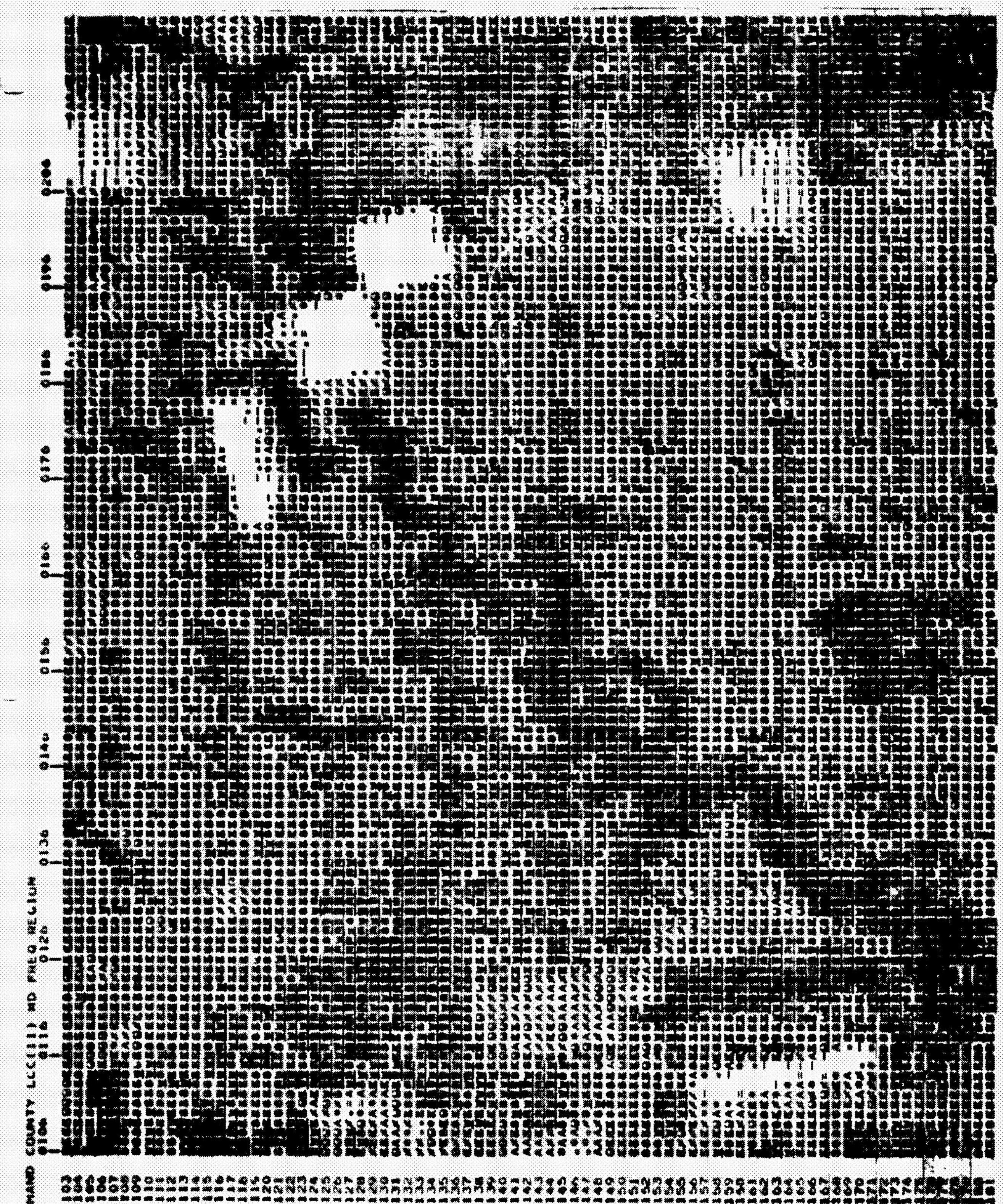

'igure 4-13(B) Hand County, Band 4, Singly Resampled Image, Medium Frequency Region

Figure 4-13(C) Hand County, Band 4, Singly Resampled Image, Low Frequency Region

Figure 4-13(D) Hand County, Band 5, Singly Resampled Image, High Frequency Region

'gure 4-13(E) Hand County, Band 5, Singly Resampled Image, Medium Frequency Region

Figure 4-13(F) Hand County, Band 5, Singly Resampled Image, Low Frequency Region

Figure 4-13(G) **Hand County, Band 6, Singly Resampled Image, High Frequency Region**

'igure 4-13(H) Hand County, Band 6, Singly Resampled Image, Medium Frequency Region

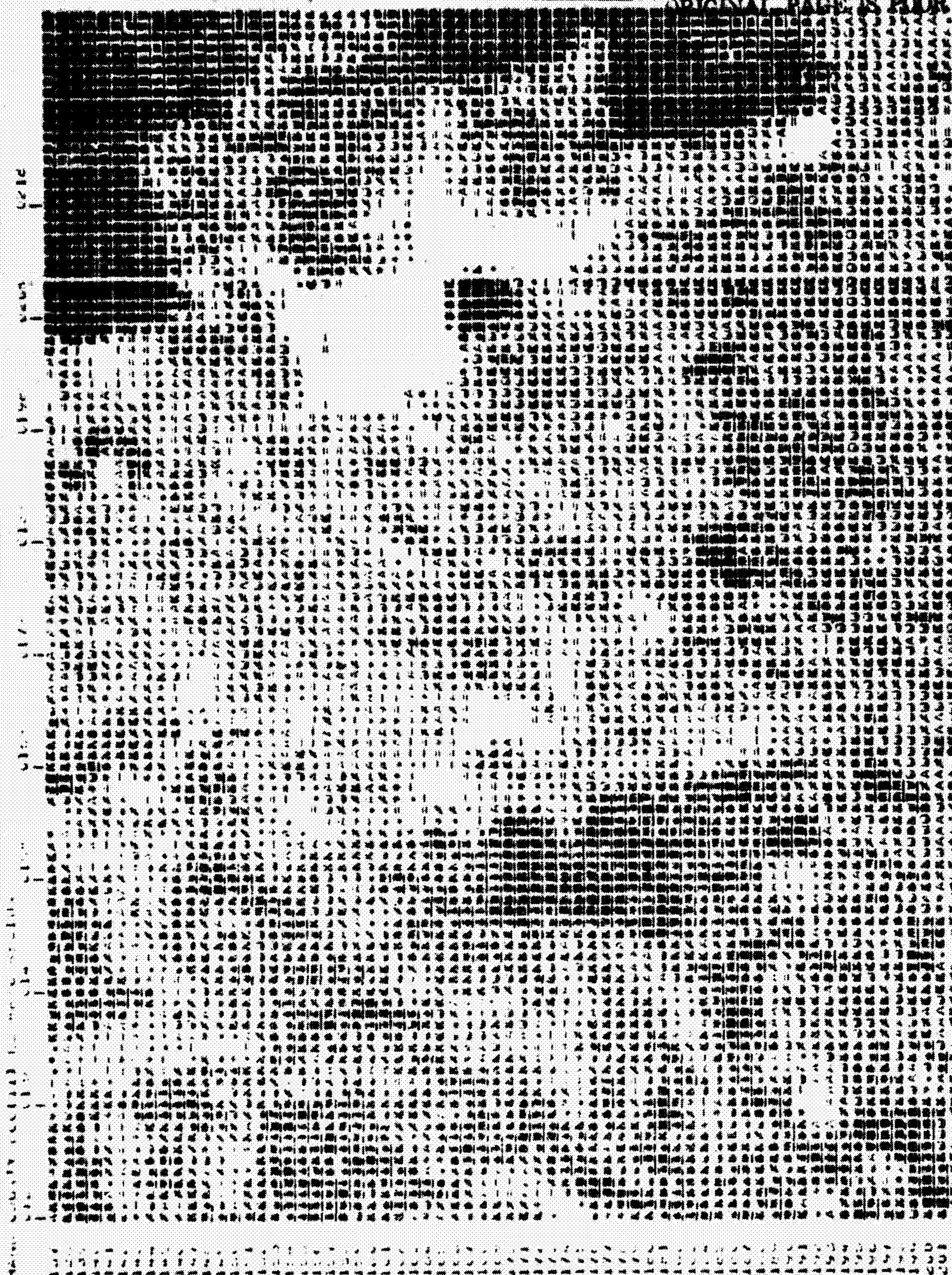

Figure 4-13(I) Hand County, Band 6, Singly Resampled Image, Low Frequency Region

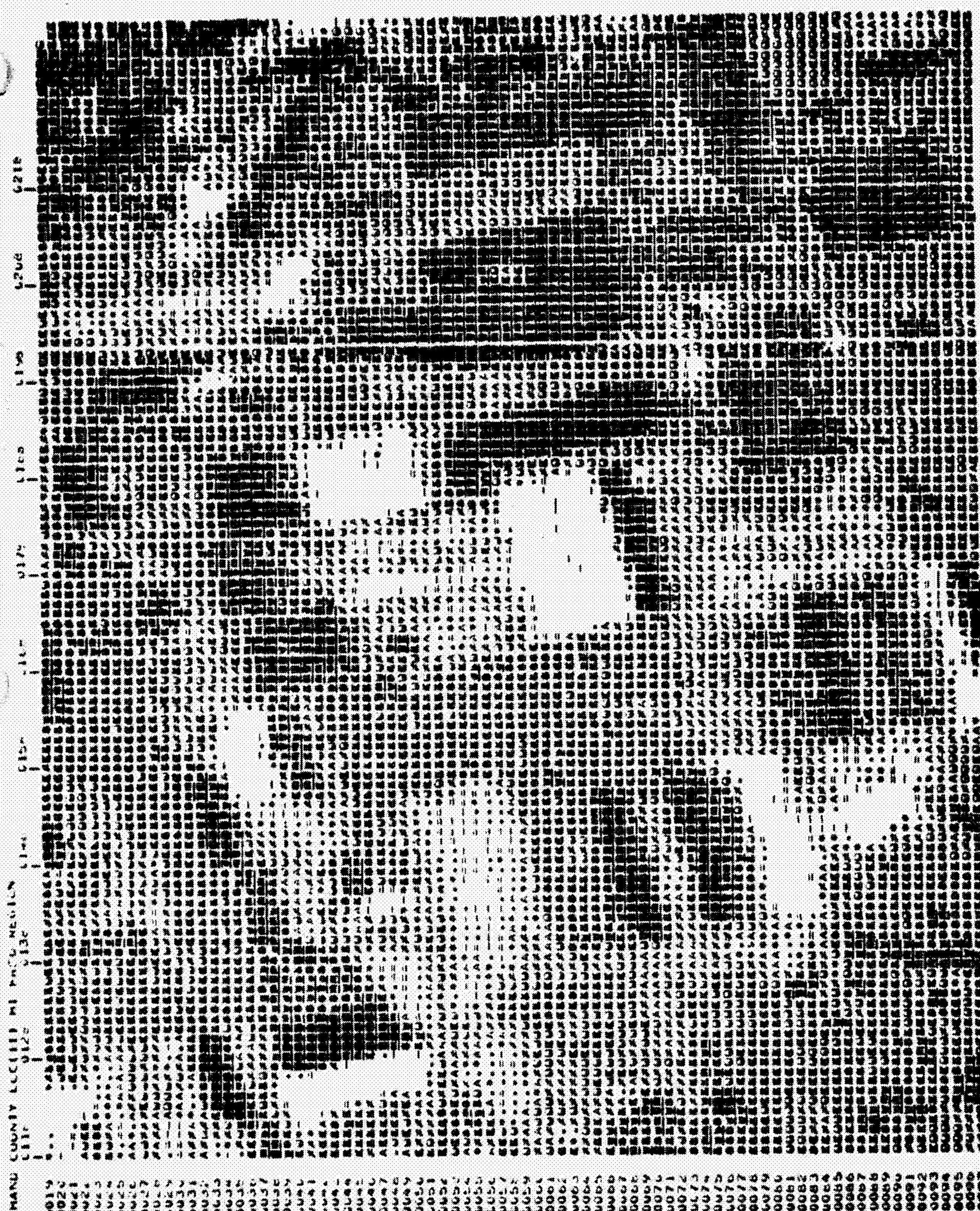

Figure 4-13(J) Hand County, Band 7, Singly Resampled Image, High Frequency Region

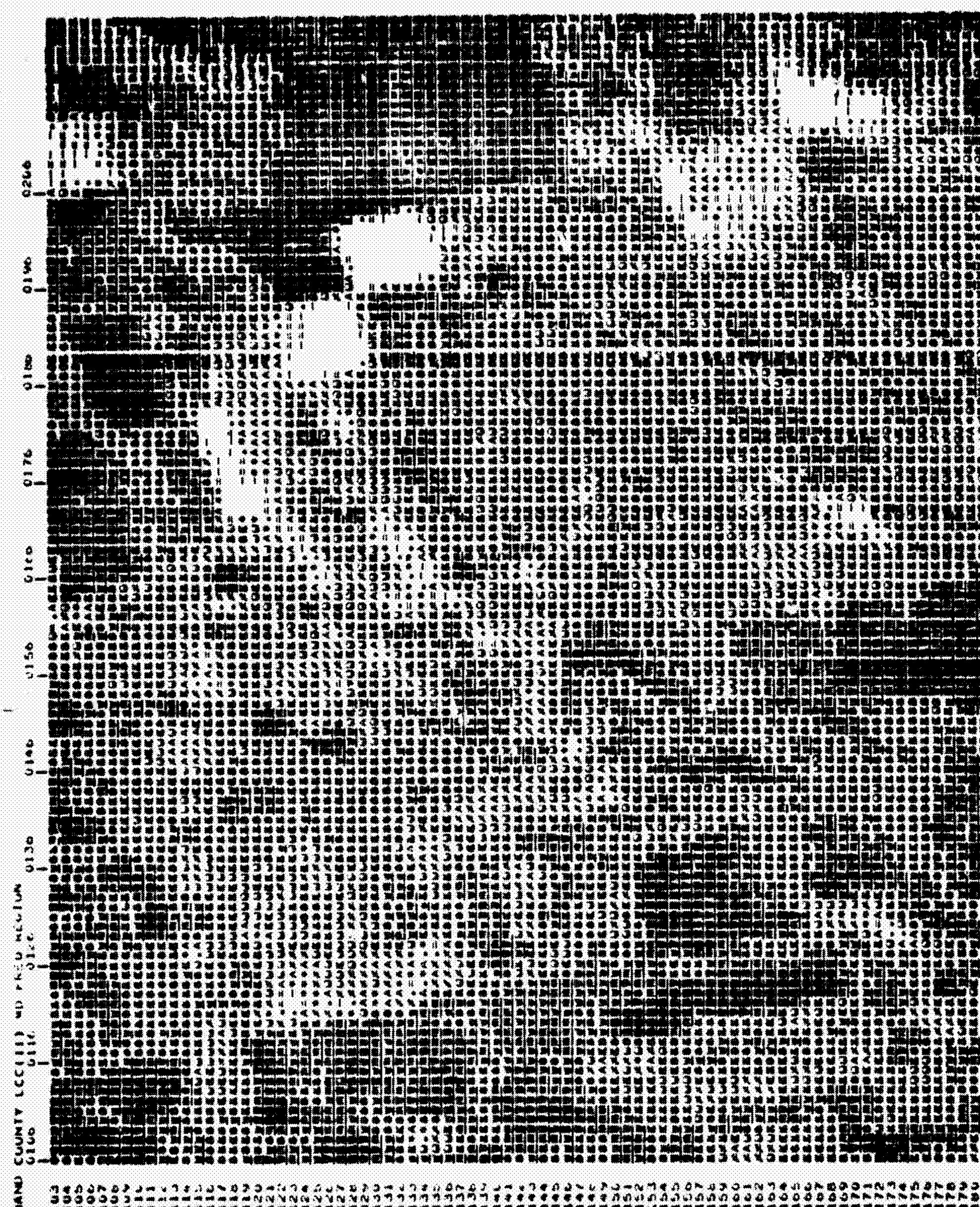

Figure 4-13(K) Hand County, Band 7, Singly Resampled Image, Medium Frequency Region

Figure 4-13(L) Hand County, Band 7, Singly Resampled Image, Low Frequency Region

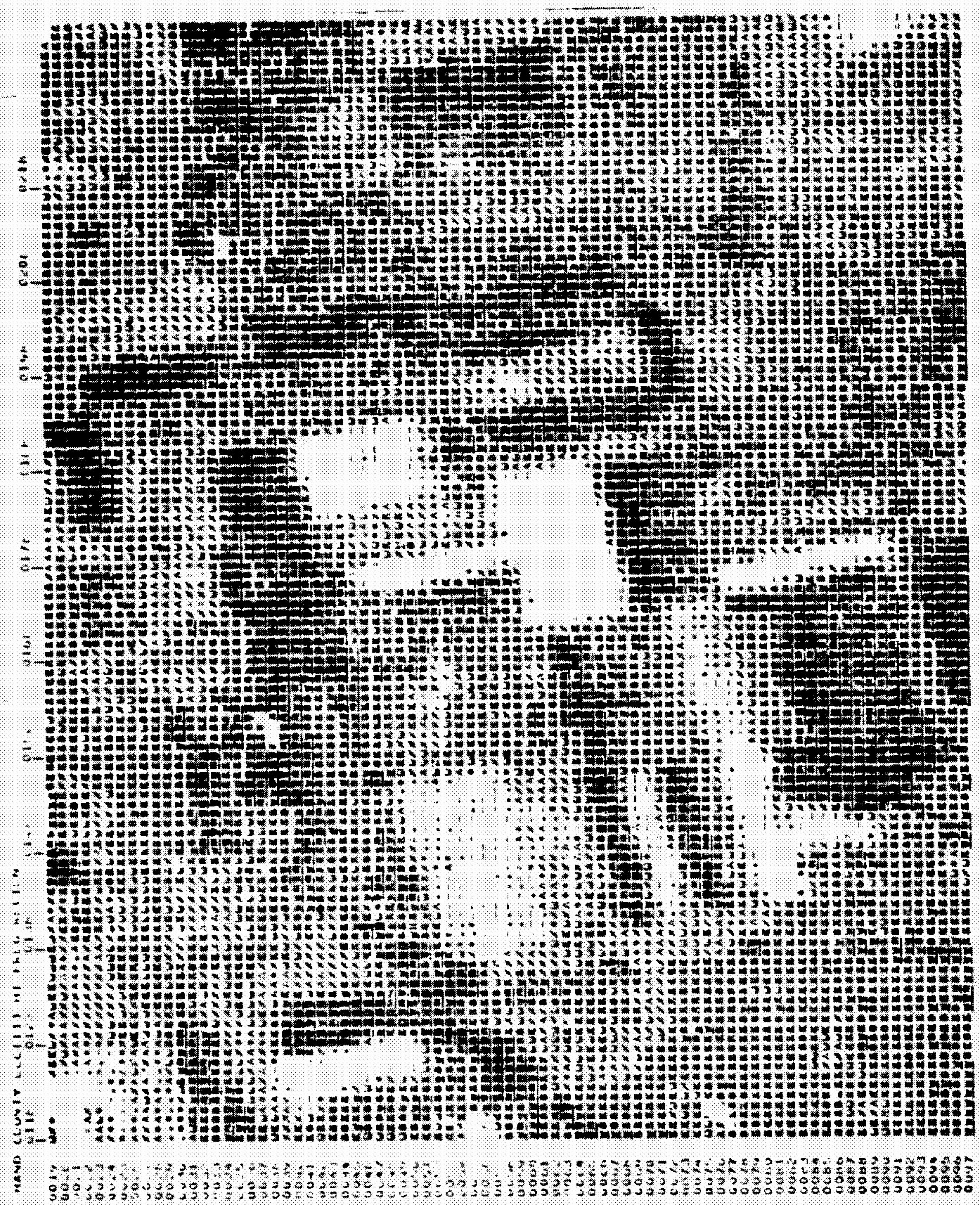

Figure 4-13(M) Hand County, Band 4, Doubly Resampled Image, High Frequency Region

igure 4-13(N) Hand County, Band 4, Doubly Resampled Image, Medium Frequency Region

Figure 4-13(0) Hand County, Band 4, Doubly Resampled Image, Low Frequency Region

Figure 4-13(P) Hand County, Band 5, Doubly Re-mpled Image, High Frequency Region

Figure 4-13(Q) Hand County, Band 5, Doubly Resampled Image, Medium Frequency Region

Figure 4-13(R) Hand County, Band 5, Doubly Resampled Image, Low Frequency Region

Figure 4-13(S) Hand County, Band 6, Doubly Resampled Image, High Frequency Region

Figure 4-13(T) Hand County, Band 6, Doubly Resampled Image, Medium Frequency Region

Figure 4-13(U) Hand County, Band 6, Doubly Resampled Image, Low Frequency Region

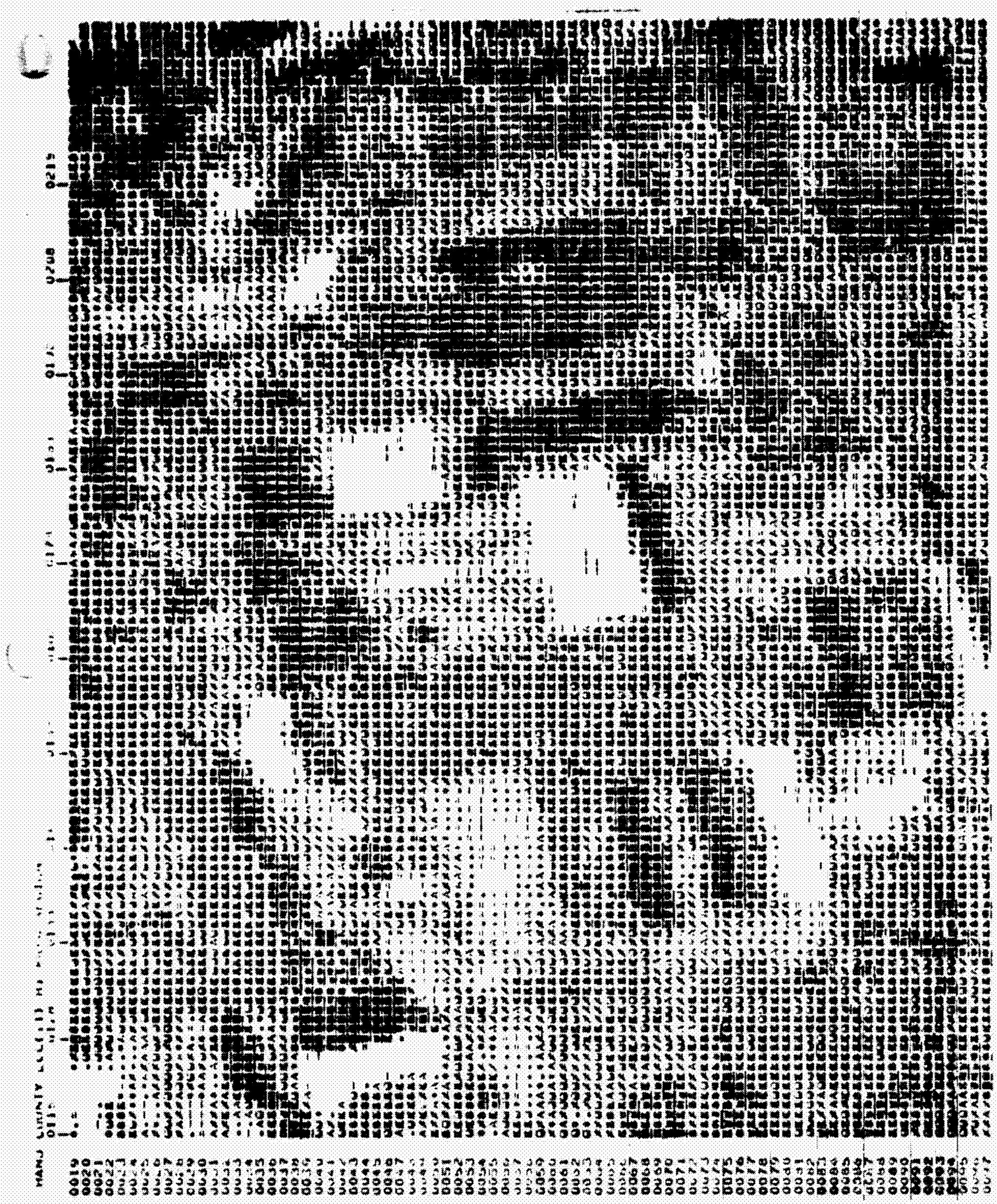

Figure 4-13(V) Hand County, Band 7, Doubly Resampled Image, High Frequency Region

Figure 4-13(W) Hand County, Band 7, Doubly Resampled Image, Medium Frequency Region

Figure 4-13(X) Hand County, Band 7, Doubly Resampled Image, Low Frequency Region

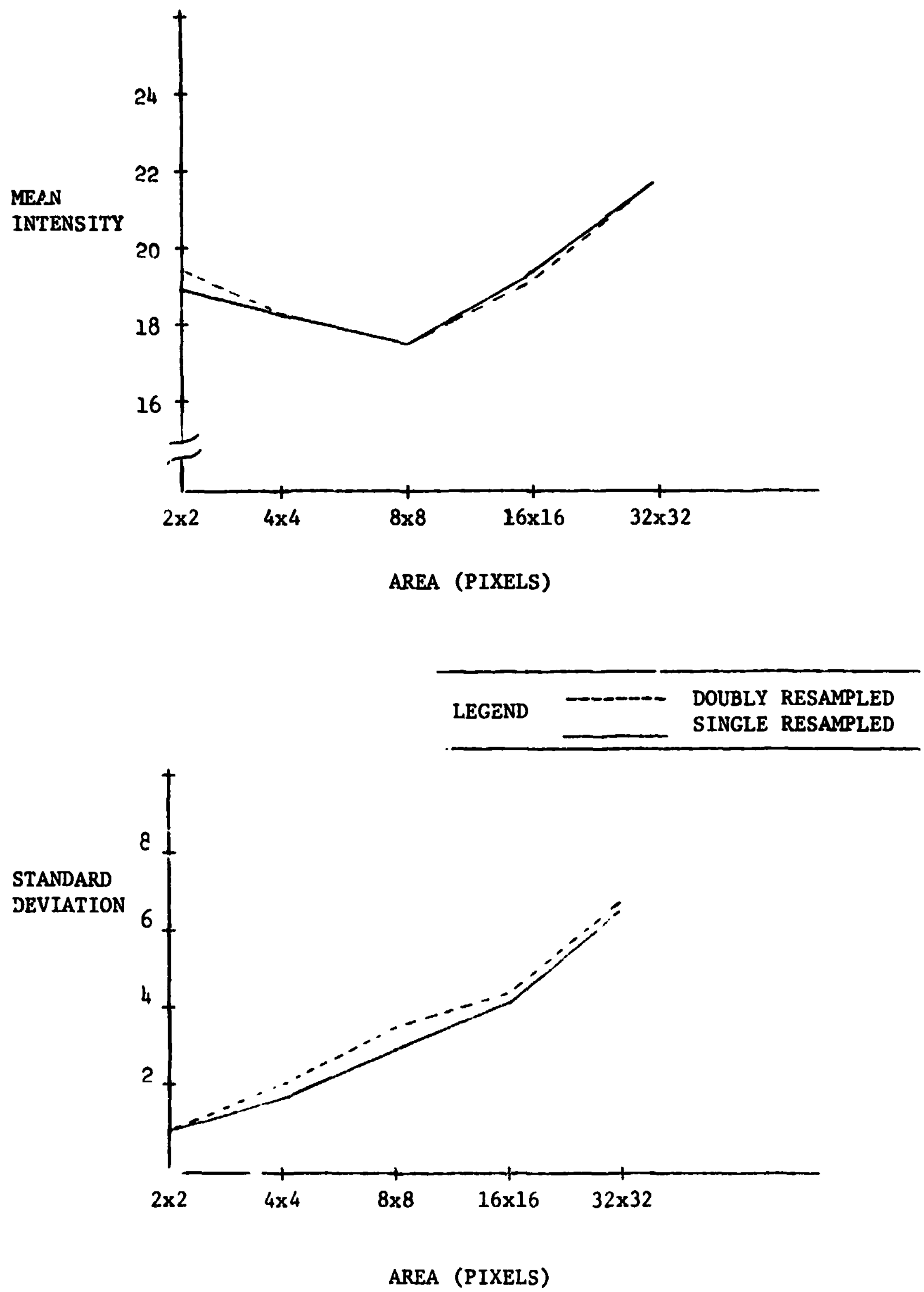

Figure 4-14(A). Scene E-1080-15192, High Frequency Region Radiometric Areal Statistics

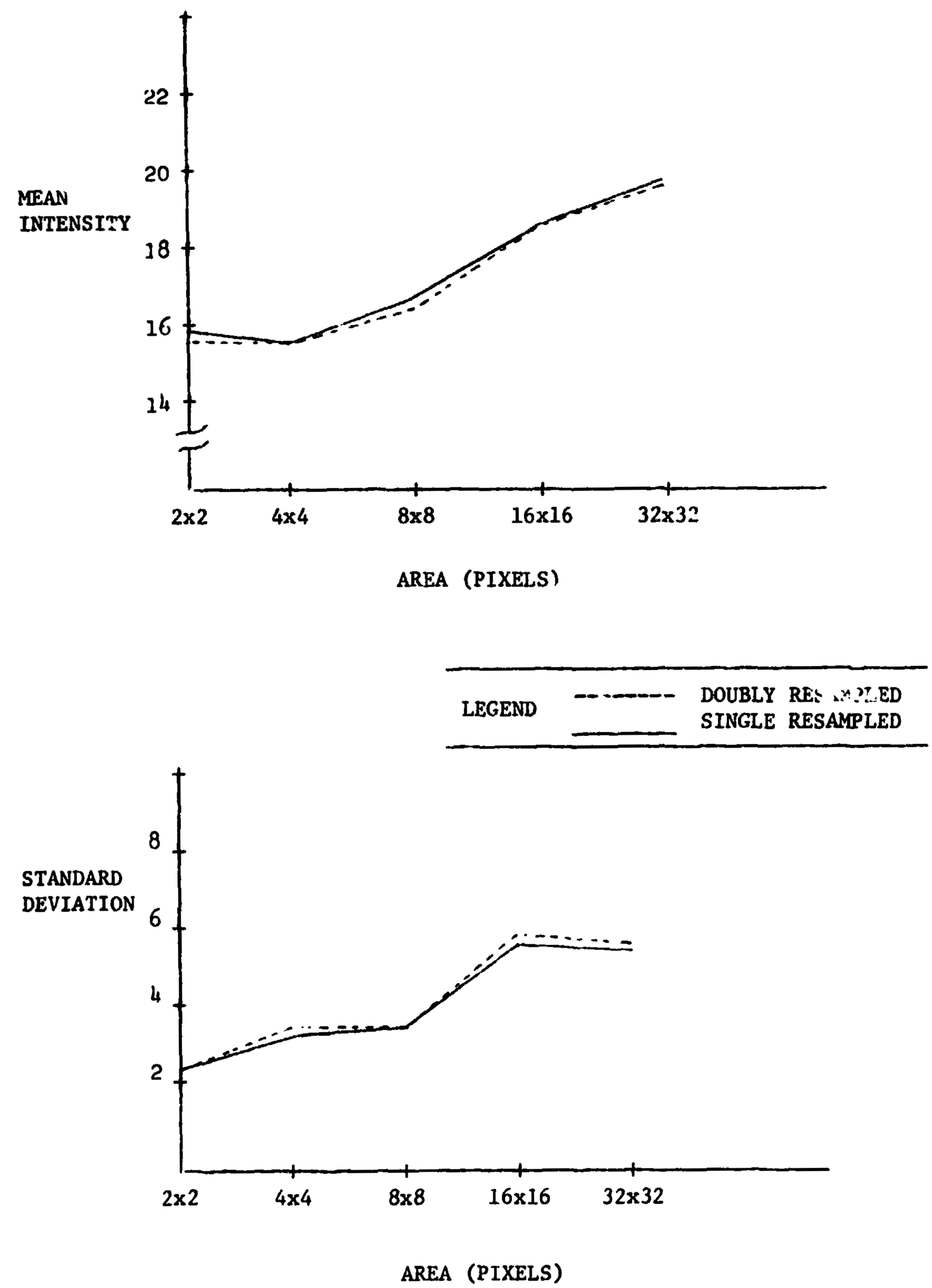

Figure 4-14(B). Scene E-1080-15192, Medium Frequency Region, Radiometric Areal Statistics

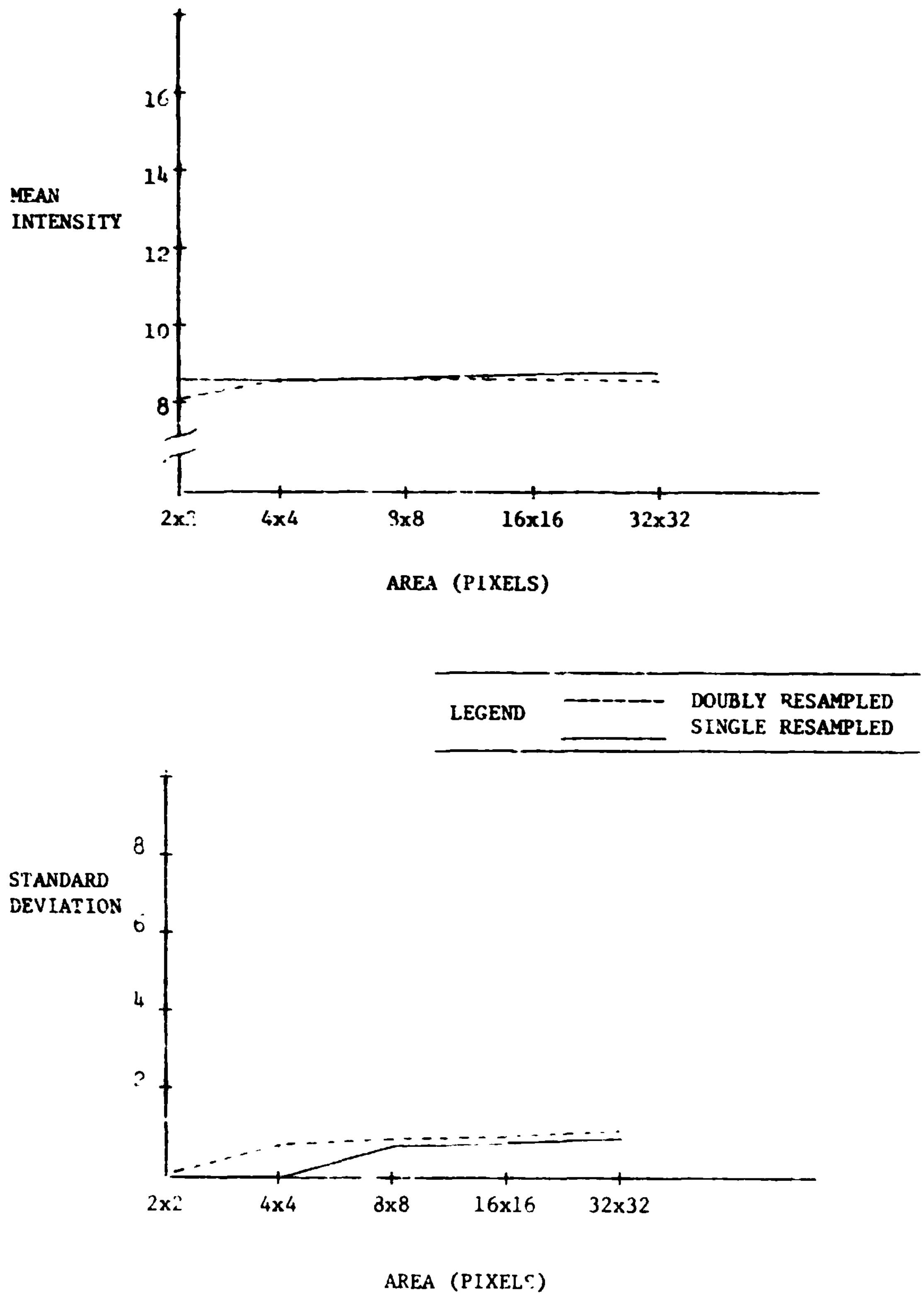

Figure 4-14(c). Scene F-1080-15192, Low Frequency Region, Radiometric Areal Statistics

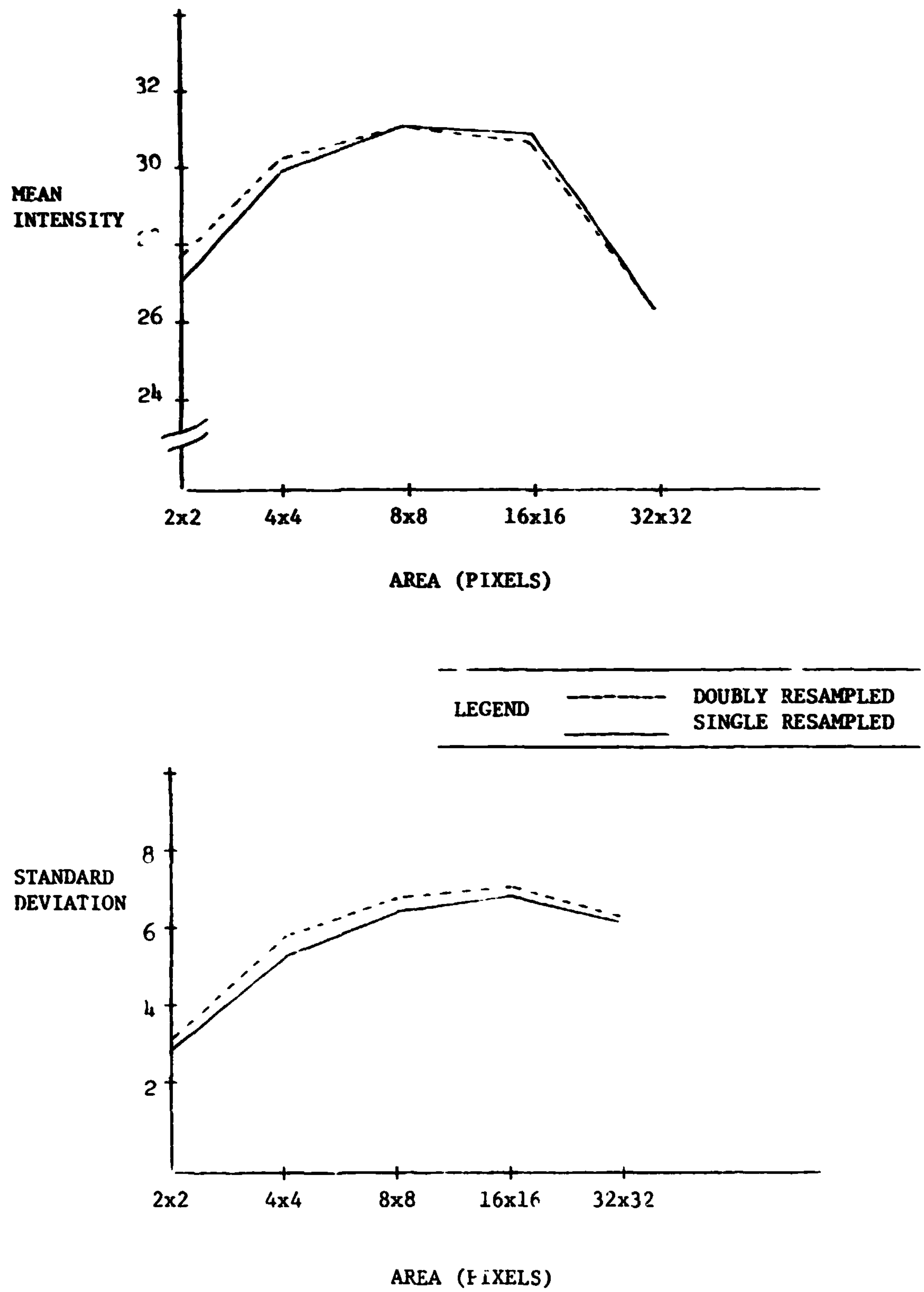

Figure 4-15([illegible]). Hani County, Band 4, High Frequency Region, Radiometric Areal Statistics

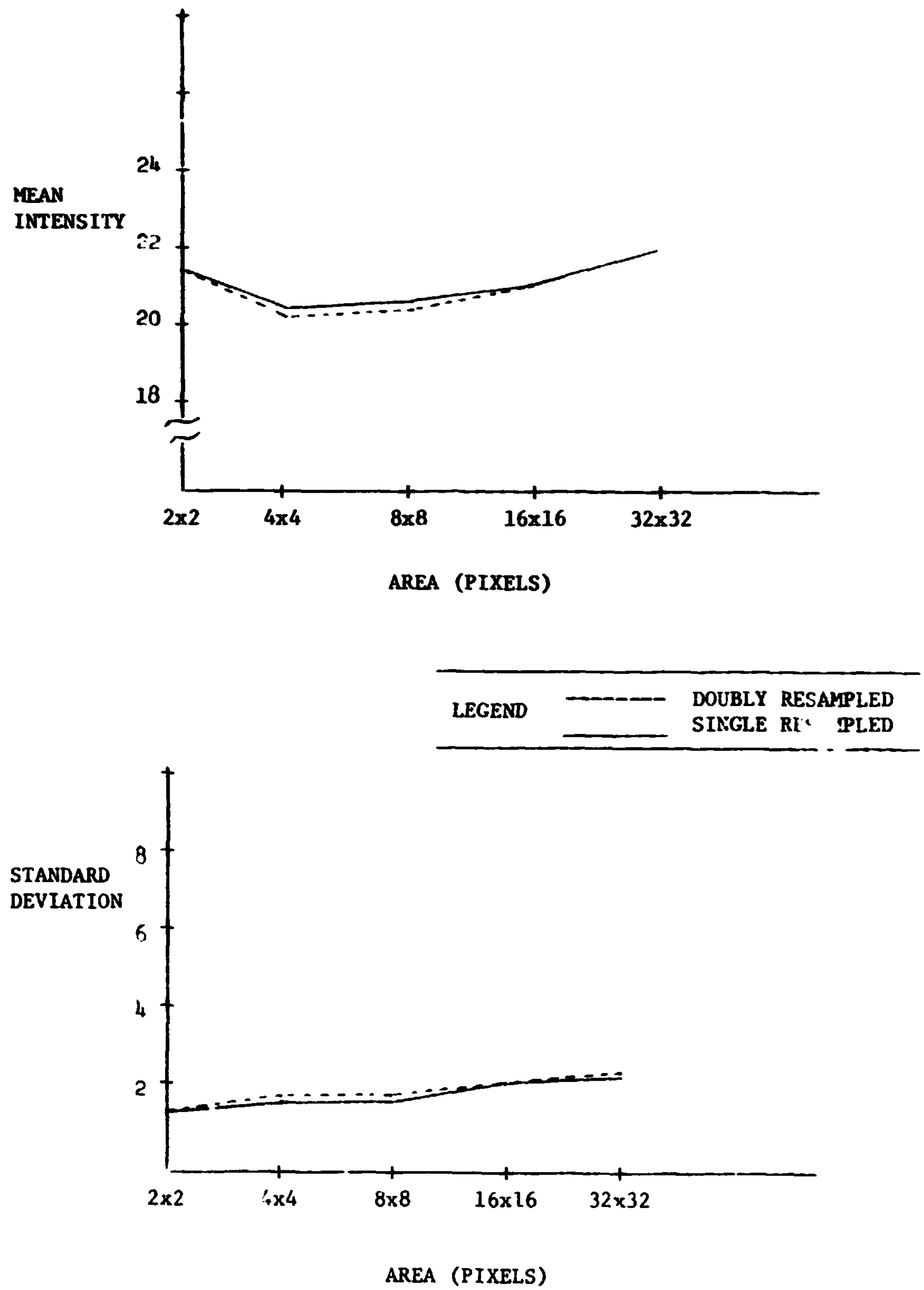

Figure 4-15(B). Hand County, Band 4, Medium Frequency Region, Radiometric Areal Statistics

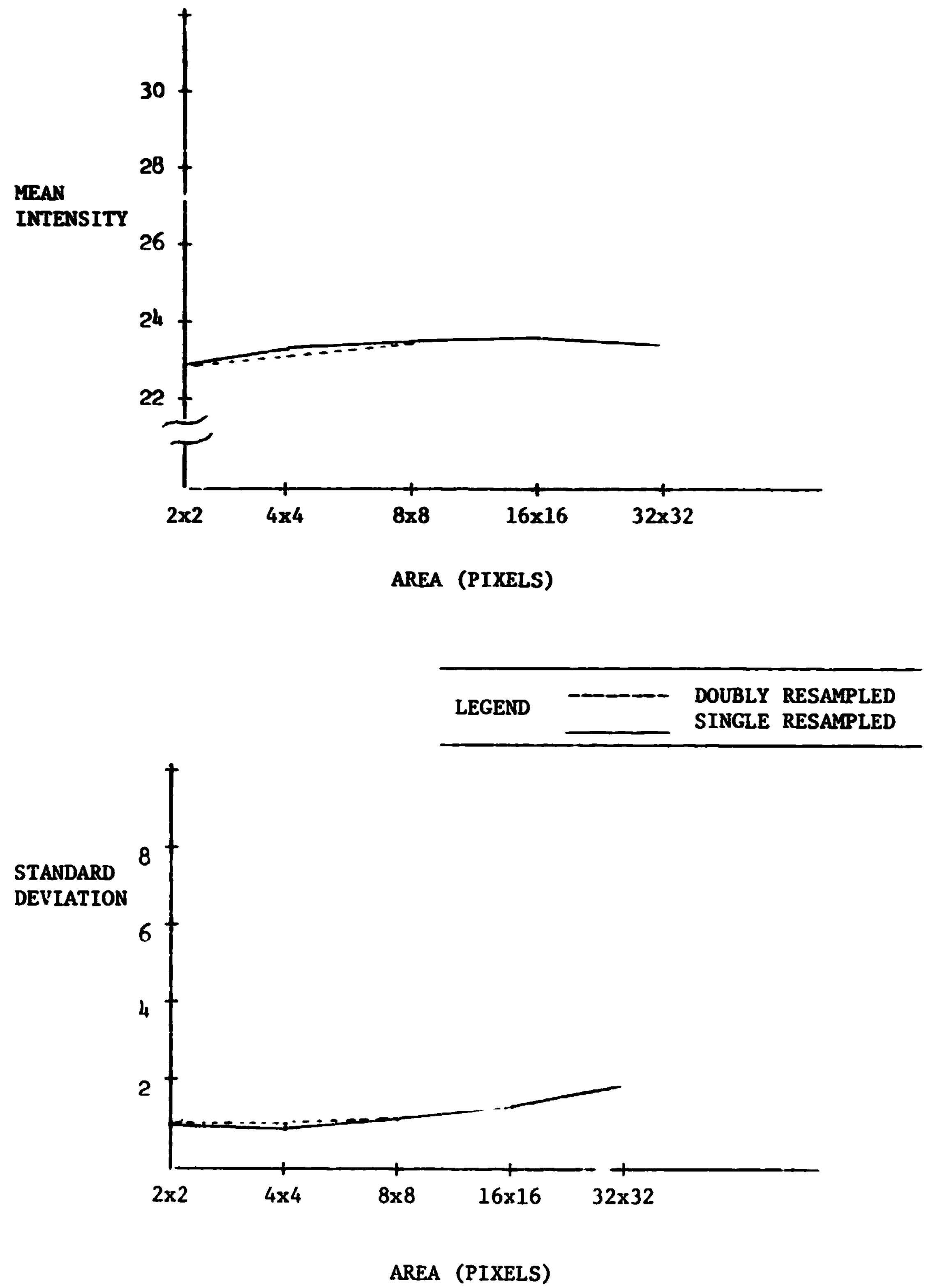

Figure 4-15(C). Hand County, Band 4, Low Frequency Region, Radiometric Areal Statistics

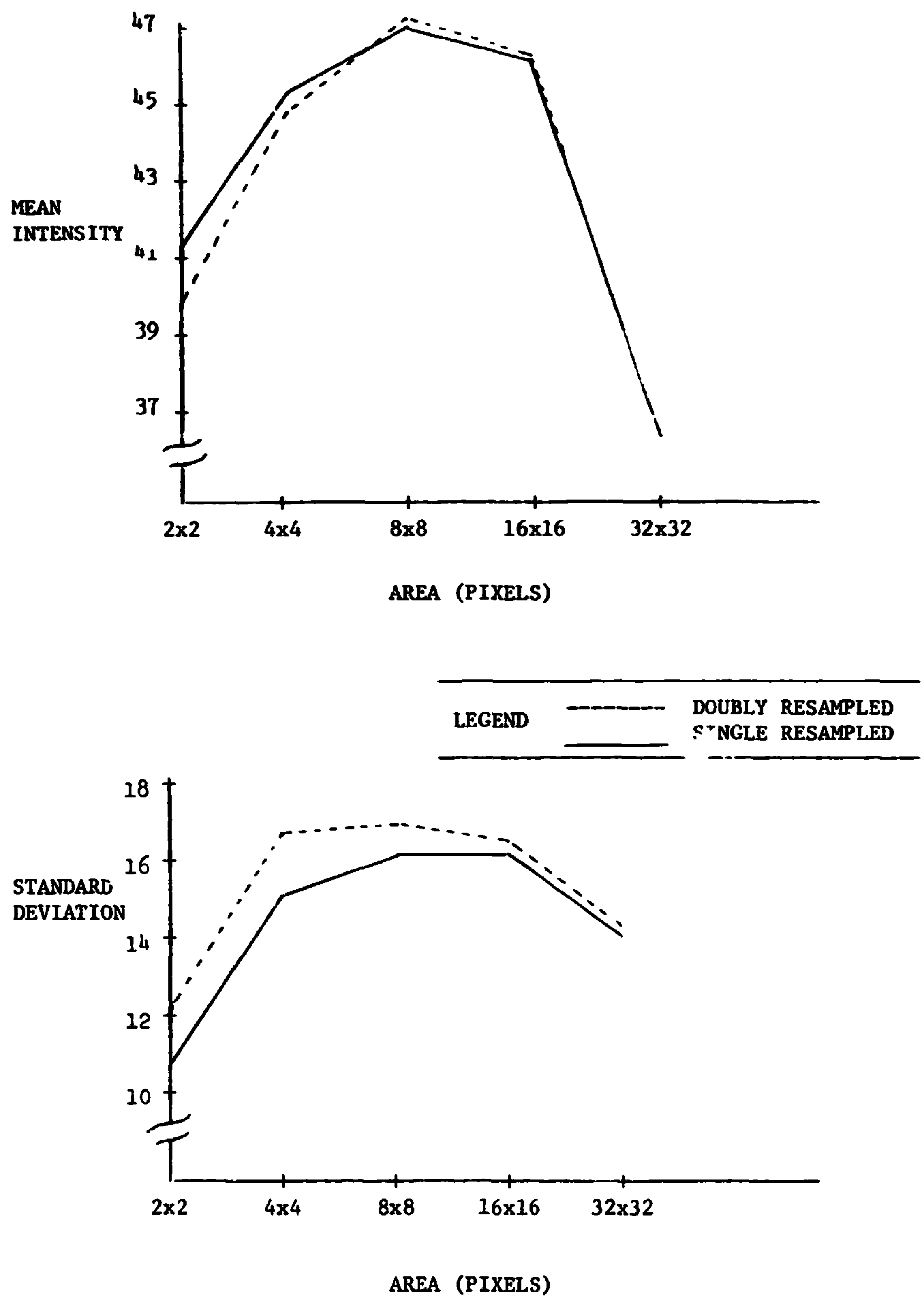

Figure 4-16(A). Hand County, Band 5, High Frequency Region, Radiometric Areal Statistics

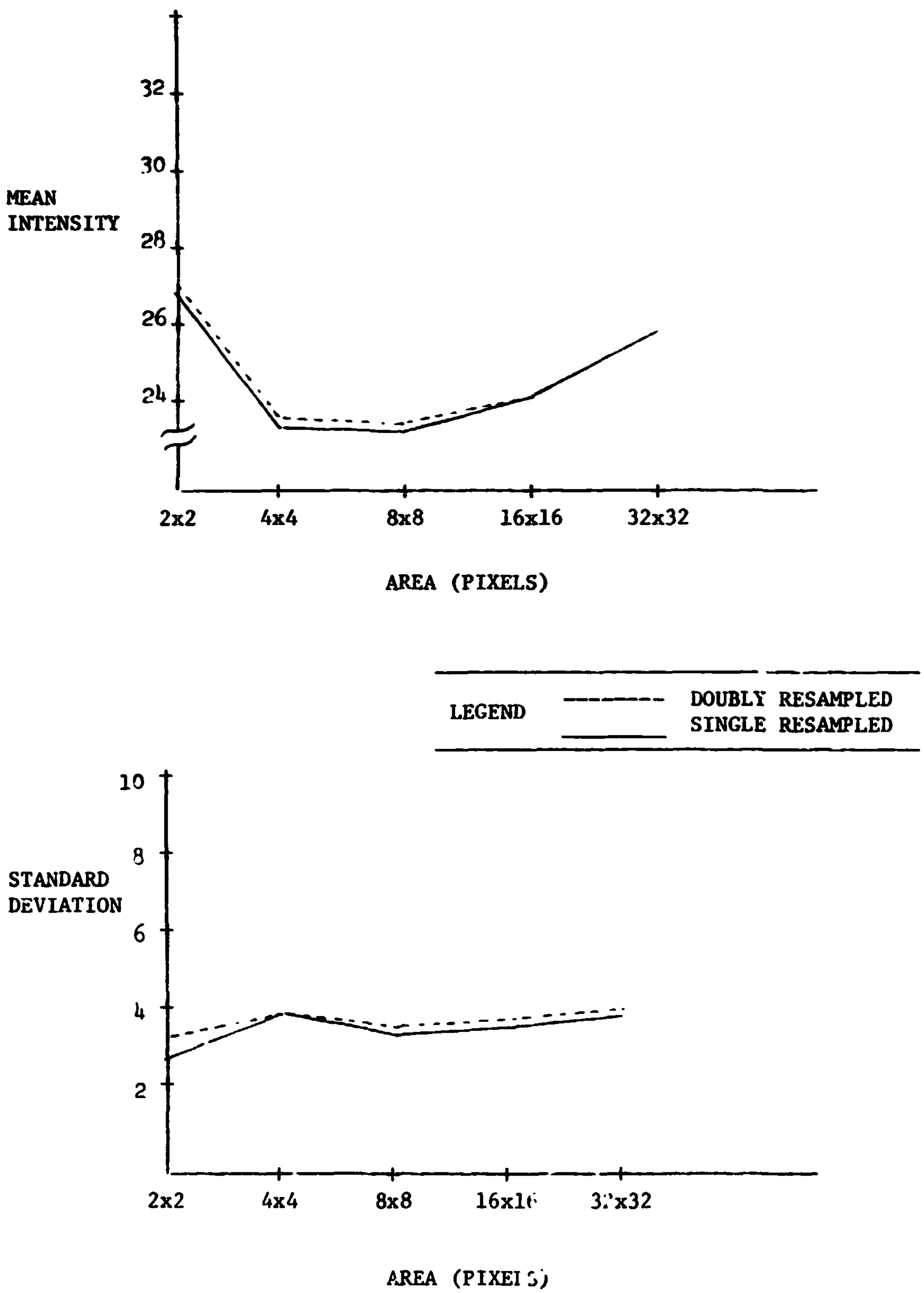

Figure 4-16(B). Hand County, Band 5, Medium Frequency Region, Radiometric Areal Statistics

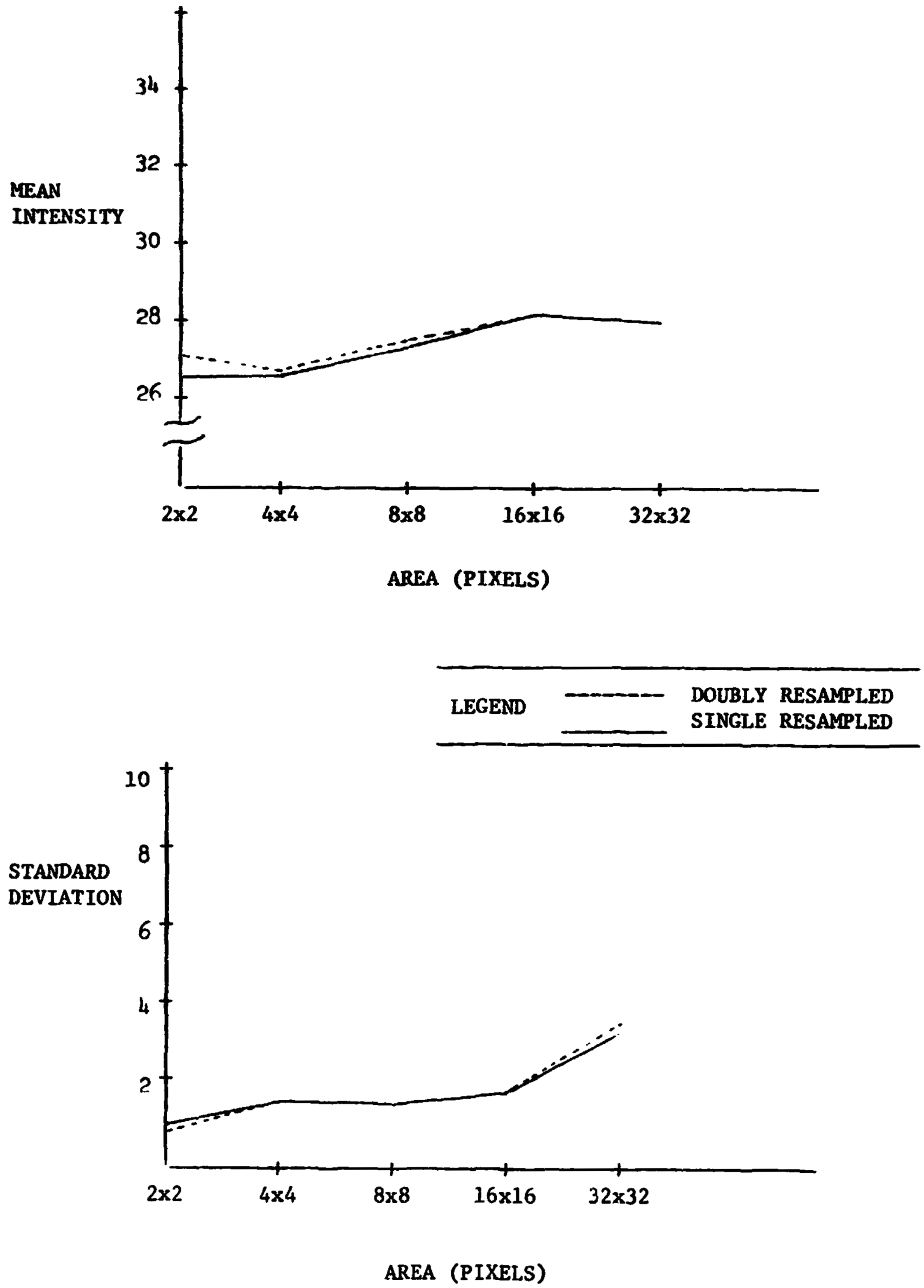

[illegible]. Land County, Band 5, Low Frequency Region, Radiometric Areal Statistics

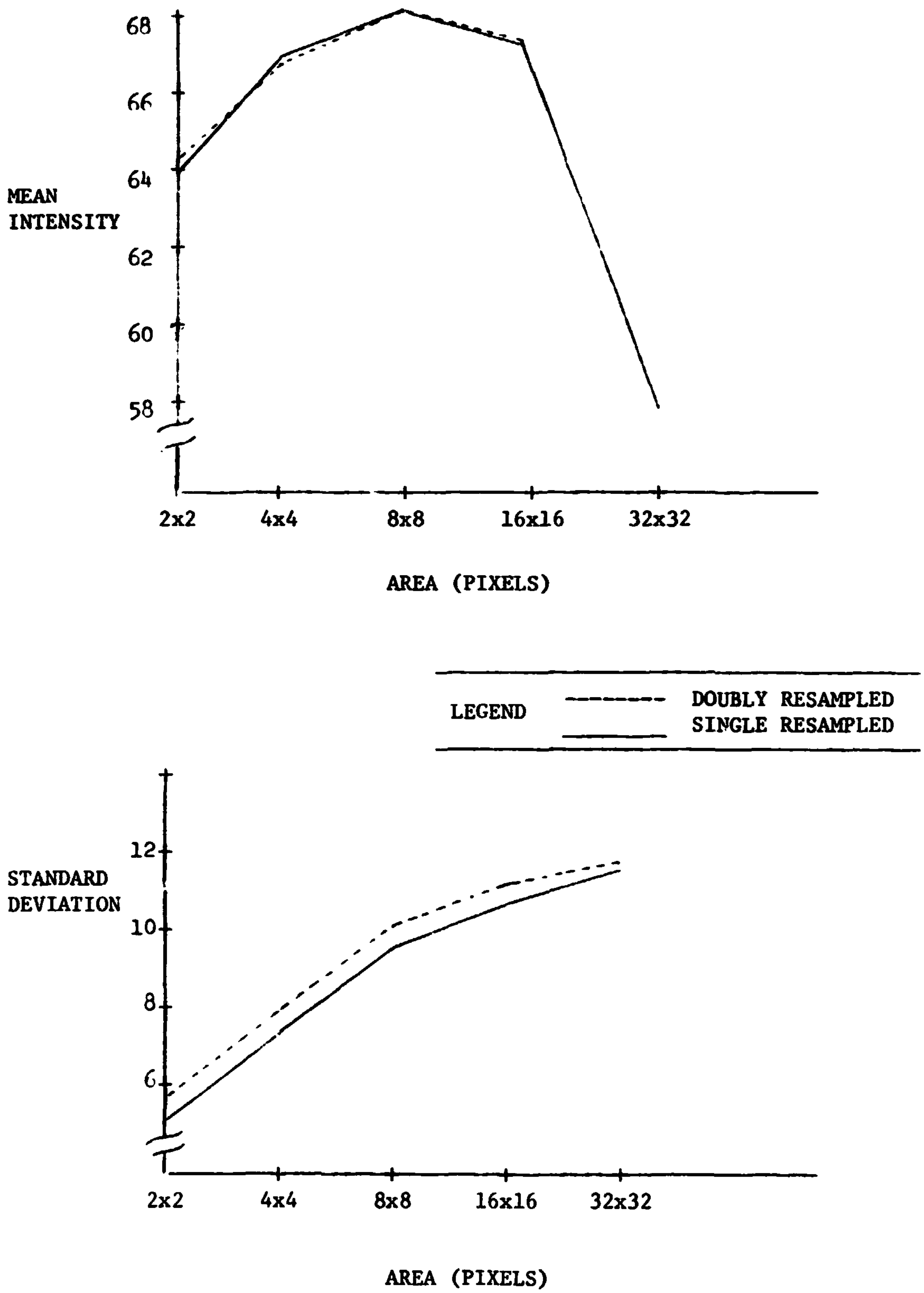

Figure 4-17(A). Hand County, Band 6, High Frequency Region, Radiometric Areal Statistics

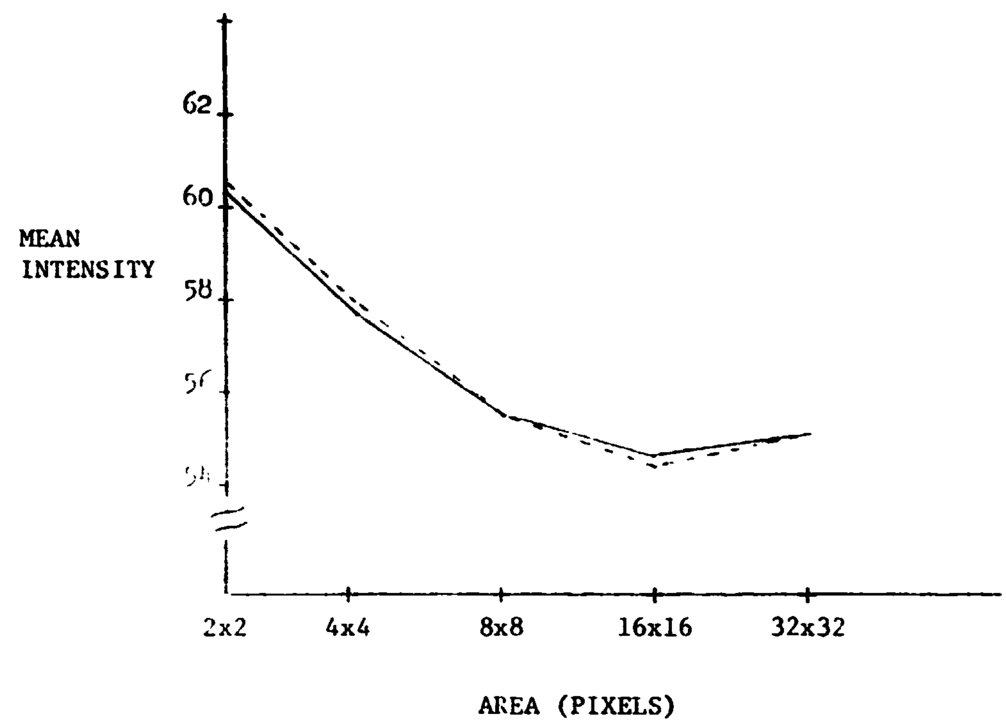

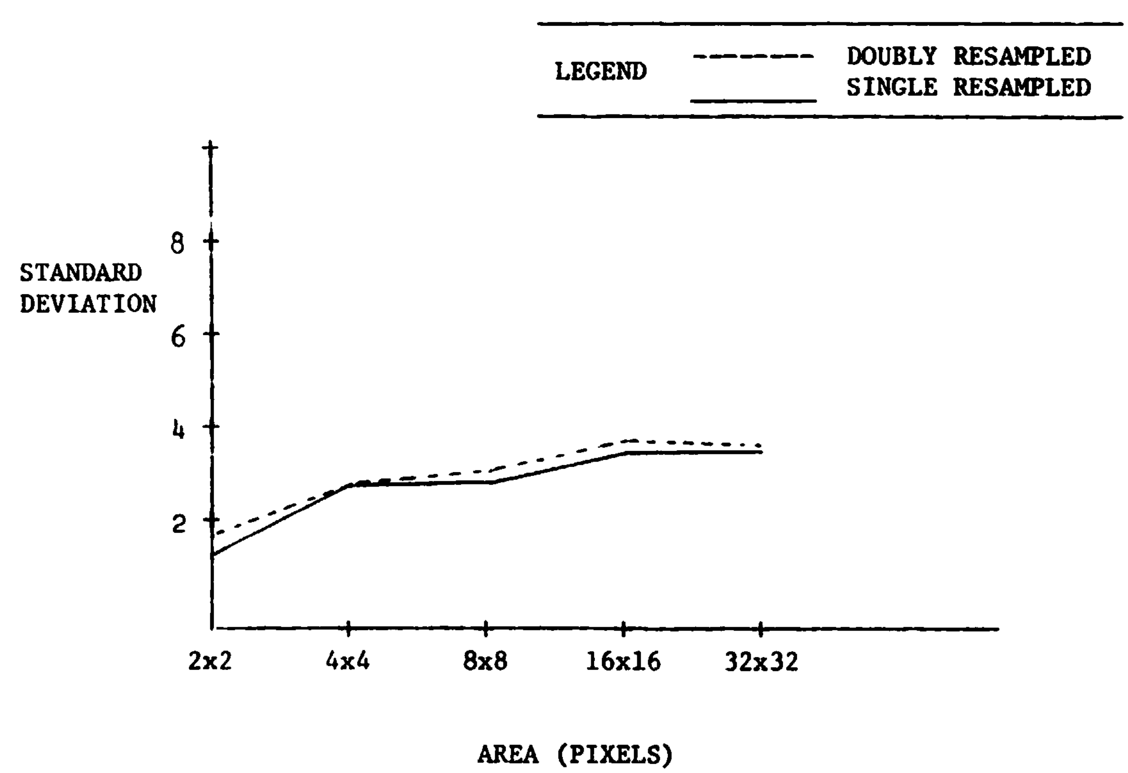

Figure 4-17(B). Hand County, Band 6, Medium Frequency Region, Radiometric Areal Statistics

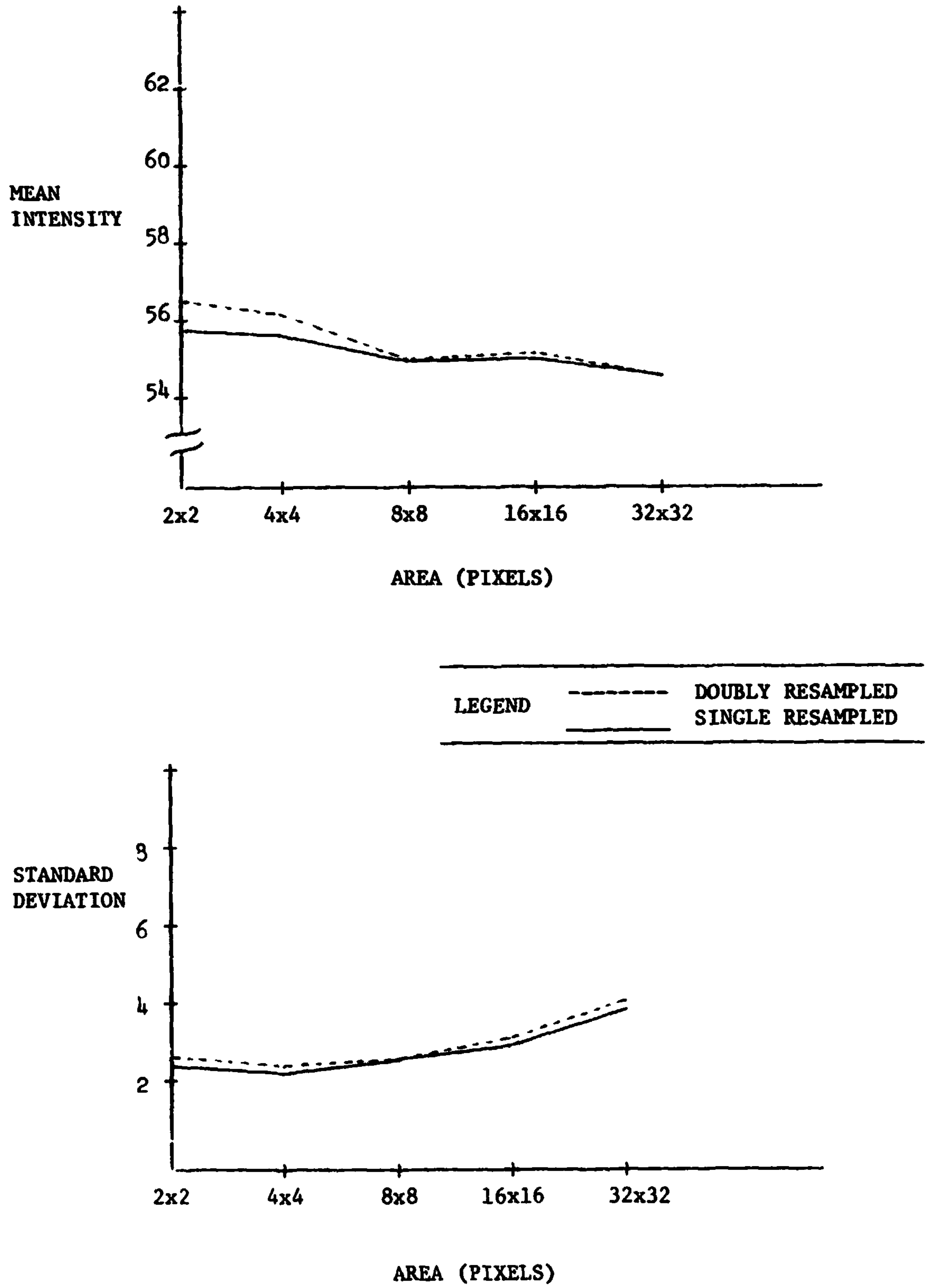

Figure 4-17(C). Hand County, Band 6, Low Frequency Region, Radiometric Areal Statistics

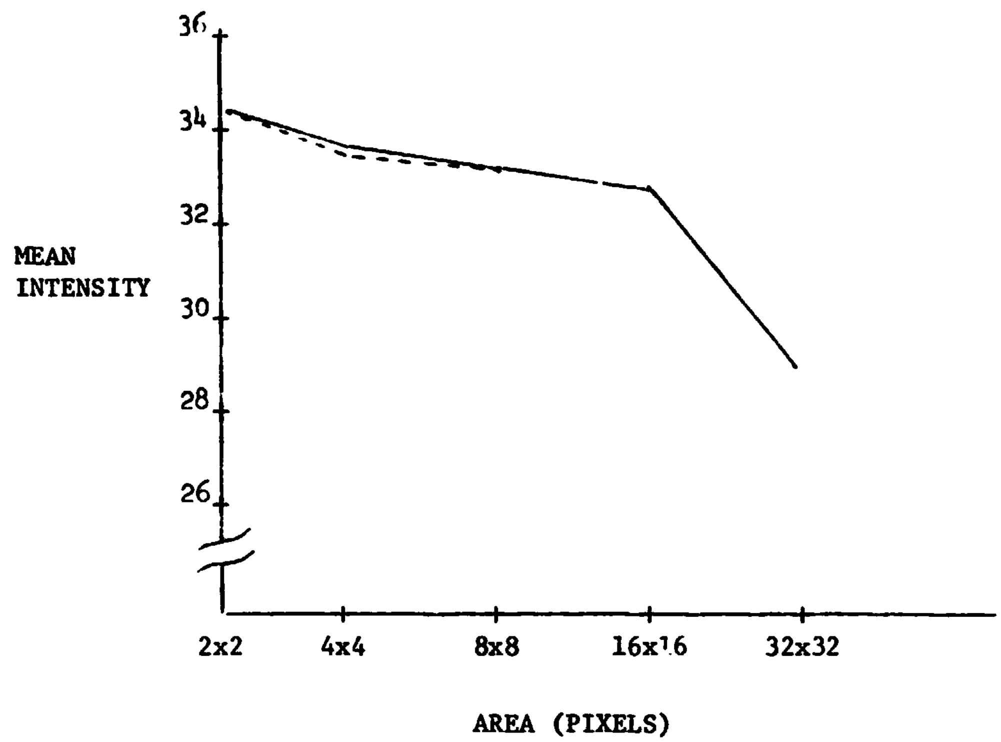

LEGEND -------- DOUBLY RESAMPLED
——— SINGLE RESAMPLED

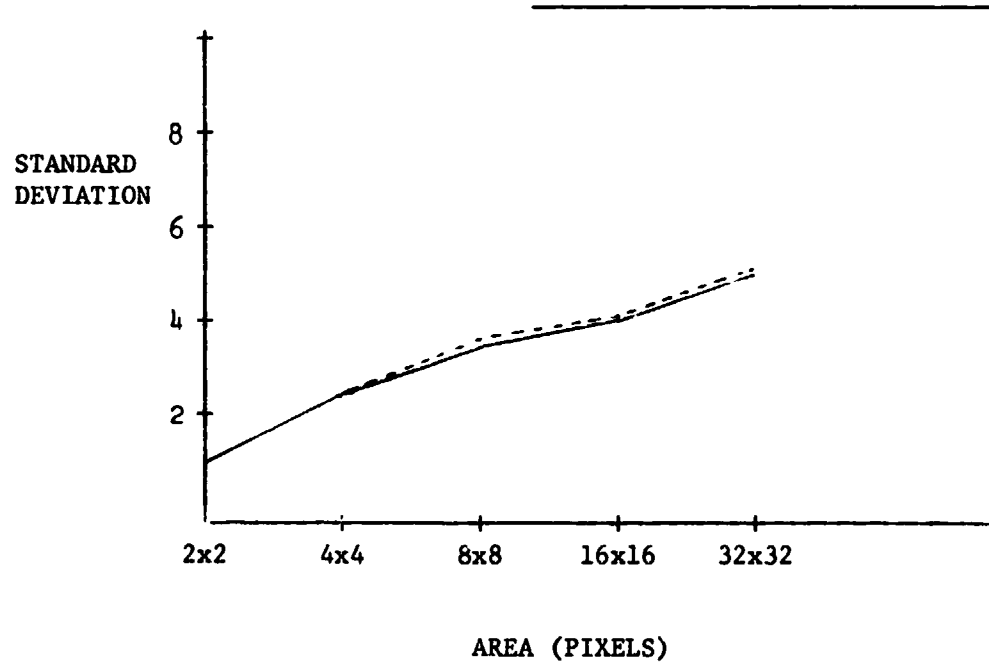

Figure 4-18(A). Hand County, Band 7. High Frequency Region, Radiometric Areal Statistics

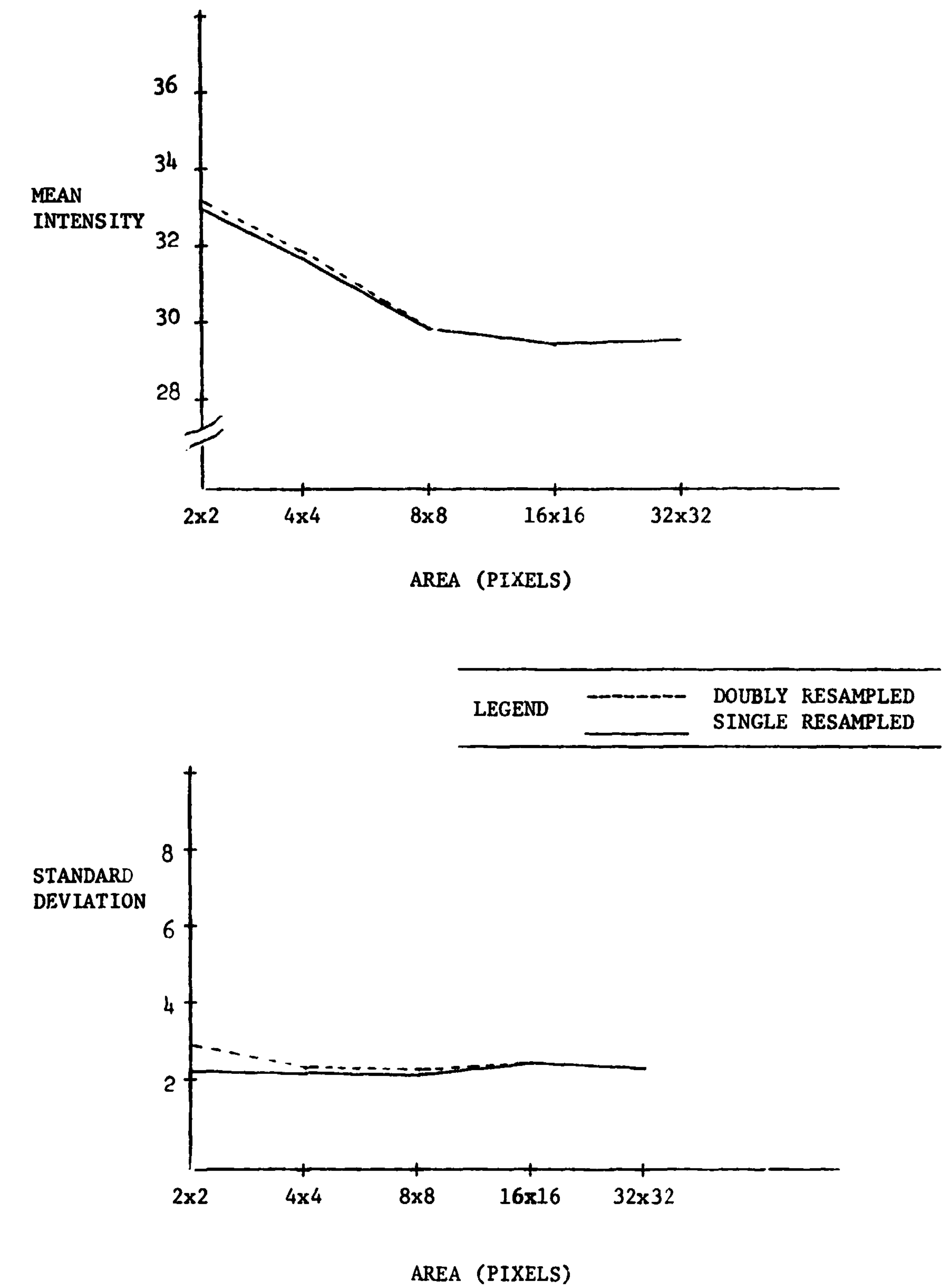

Figure 4-18(B). Hand County, Band 7, Medium Frequency Region, Radiometric Areal Statistics

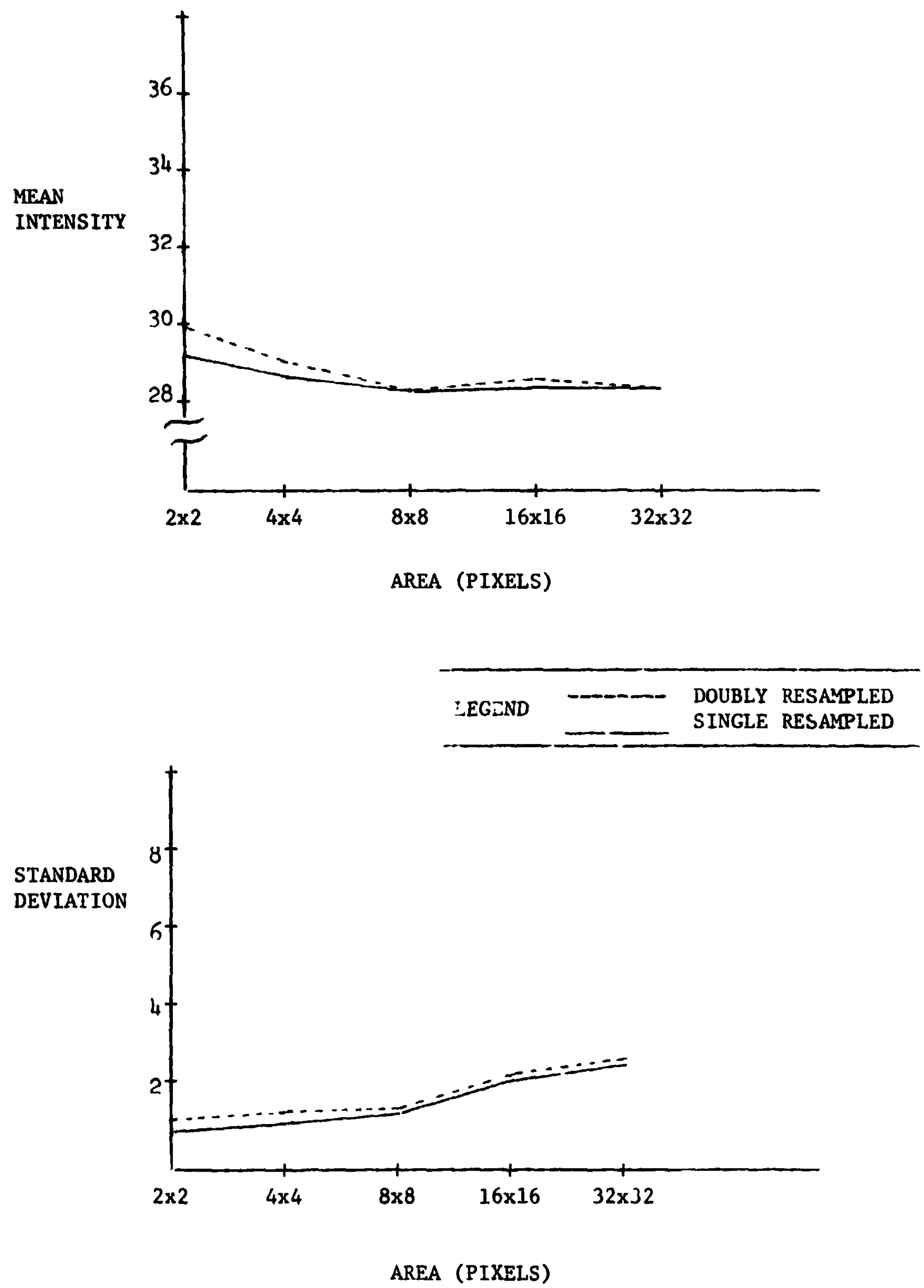

Figure 4-18(C). Hand County, Band 7, Low Frequency Region,
Radiometric Areal Statistics

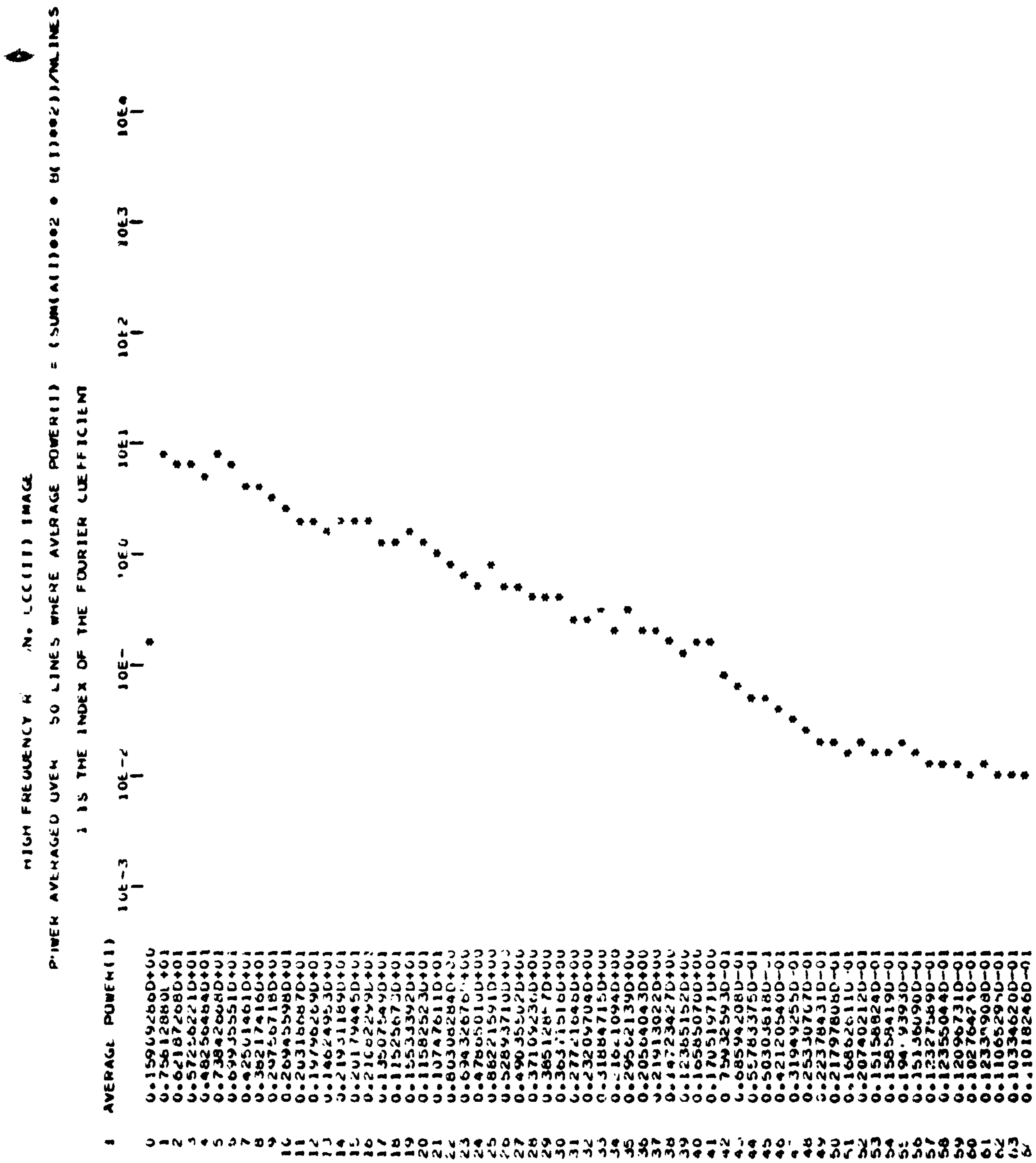

Figure 4-19 Horizontal Spectrum, High Frequency Region, Singly Resampled Image of Scene E-1080-15192

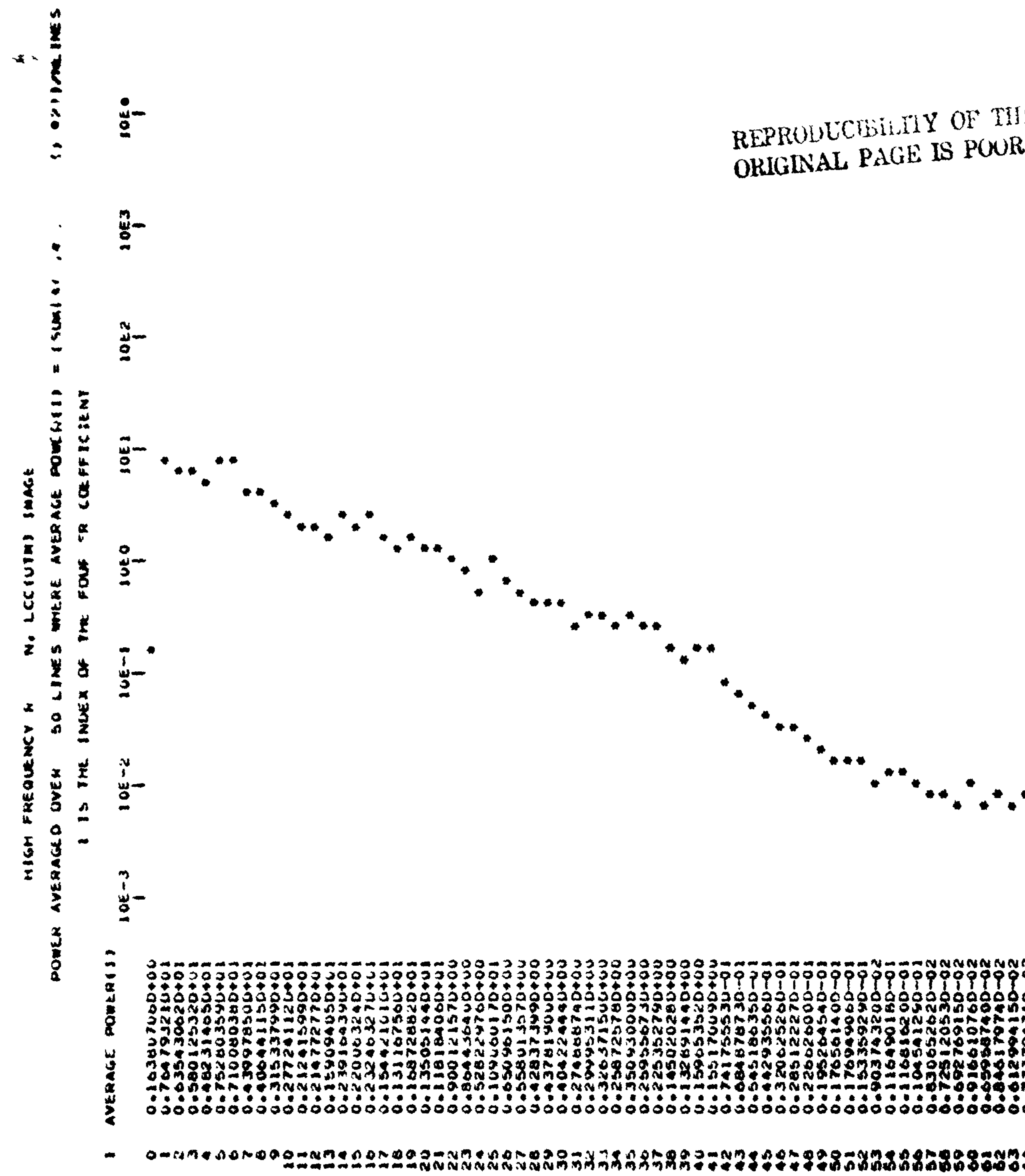

Figure 4-20 Horizontal Spectrum, High Frequency Region, Doubly Resampled Image of Scene E-1080-15192

ABSOLUTE DIFFERENCE OF THE TWO SPECTRA, HIGH FREQUENCY REGION

POWER AVERAGED OVER 50 LINES WHERE AVERAGE POWER(I) = (SUM(A(I)**2 + B(I)**2))/NLINES

I IS THE INDEX OF THE FOURIER COEFFICIENT

I	AVERAGE POWER(I)
0	0.47141964D-02
1	0.66644119D-01
2	0.13557944D+00
3	0.75631045D-01
4	0.25018655D-02
5	0.14376907D+00
6	0.10724876D+00
7	0.14963688D+00
8	0.24266991D+00
9	0.17770813D+00
10	0.77851404D-01
11	0.92291136D-01
12	0.16810074D+00
13	0.12844518D+00
14	0.19852500D+00
15	0.18268793D+00
16	0.21640279D+00
17	0.19345523D+00
18	0.15910836D+00
19	0.13394892D+00
20	0.19226213D+00
21	0.10707951D+00
22	0.97038735D-01
23	0.17010963D+00
24	0.49579659D-01
25	0.20838575D+00
26	0.12202440D+00
27	0.67656548D-01
28	0.[illegible]7281623D-01
29	0.[illegible]26904240D-01
30	0.40509274D-01
31	0.23277225D-02
32	0.67856077D-01
33	0.75243492D-02
34	0.42514834D-01
35	0.55308618D-01
36	0.53916303D-01
37	0.62225626D-02
38	0.22139938D-02
39	0.90399259D-02
40	0.61971745D-02
41	0.15349623D-01
42	0.17570793D-02
43	0.10633468D-03
44	0.12647396D-02
45	0.60102616D-02
46	0.10058014D-01
47	0.34370274D-02
48	0.26681070D-02
49	0.28519766D-02
50	0.41416674D-02
51	0.83229473D-03
52	0.54042829D-02
53	0.61213925D-02
54	0.42094009D-02
55	0.77877727D-02
56	0.46819605D-02
57	0.40210626D-02
58	0.51038388D-02
59	0.51690395D-02
60	0.11103162D-02
61	0.57430335D-02
62	0.26034985D-02
63	0.42046785D-02
64	0.36803033D-02

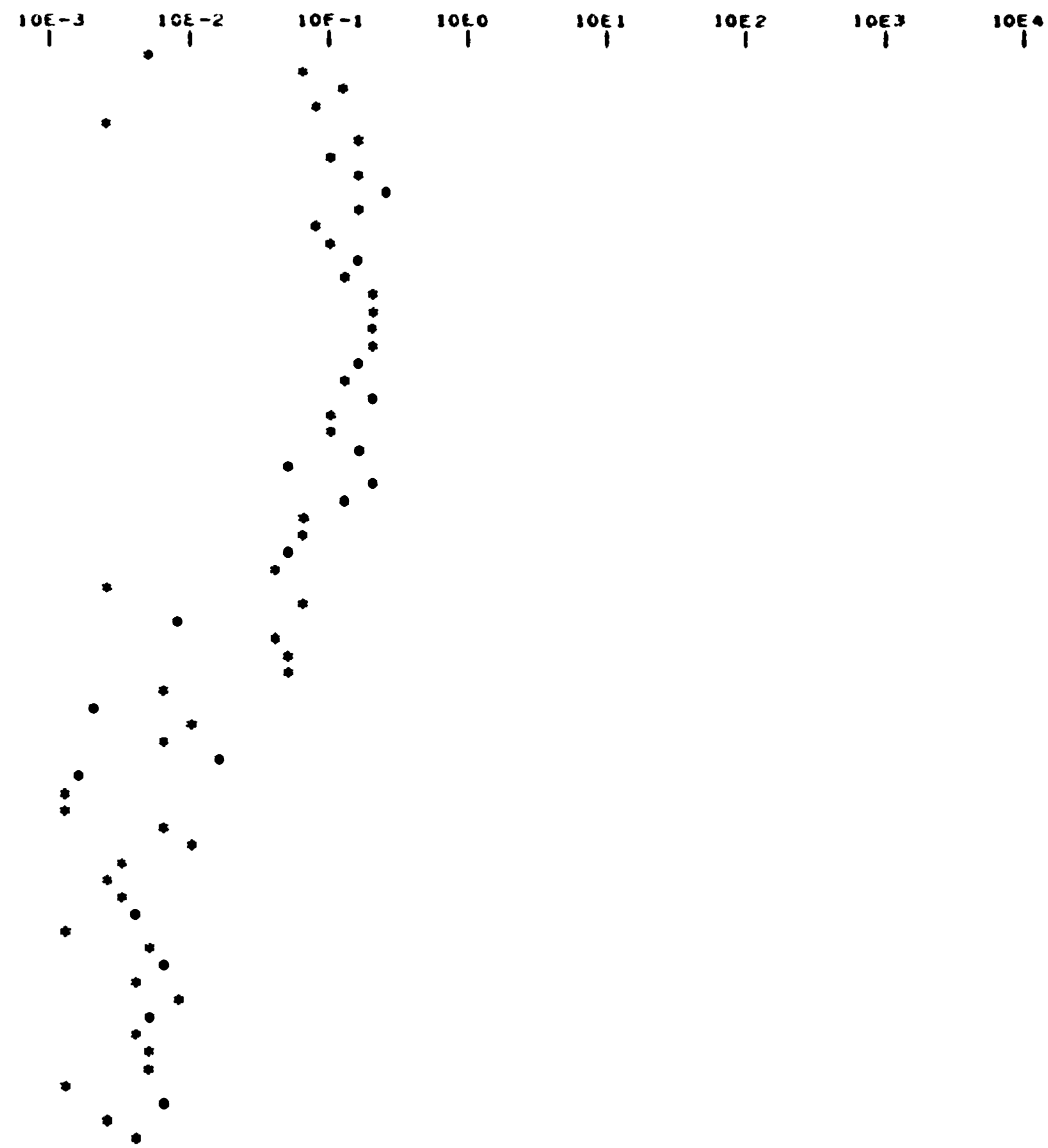

Figure 4-21 Absolute Difference of Horizontal Spectra, High Frequency Region, Scene E-1080-15192

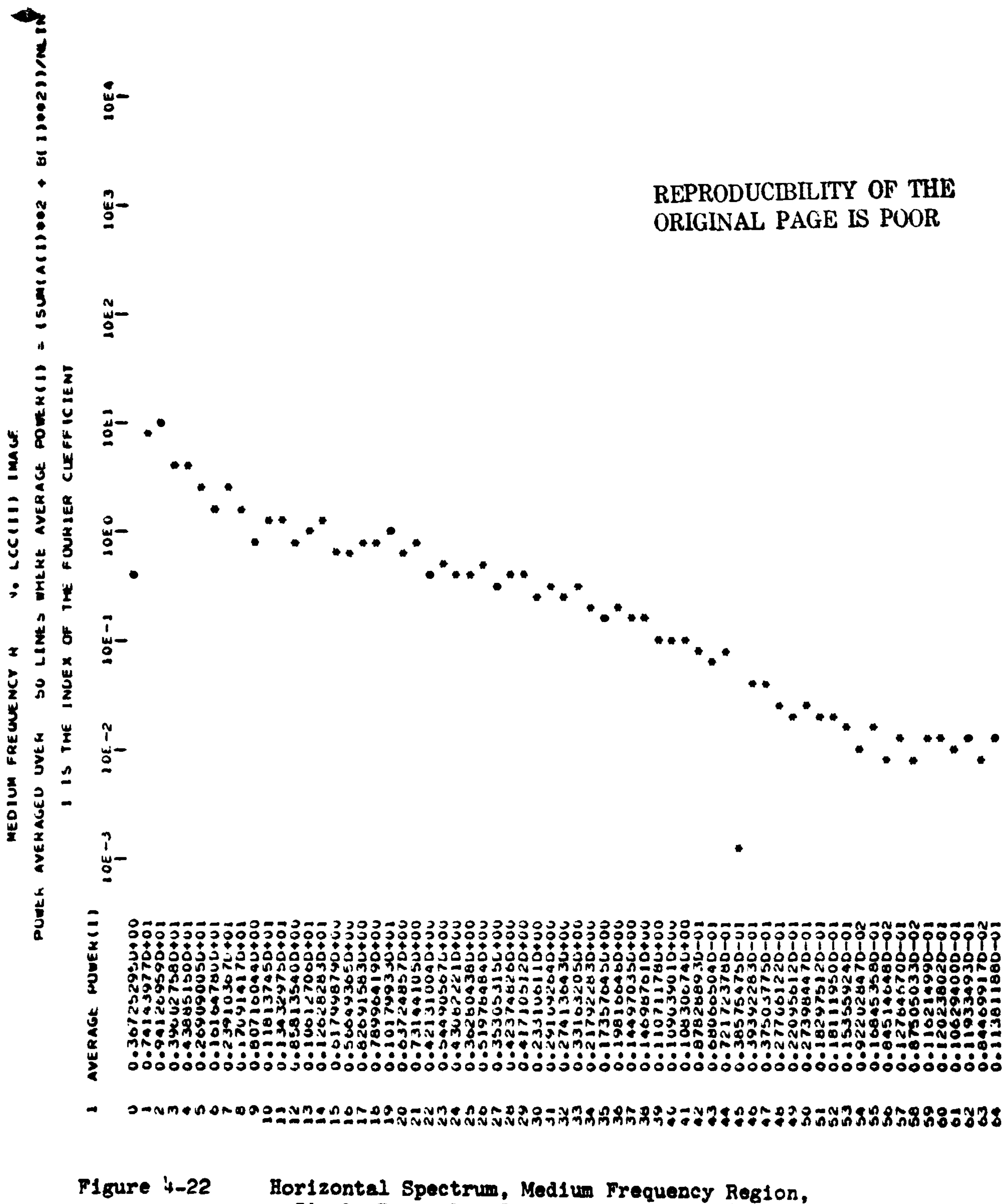

Figure 4-22 Horizontal Spectrum, Medium Frequency Region, Singly Resampled Image of Scene E-1080-15192

MEDIUM FREQUENCY ... ION, LCC(UTM) IMAGE

POWER AVERAGED OVER 50 LINES WHERE AVERAGE POWER(I) = (SUM(A(I)**2 + B(I)**2))/NLINES

I IS THE INDEX OF THE FOURIER COEFFICIENT

I	AVERAGE POWER(I)
0	0.38711729D+00
1	0.76340076D+01
2	0.94985554D+01
3	0.40315772D+01
4	0.44029722D+01
5	0.28012635D+01
6	0.17067946D+01
7	0.25201295D+01
8	0.17719517D+01
9	0.89773394D+00
10	0.13226249D+01
11	0.14469369D+01
12	0.89310045D+00
13	0.11974927D+01
14	0.13547555D+01
15	0.69338791D+00
16	0.63256461D+00
17	0.91379084D+00
18	0.87573755D+00
19	0.10851530D+01
20	0.72449825D+00
21	0.83680986D+00
22	0.48905935D+00
23	0.63799935D+00
24	0.47936973D+00
25	0.41790585D+00
26	0.59393141D+00
27	0.39624050D+00
28	0.49089935D+00
29	0.44891549D+00
30	0.26654671D+00
31	0.33003552D+00
32	0.28394750D+00
33	0.37509550D+00
34	0.23444762D+00
35	0.19670948D+00
36	0.20020161D+00
37	0.16477779D+00
38	0.15337100D+00
39	0.11127778D+00
40	0.11299673D+00
41	0.10357709D+00
42	0.82101859D-01
43	0.68740659D-01
44	0.69385749D-01
45	0.43929954D-01
46	0.35704159D-01
47	0.31612187D-01
48	0.27031654D-01
49	0.22359540D-01
50	0.22329290D-01
51	0.15306402D-01
52	0.13121202D-01
53	0.95810117D-02
54	0.85799573D-02
55	0.10405512D-01
56	0.79224452D-02
57	0.96183817D-02
58	0.71009525D-02
59	0.84497035D-02
60	0.84905433D-02
61	0.73748312D-02
62	0.87983802D-02
63	0.61196285D-02
64	0.83729760D-02

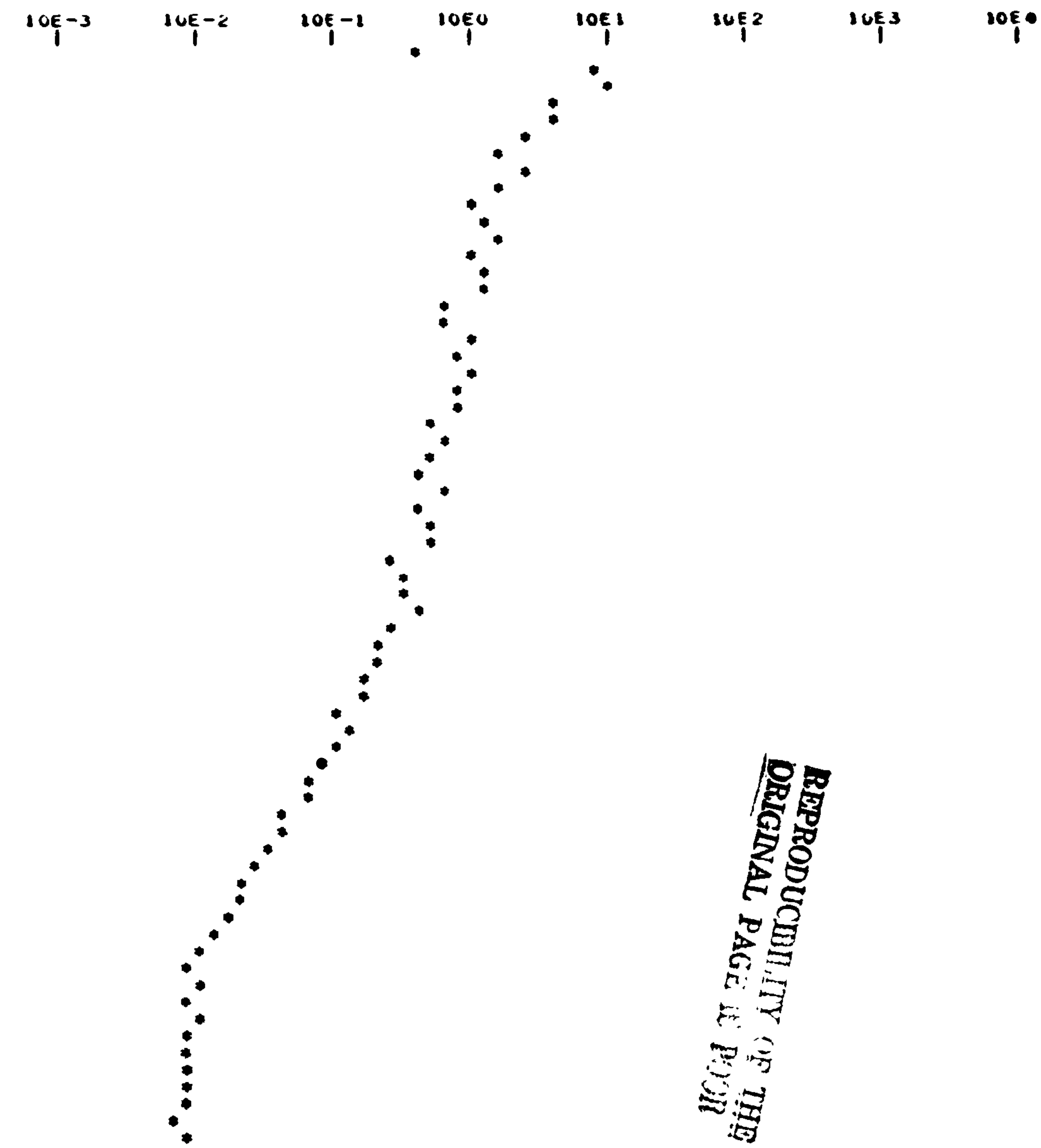

Figure 4-23 Horizontal Spectrum, Medium Frequency Region, Doubly Resampled Image of Scene E-1080-15192

ABSOLUTE DIFFE[illegible] OF THE TWO SPECTRA, MEDIUM FREQUENCY REGION

POWER AVERAGED OVER 50 LINES WHERE AVERAGE POWER(I) = (SUM(A(I)**2 + B(I)**2))/NLINES

I IS THE INDEX OF THE FOURIER COEFFICIENT

I	AVERAGE POWER(I)
0	0.19864332D-01
1	0.21960965D+00
2	0.85859496D-01
3	0.71301383D-01
4	0.14457183D-01
5	0.11036306D+00
6	0.90316039D-01
7	0.12909282D+00
8	0.62810031D-01
9	0.90573560D-01
10	0.14125036D+00
11	0.10364137D+00
12	0.34960507D-01
13	0.13622206D+00
14	0.91927208D-01
15	0.75389121D-01
16	0.66070960D-01
17	0.86881008D-01
18	0.85773358D-01
19	0.67159702D-01
20	0.87249683D-01
21	0.10536883D+00
22	0.67749306D-01
23	0.93093677D-01
24	0.48547517D-01
25	0.55101470D-01
26	0.74146571D-01
27	0.43167355D-01
28	0.67151095D-01
29	0.31810364D-01
30	0.33440593D-01
31	0.38942875D-01
32	0.98110697D-02
33	0.43463452D-01
34	0.16524786D-01
35	0.23133026D-01
36	0.20353274D-02
37	0.19807442D-01
38	0.63833893D-02
39	0.56600502D-03
40	0.39577192D-02
41	0.47296552D-02
42	0.57270339D-02
43	0.67415532D-03
44	0.27866285D-02
45	0.53544787D-02
46	0.36881234D-02
47	0.58915886D-02
48	0.67446729D-03
49	0.26392733D-03
50	0.50691573D-02
51	0.29911103D-02
52	0.49907481D-02
53	0.57749121D-02
54	0.64032735D-03
55	0.64398461D-02
56	0.52901963D-03
57	0.31662879D-02
58	0.16495508D-02
59	0.31717952D-02
60	0.35332590D-02
61	0.32545685D-02
62	0.31351123D-02
63	0.23273632D-02
64	0.30082117D-02

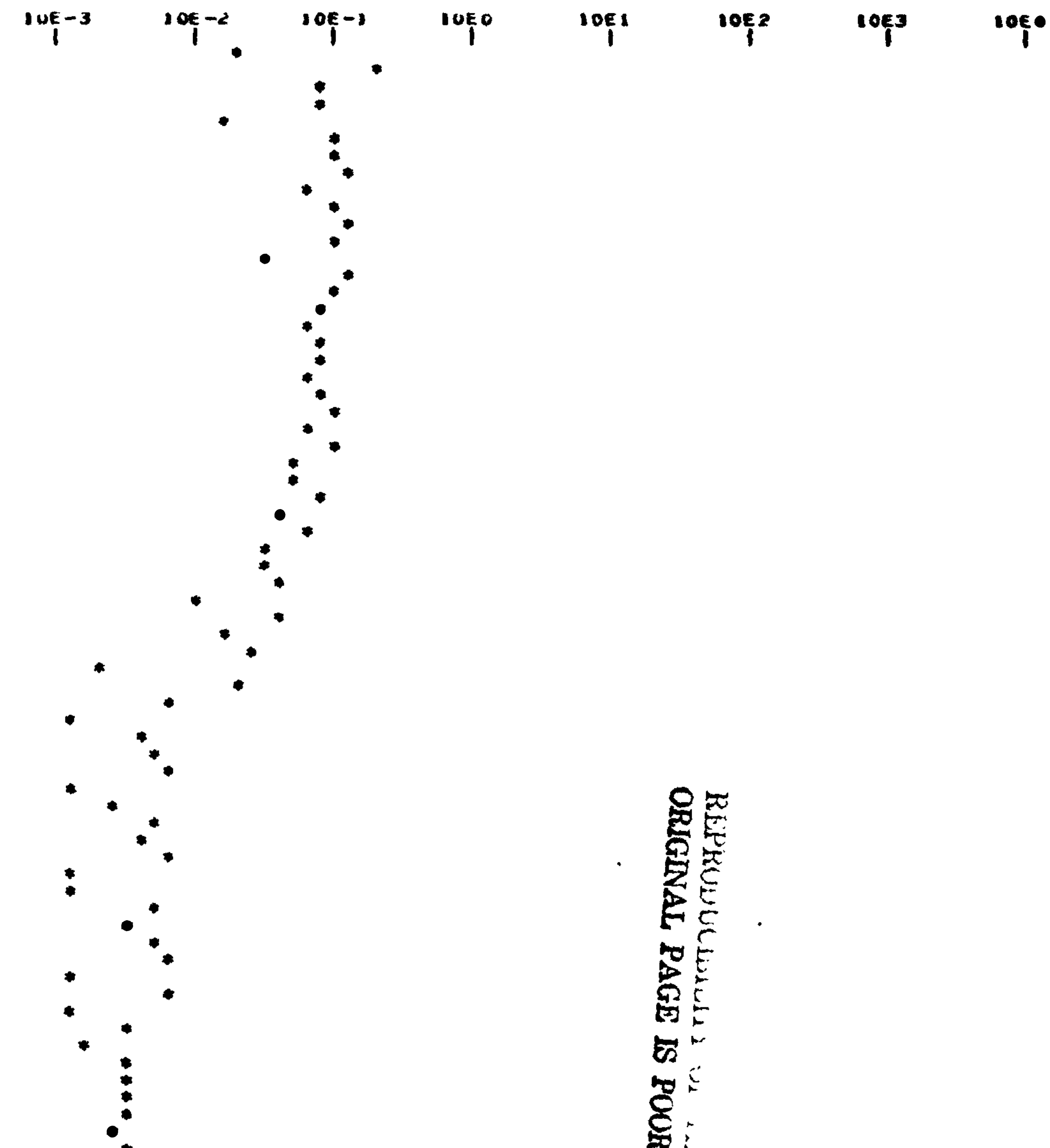

Figure 4-24 Absolute Difference of Horizontal Spectra,
Medium Frequency Region, Scene E-1080-15192

LOW FREQUENCY I   ON. LCC(11) IMAGE

POWER AVERAGED OVER   50 LINES WHERE AVERAGE POWER(I) = (SUM(A(I)**2 + B(I)**2))/NLINES

I IS THE INDEX OF THE FOURIER COEFFICIENT

I	AVERAGE POWER(I)
0	0.18719826D-02
1	0.13468078D+00
2	0.15153594D+00
3	0.17253996D-01
4	0.18781102D-01
5	0.13326225D-01
6	0.13516219D-01
7	0.10568647D-01
8	0.18423023D-01
9	0.13449602D-01
10	0.99952874D-02
11	0.96063758D-02
12	0.91601061D-02
13	0.11205465D-01
14	0.76752144D-02
15	0.11484169D-01
16	0.10252558D-01
17	0.97813675D-02
18	0.85941661D-02
19	0.11967039D-01
20	0.99317915D-02
21	0.15020698D-01
22	0.14635385D-01
23	0.97342876D-02
24	0.71884603D-02
25	0.10833866D-01
26	0.74860339D-02
27	0.11381373D-01
28	0.91840412D-02
29	0.13165376D-01
30	0.12990741D-01
31	0.90268640D-02
32	0.73886347D-02
33	0.94777228D-02
34	0.67447126D-02
35	0.66256171D-02
36	0.73801471D-02
37	0.86758747D-02
38	0.63525260D-02
39	0.81263435D-02
40	0.81570628D-02
41	0.60192940D-02
42	0.79047159D-02
43	0.60090741D-02
44	0.66074330D-02
45	0.59672460D-02
46	0.48610193D-02
47	0.45878765D-02
48	0.41120419D-02
49	0.44403995D-02
50	0.30571386D-02
51	0.48195358D-02
52	0.36703733D-02
53	0.49671401D-02
54	0.33539175D-02
55	0.36644773D-02
56	0.30111665D-02
57	0.27331583D-02
58	0.37922309D-02
59	0.35684882D-02
60	0.34665839D-02
61	0.31863787D-02
62	0.32371058D-02
63	0.29258599D-02
64	0.31616111D-02

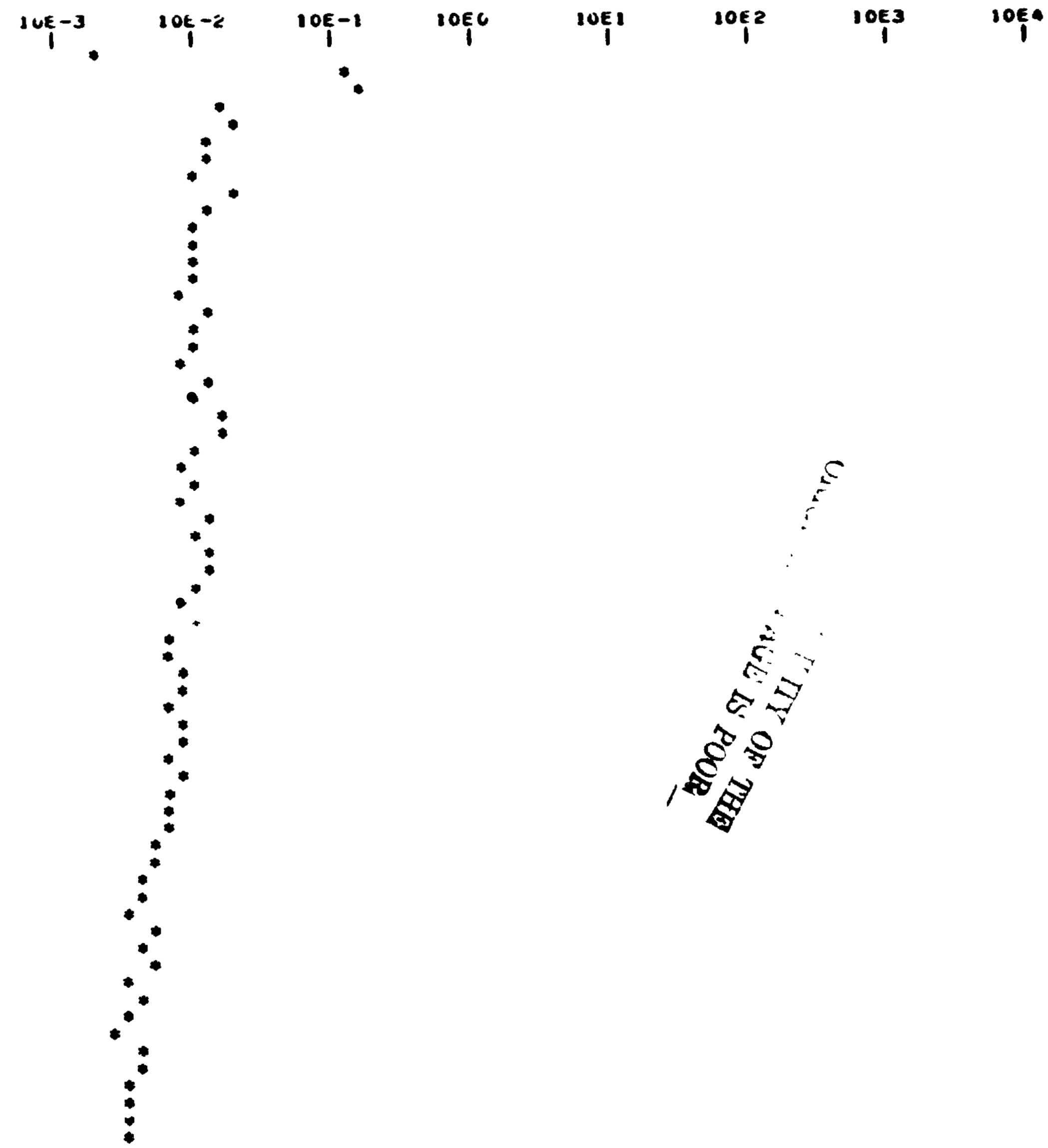

Figure 4-25 Horizontal Spectrum, Low Frequency Region, Singly Resampled Image of Scene E-1080-15192

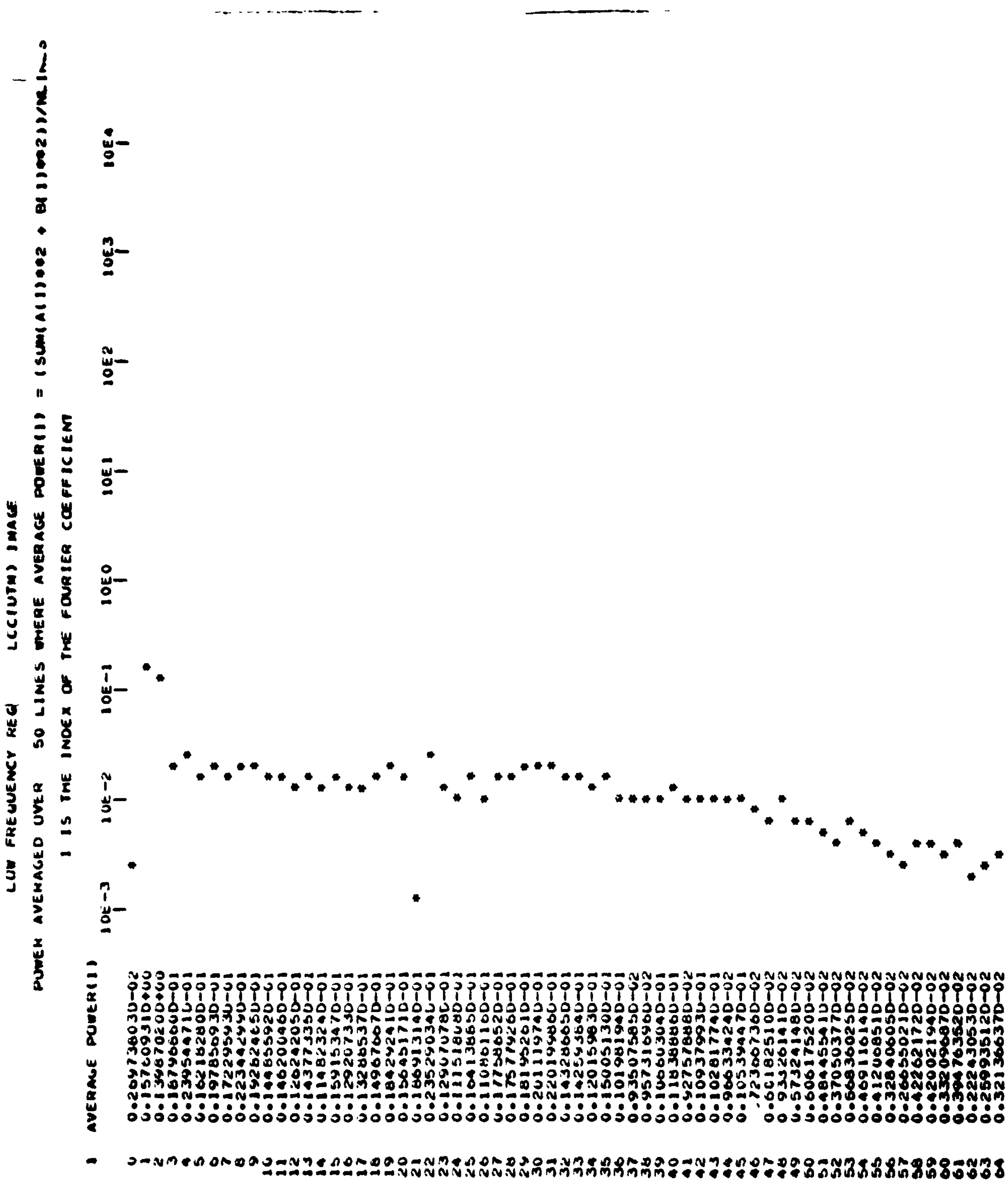

Figure 4-26 Horizontal Spectrum, Low Frequency Region, Doubly Resampled Image of Scene E-1080-15192

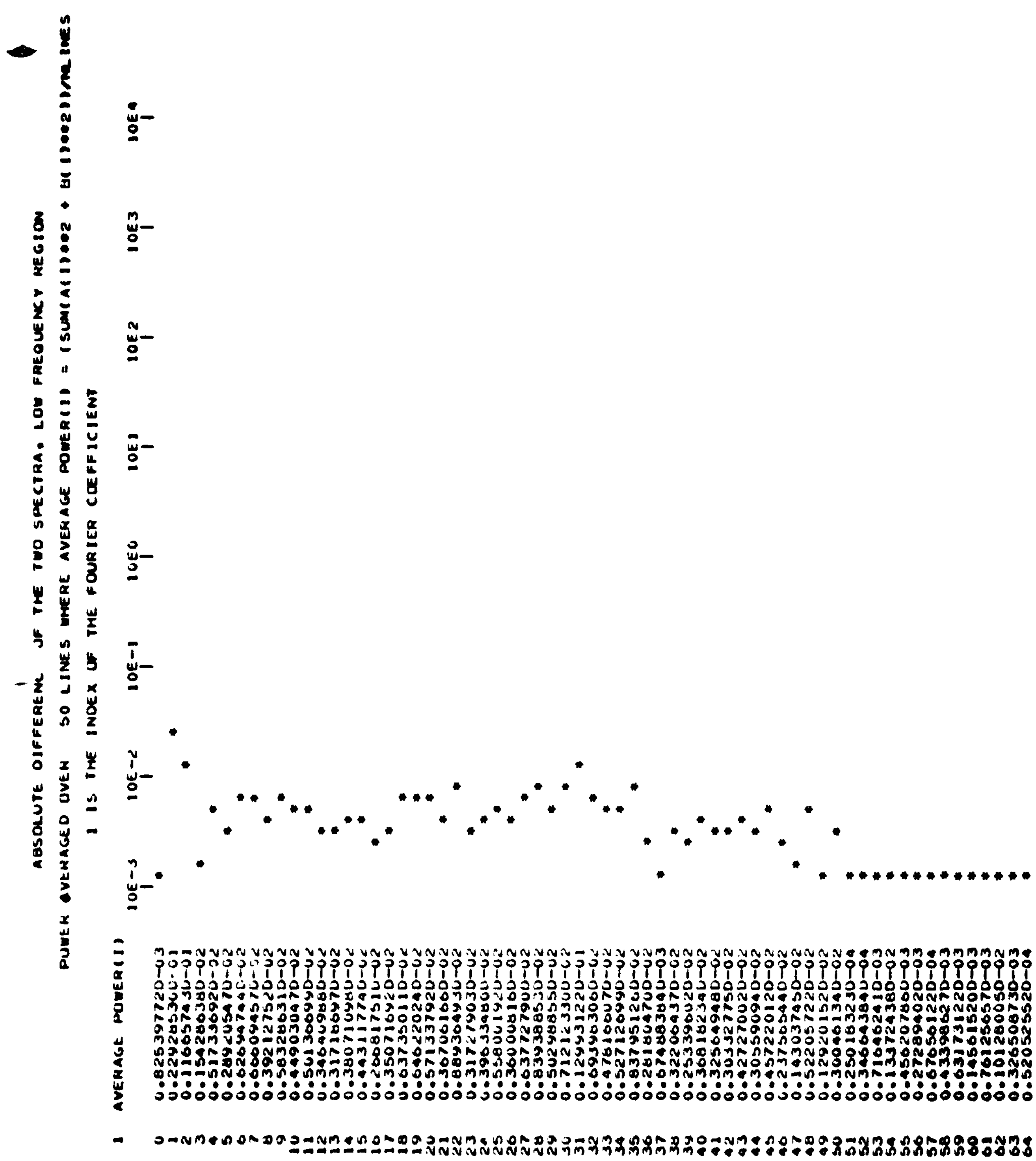

Figure 4-27 Absolute Difference of Horizontal Spectra, Low Frequency Region, Scene E-1080-15192

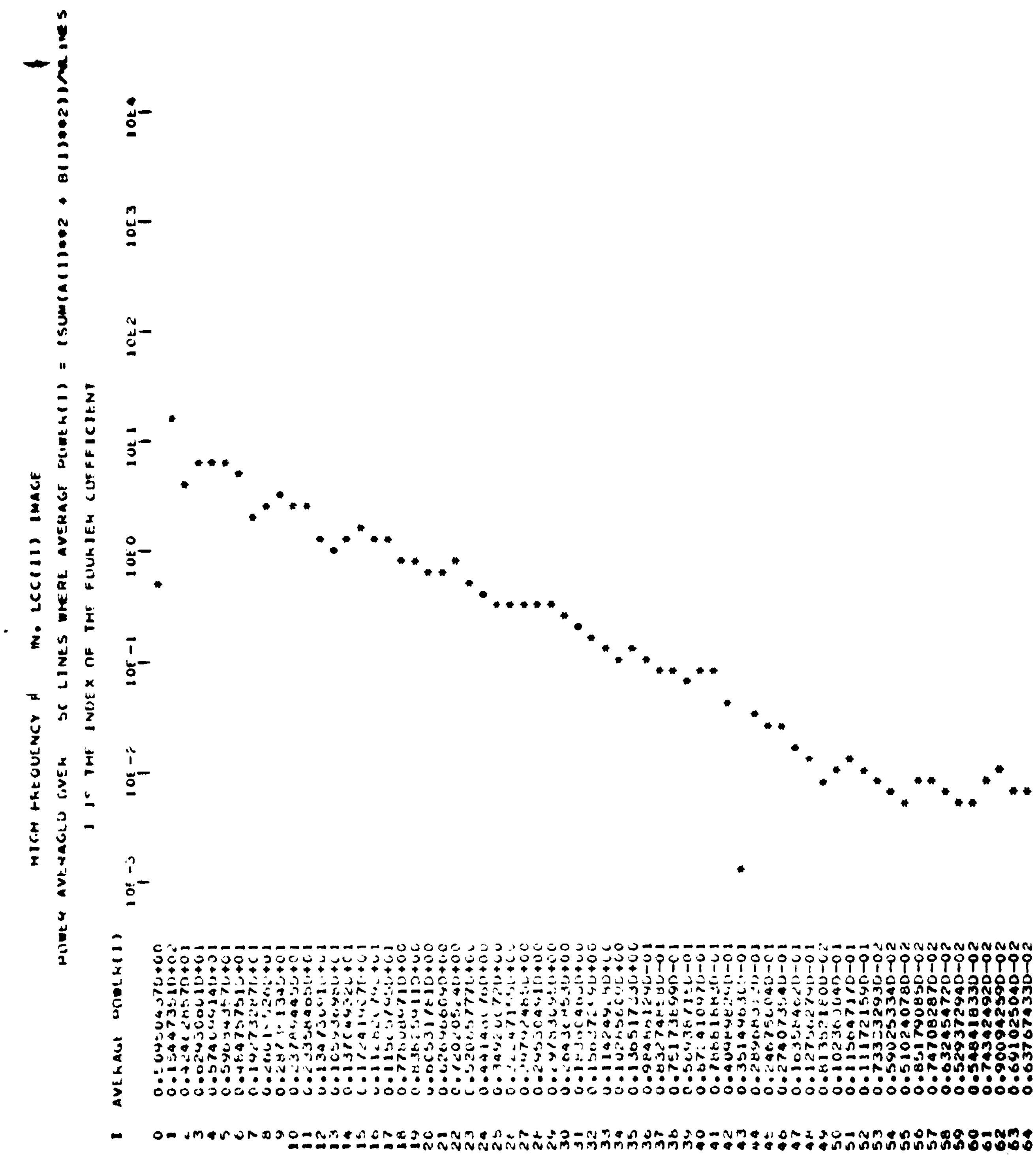

Figure 4-28 Vertical Spectrum, High Frequency Region, Singly Resampled Image of Scene E-1080-15192

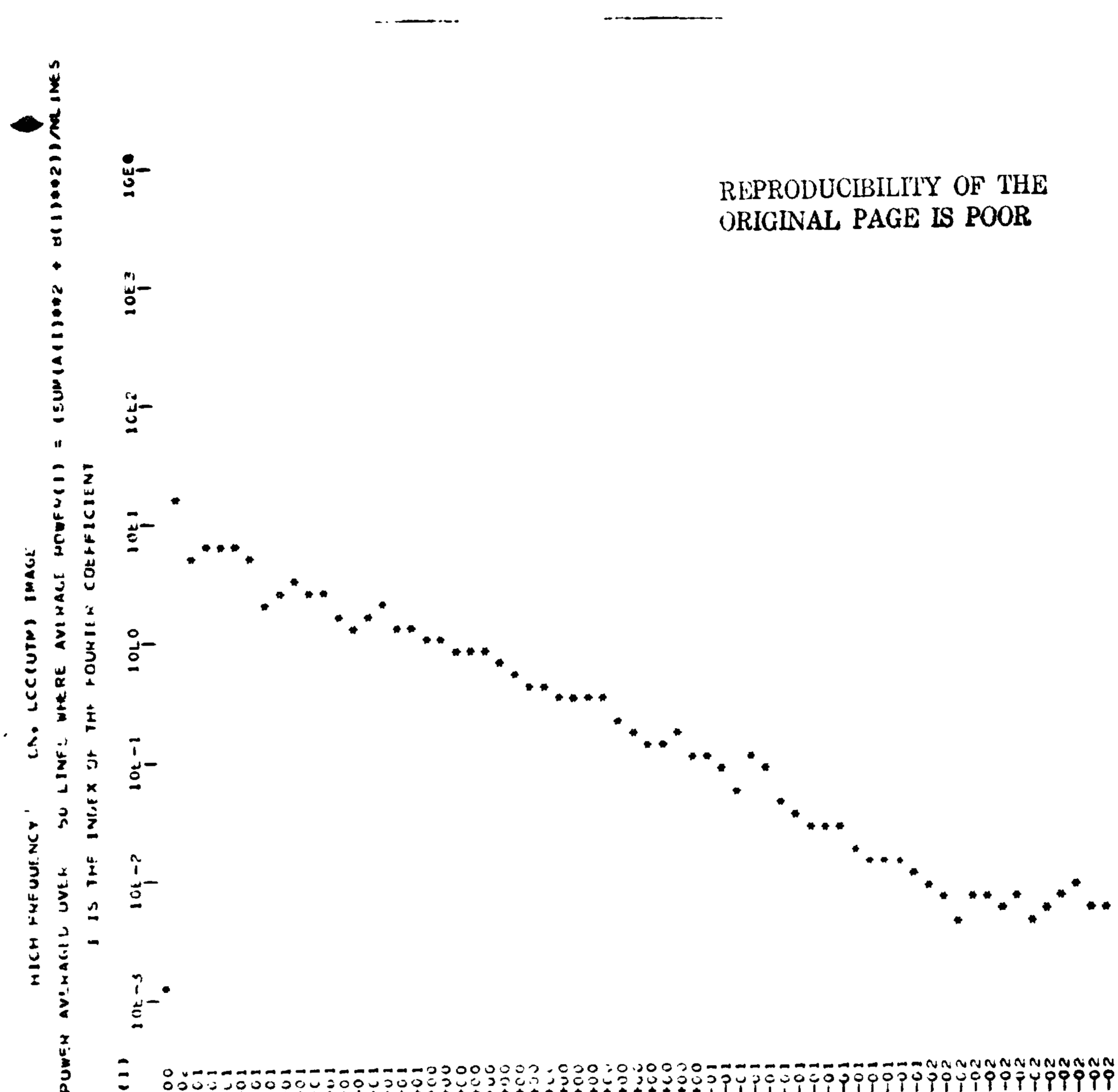

Figure 4-29 **Vertical Spectrum, High Frequency Region, Doubly Resampled Image of Scene E-1080-15192**

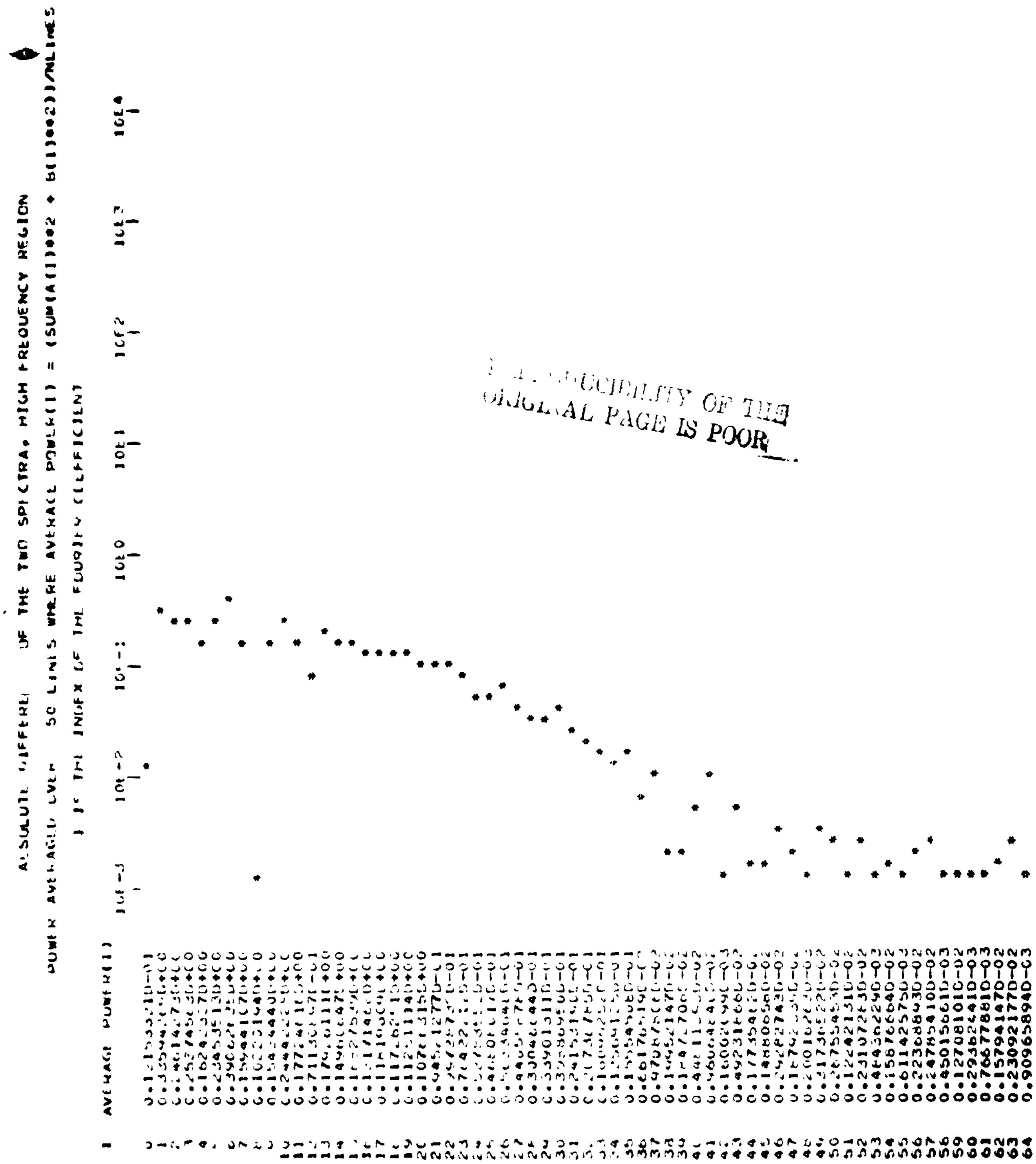

Figure 4-30 Absolute Difference of Vertical Spectra, High Frequency Region, Scene E-1080-15192

MEDIUM FREQUENCY ICN. LCC(II) IMAGE

POWER AVERAGED OVER 50 LINES WHERE AVERAGE POWER(I) = (SUM(A(I)**2 + B(I)**2))/NLINES

I IS THE INDEX OF THE FOURIER COEFFICIENT

I	AVERAGE POWER(I)
0	0.314355F3D+00
1	0.11341213D+02
2	0.20838097D+01
3	0.37977861D+01
4	0.30567009D+01
5	0.26675990D+01
6	0.30766925D+01
7	0.19402442D+01
8	0.16930570D+01
9	0.21763761D+01
10	0.17026497D+01
11	0.12720100D+01
12	0.10001363D+01
13	0.13195F30D+01
14	0.97506220D+00
15	0.11132FC1D+01
16	0.10390271D+01
17	0.10162549D+01
18	0.99045C57D+00
19	0.86874470D+00
20	0.85410908D+00
21	0.65643195D+00
22	0.49971993D+00
23	0.61366604D+00
24	0.63181315D+00
25	0.51492769D+00
26	0.42602547D+00
27	0.43710071D+00
28	0.26128101D+00
29	0.35821447D+00
30	0.26798274D+00
31	0.29434972D+00
32	0.23488340D+00
33	0.29559560D+00
34	0.17312211D+00
35	0.15178993D+00
36	0.12500303D+00
37	0.12715058D+00
38	0.99084390D-01
39	0.98758583D-01
40	0.99521133D-01
41	0.87453734D-01
42	0.68349962D-01
43	0.44491889D-01
44	0.44356960D-01
45	0.30404610D-01
46	0.36803540D-01
47	0.22588647D-01
48	0.24678579D-01
49	0.16261272D-01
50	0.15104813D-01
51	0.90259506D-02
52	0.92499390D-02
53	0.99253925D-02
54	0.59277033D-02
55	0.68629847D-02
56	0.61028155D-02
57	0.44551660D-02
58	0.57448687D-02
59	0.43664009D-02
60	0.55436716D-02
61	0.66230653D-02
62	0.78448190D-02
63	0.81229887D-02
64	0.70427624D-02

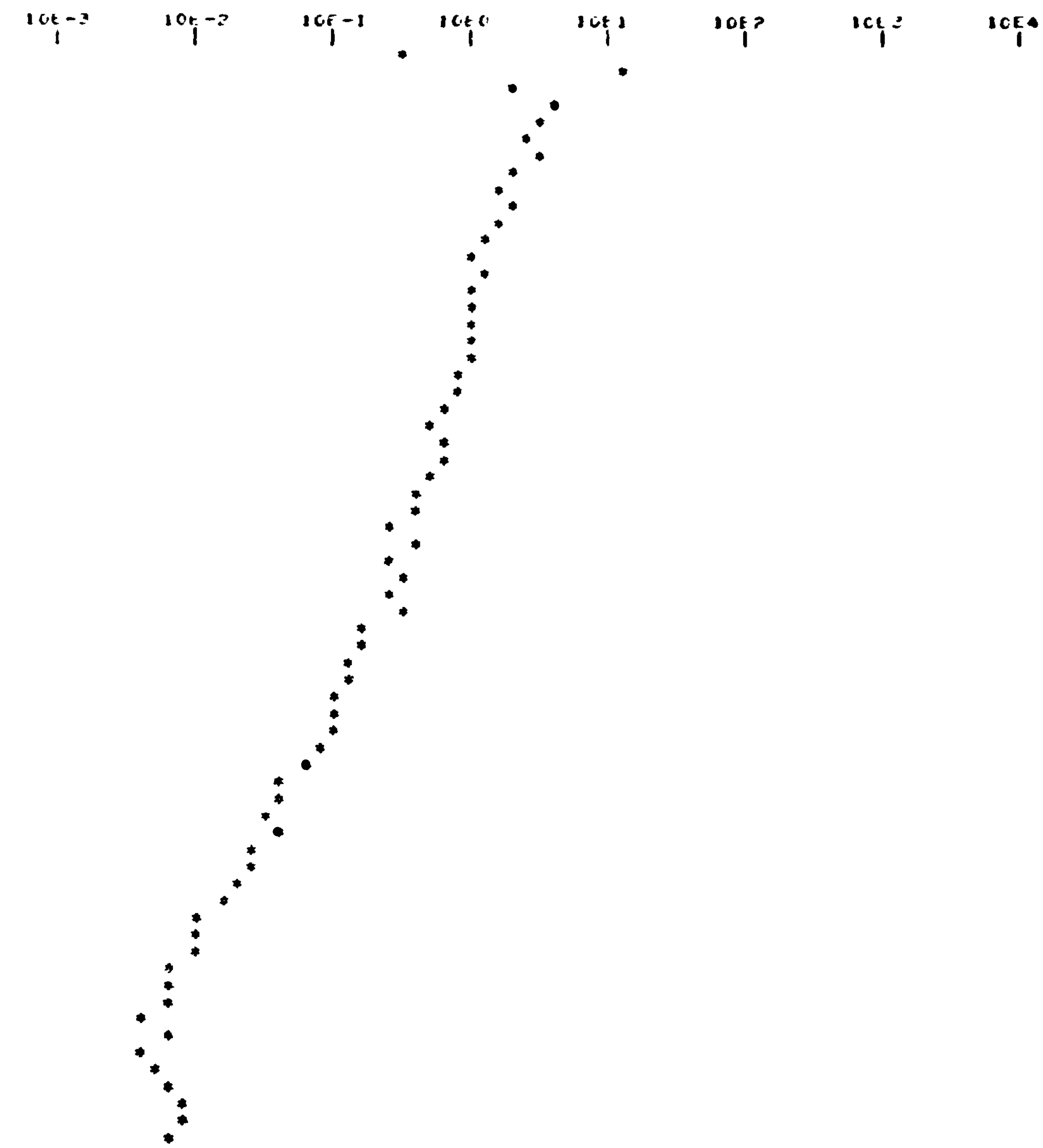

Figure 4-31 Vertical Spectrum, Medium Frequency Region, Singly Resampled Image of Scene E-1080-15192

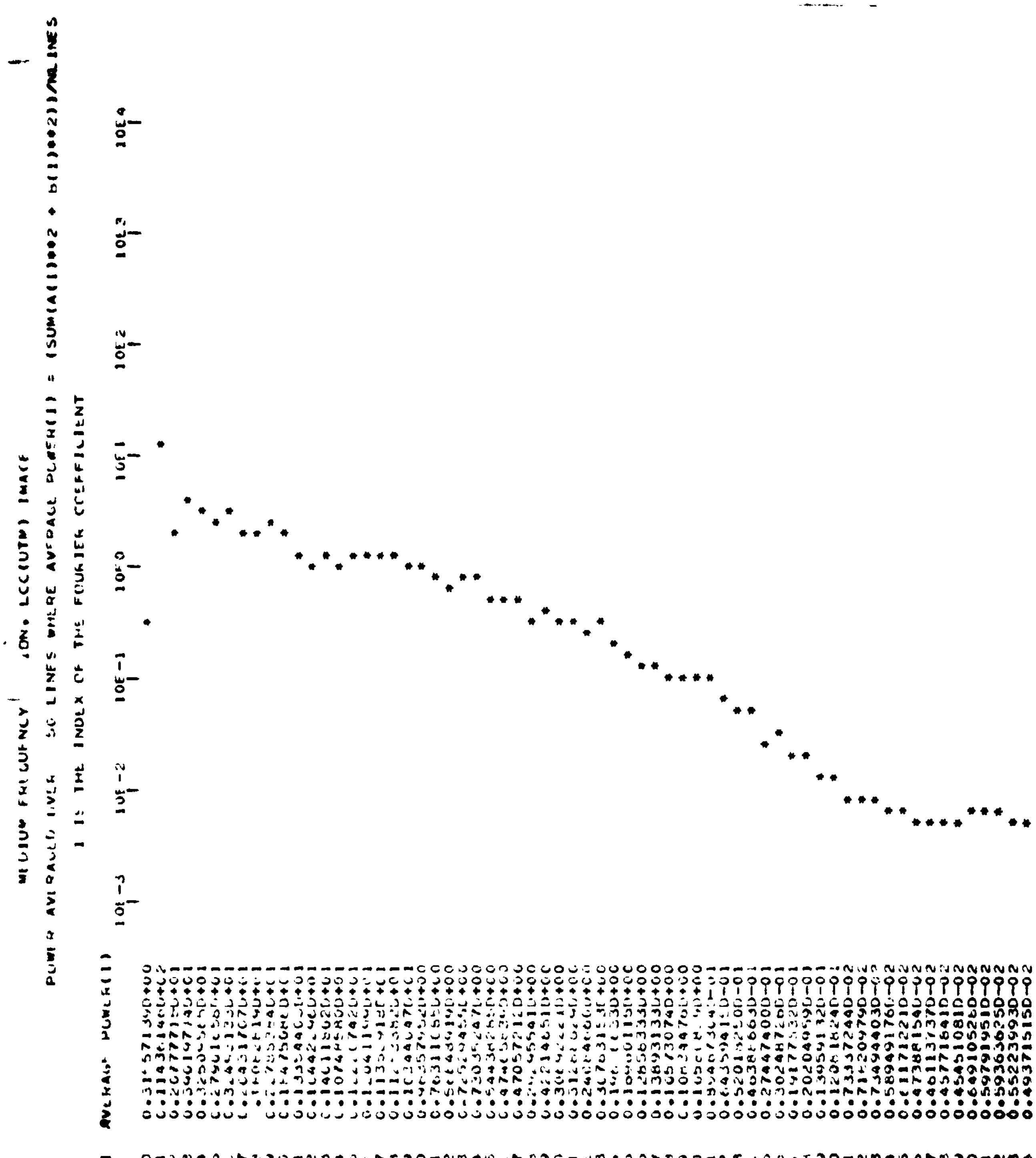

Figure 4-32 Vertical Spectrum, Medium Frequency Region, Doubly Resampled Image of Scene E-1080-15192

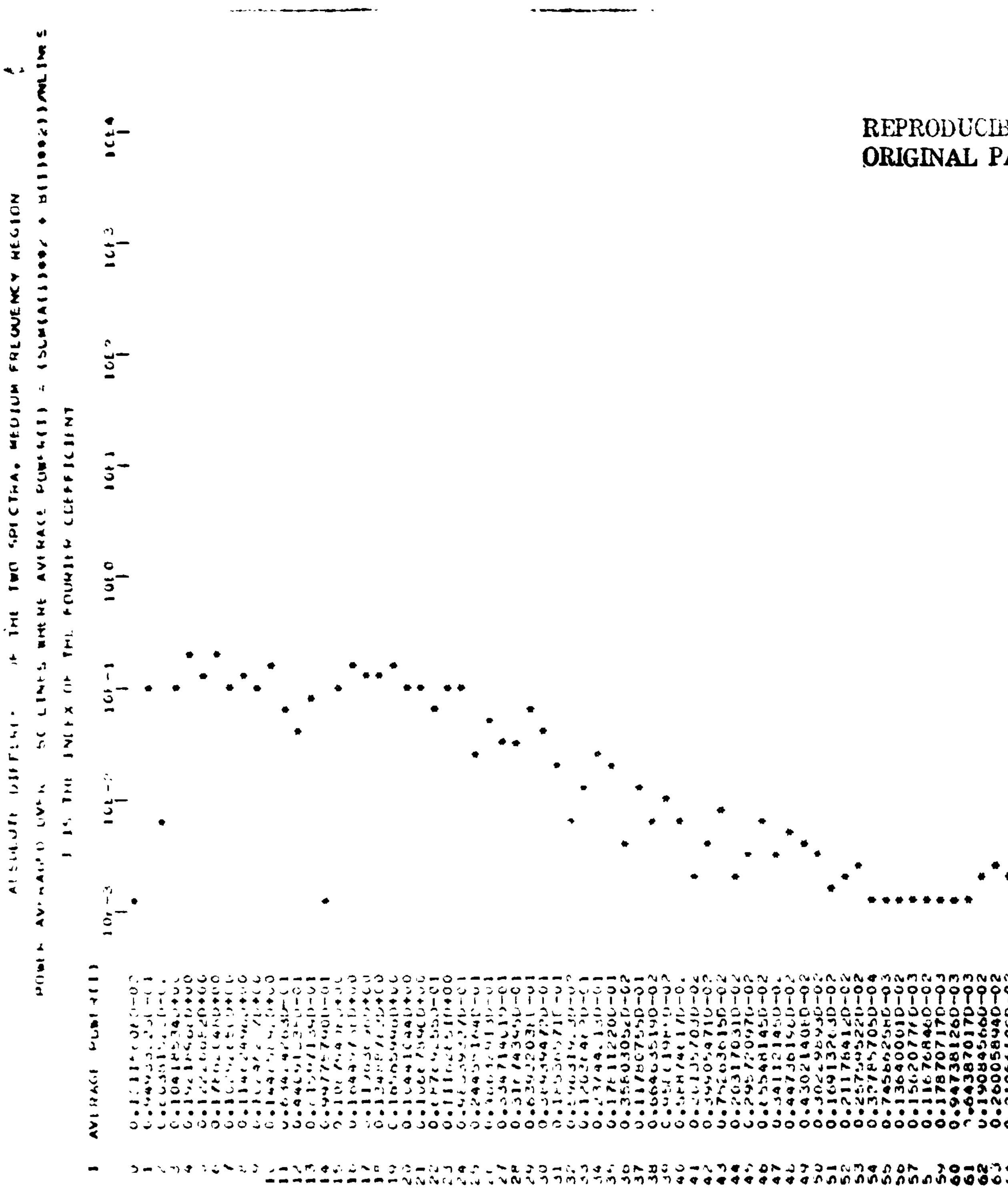

Figure 4-33 Absolute Difference of Vertical Spectra, Medium Frequency Region, Scene E-1080-15192

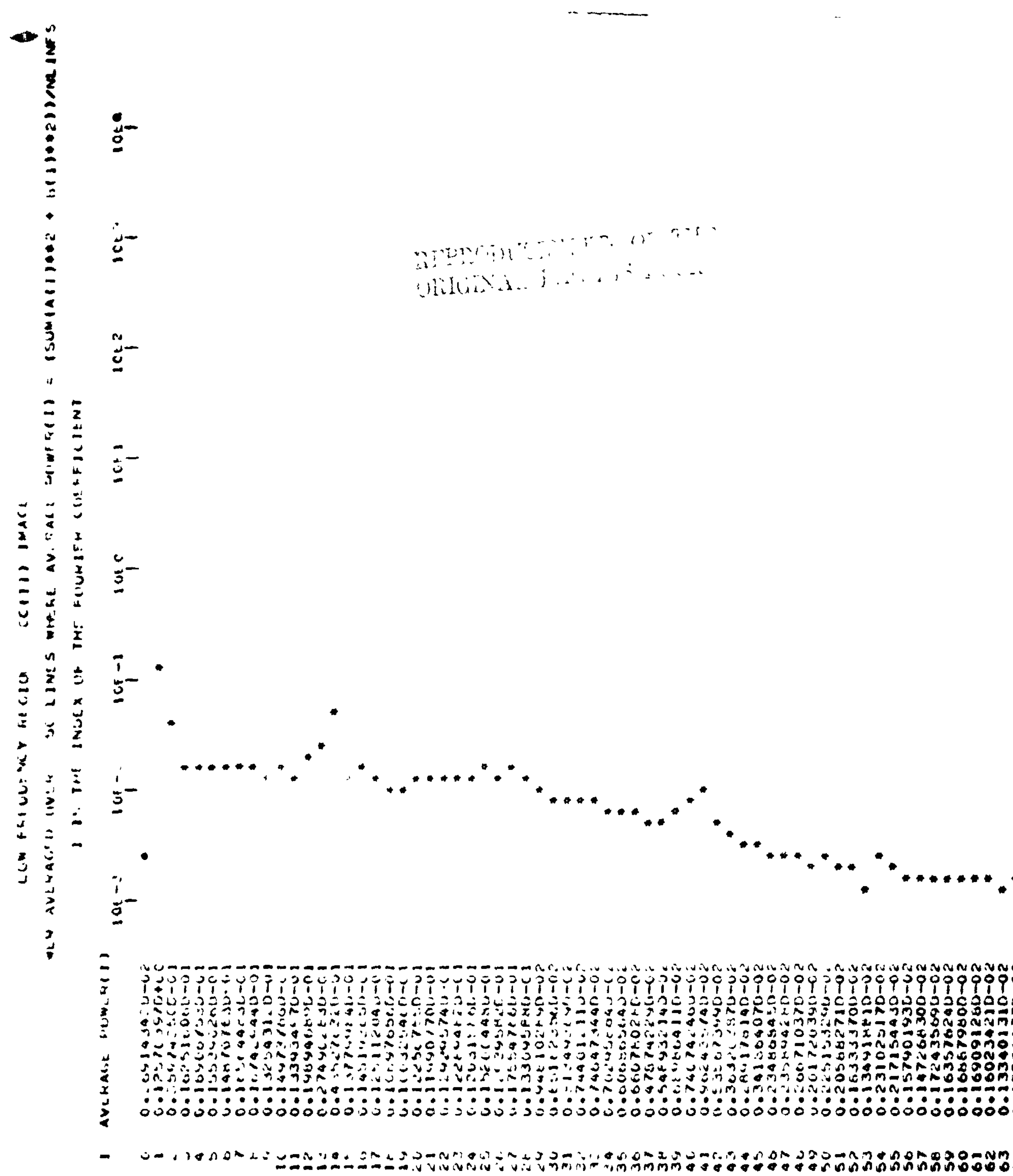

Figure 4-34 Vertical Spectrum, Low Frequency Region, Singly Resampled Image of Scene E-1080-15192

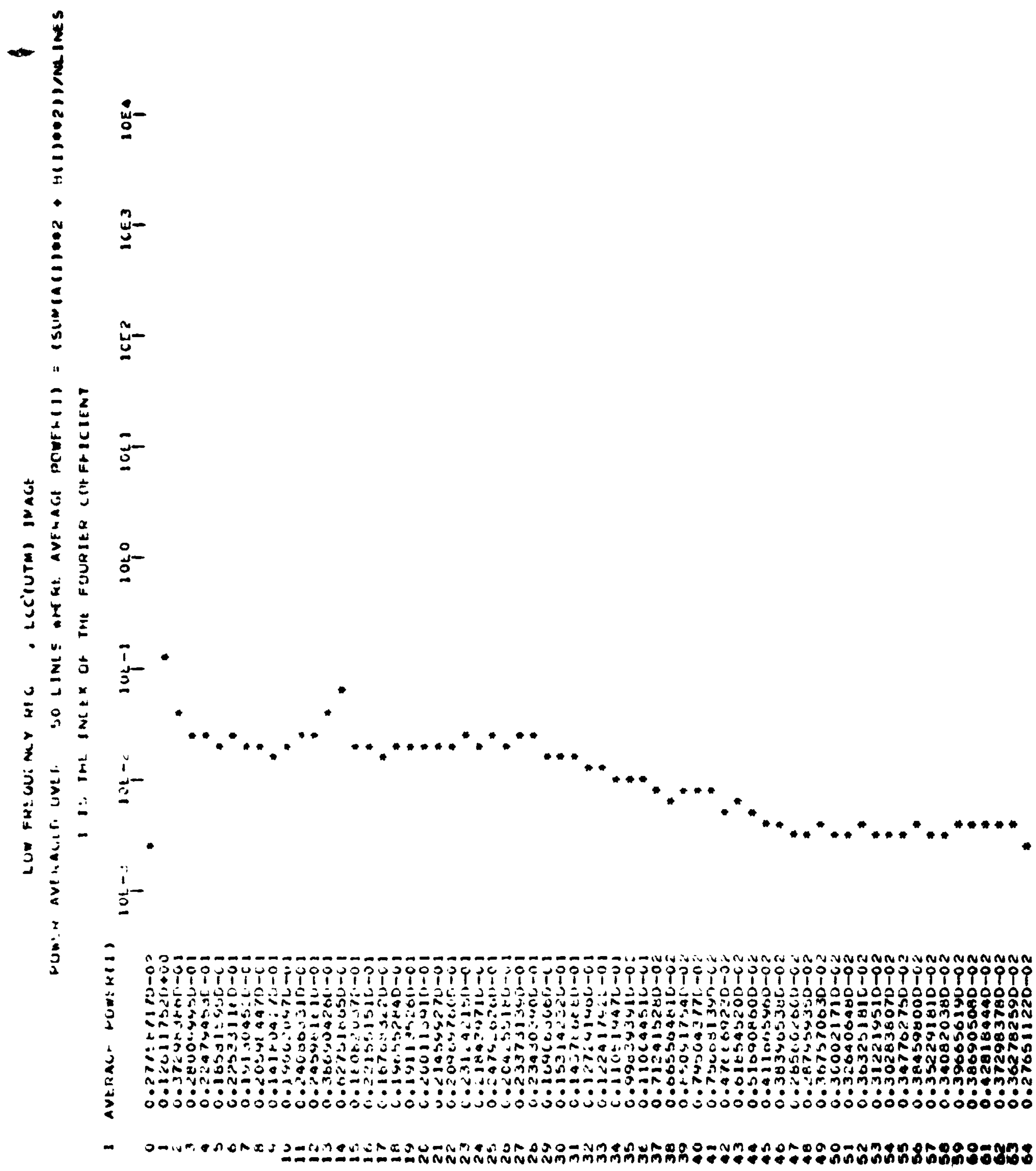

Figure 4-35 Vertical Spectrum, Low Frequency Region, Doubly Resampled Image of Scene ?-1080-15192

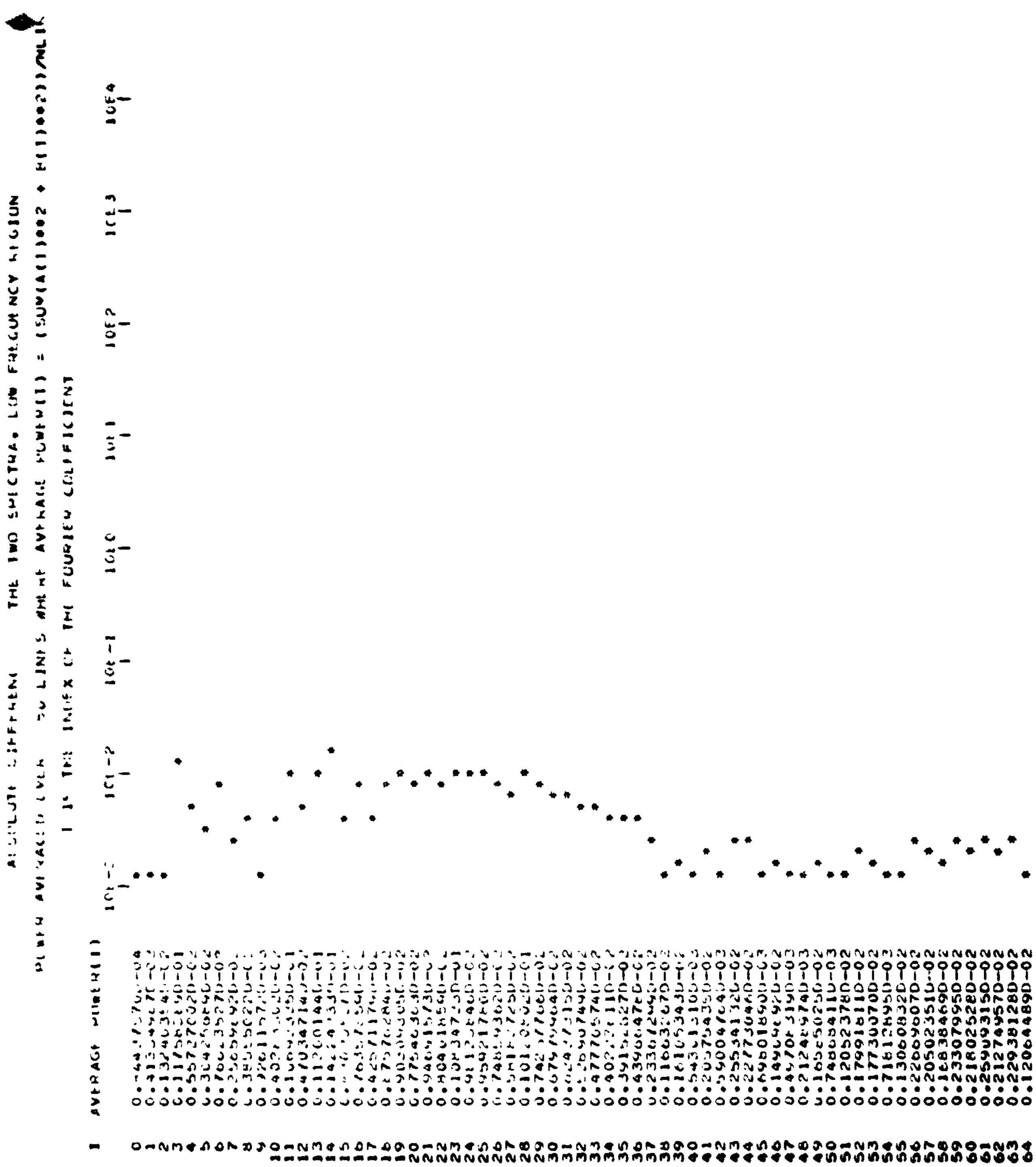

Figure 4-36   Absolute Difference of Vertical Spectra, Low Frequency Region, Scene E-1080-15?92

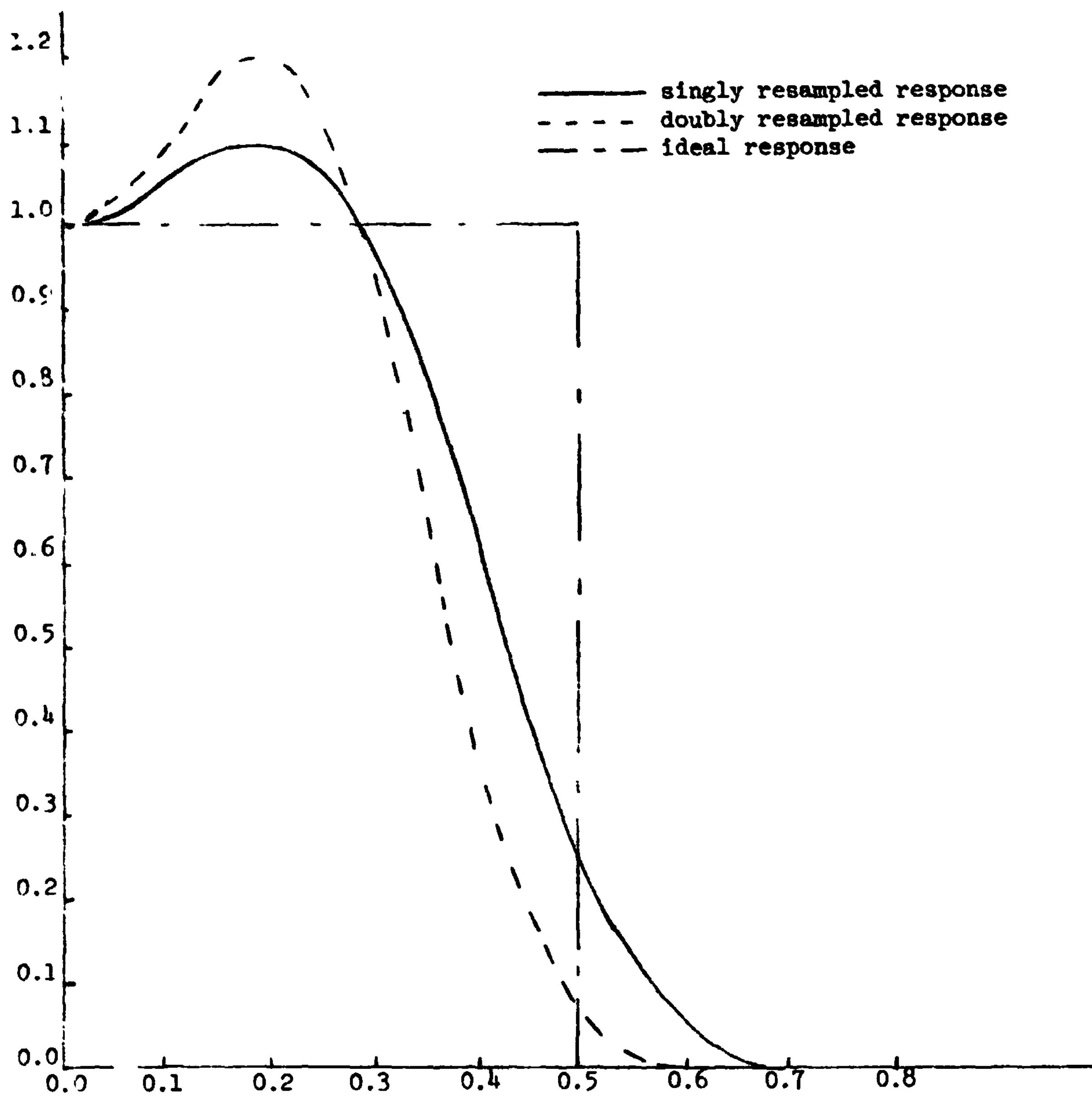

Figure 4-37. Power Spectrum Response of Various Resamplers

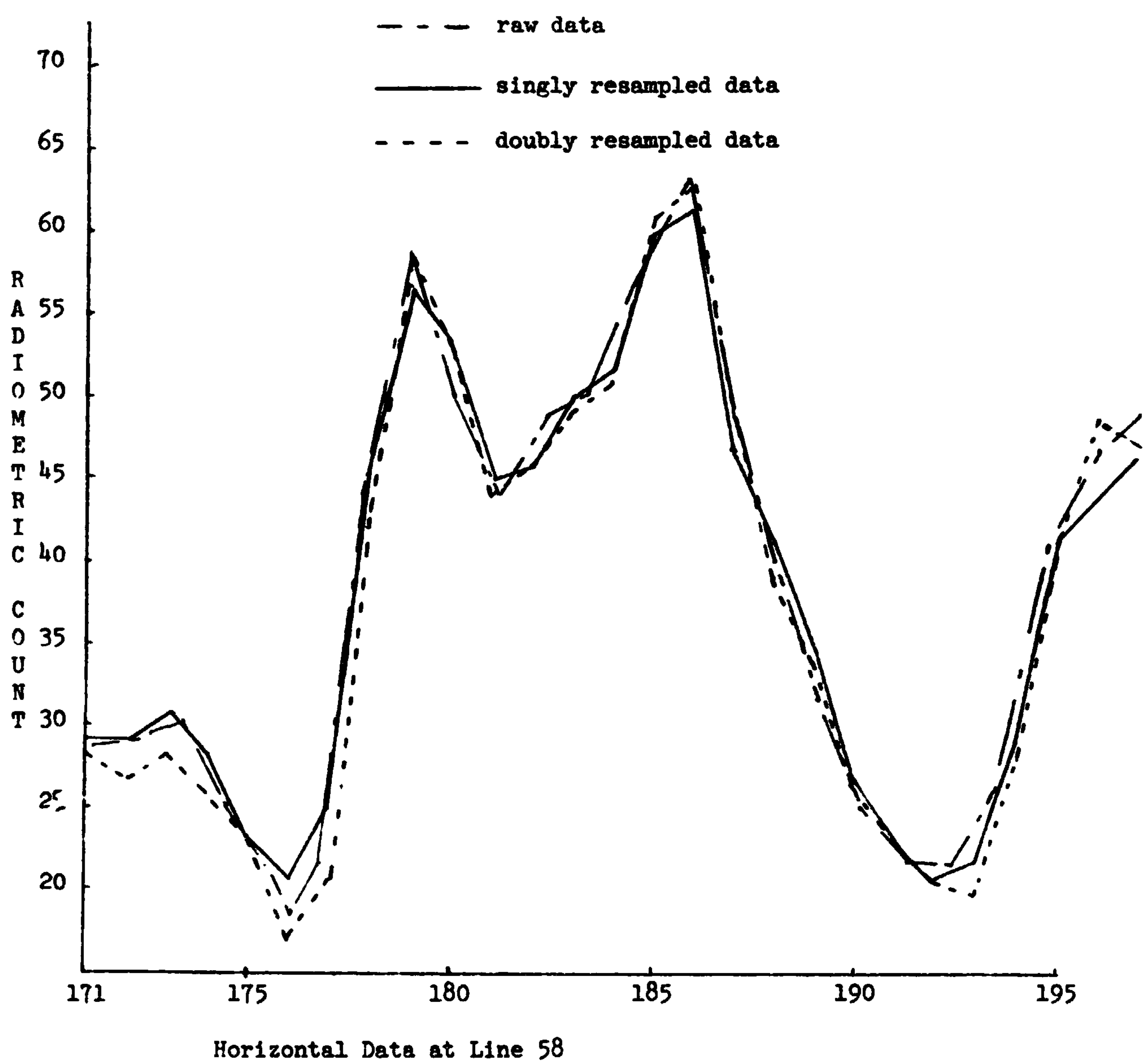

Figure 4-38. Edge Effects of Bi-resampling, Hand County, Band 5, High Frequency Region

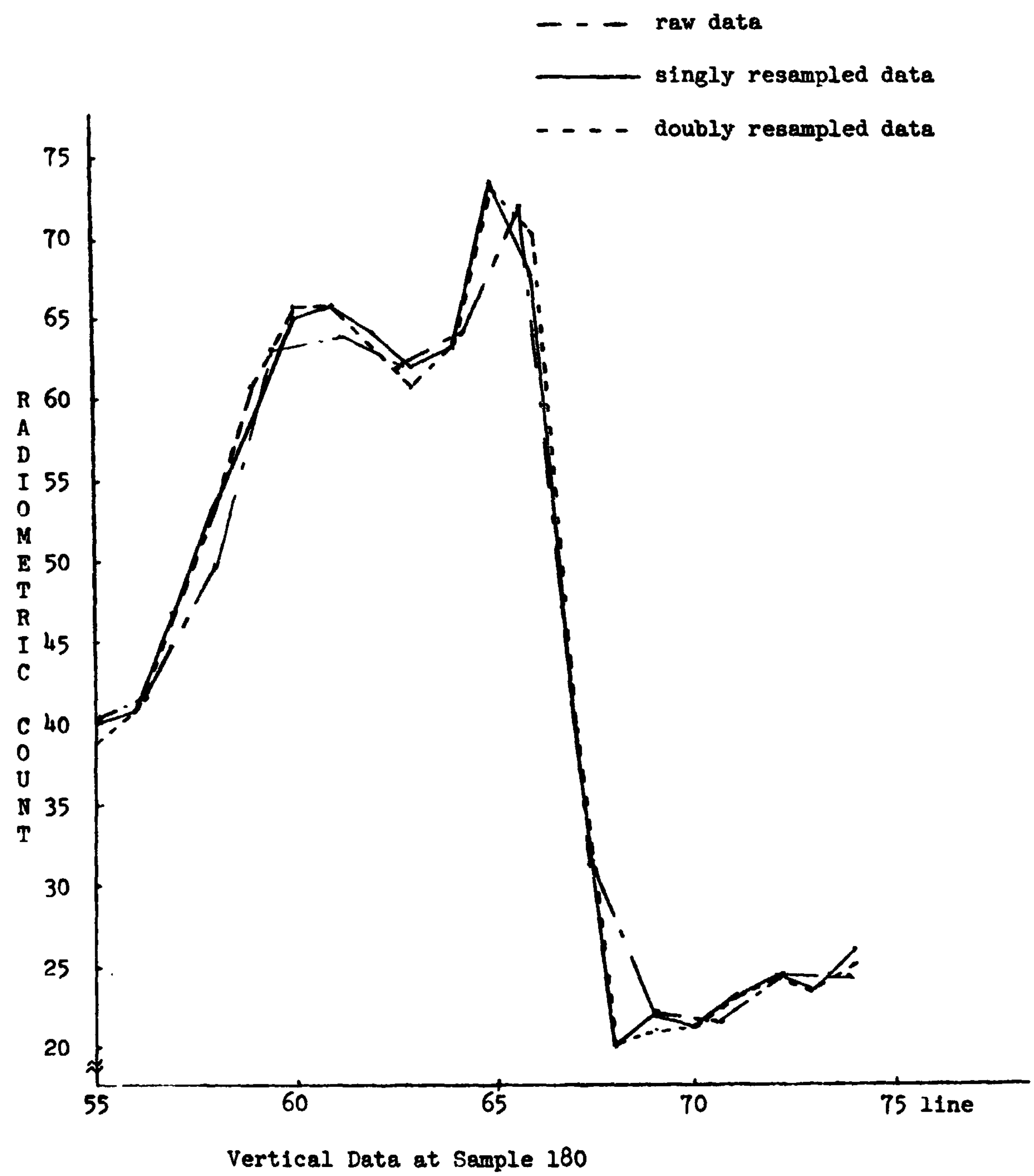

Figure 4-39. Edge Effects of Bi-resampling, Hand County, Band 5, High Frequency Region

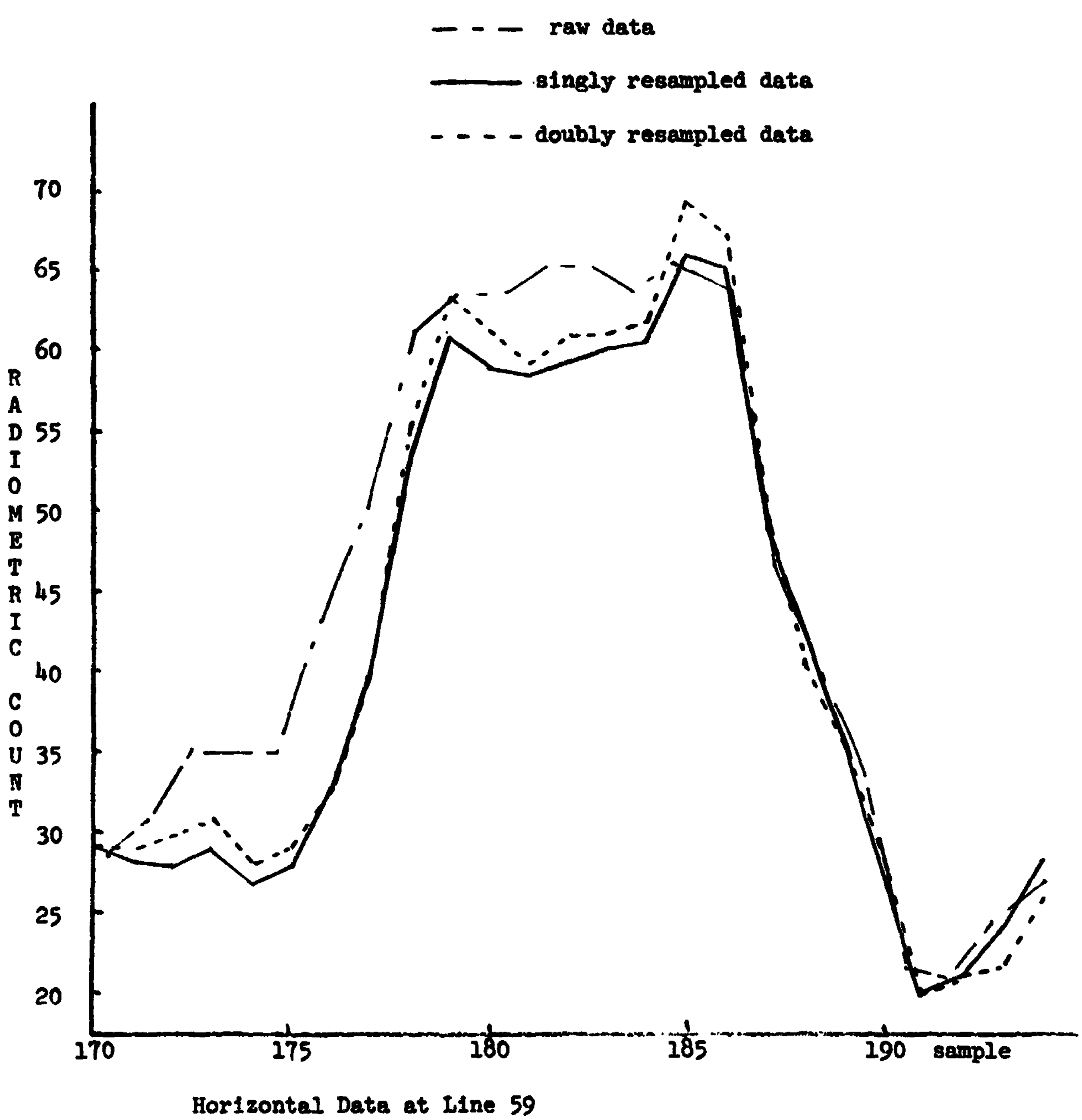

Figure 4-40. Edge Effects of Bi-resampling, Hand County, Band 5, High Frequency Region

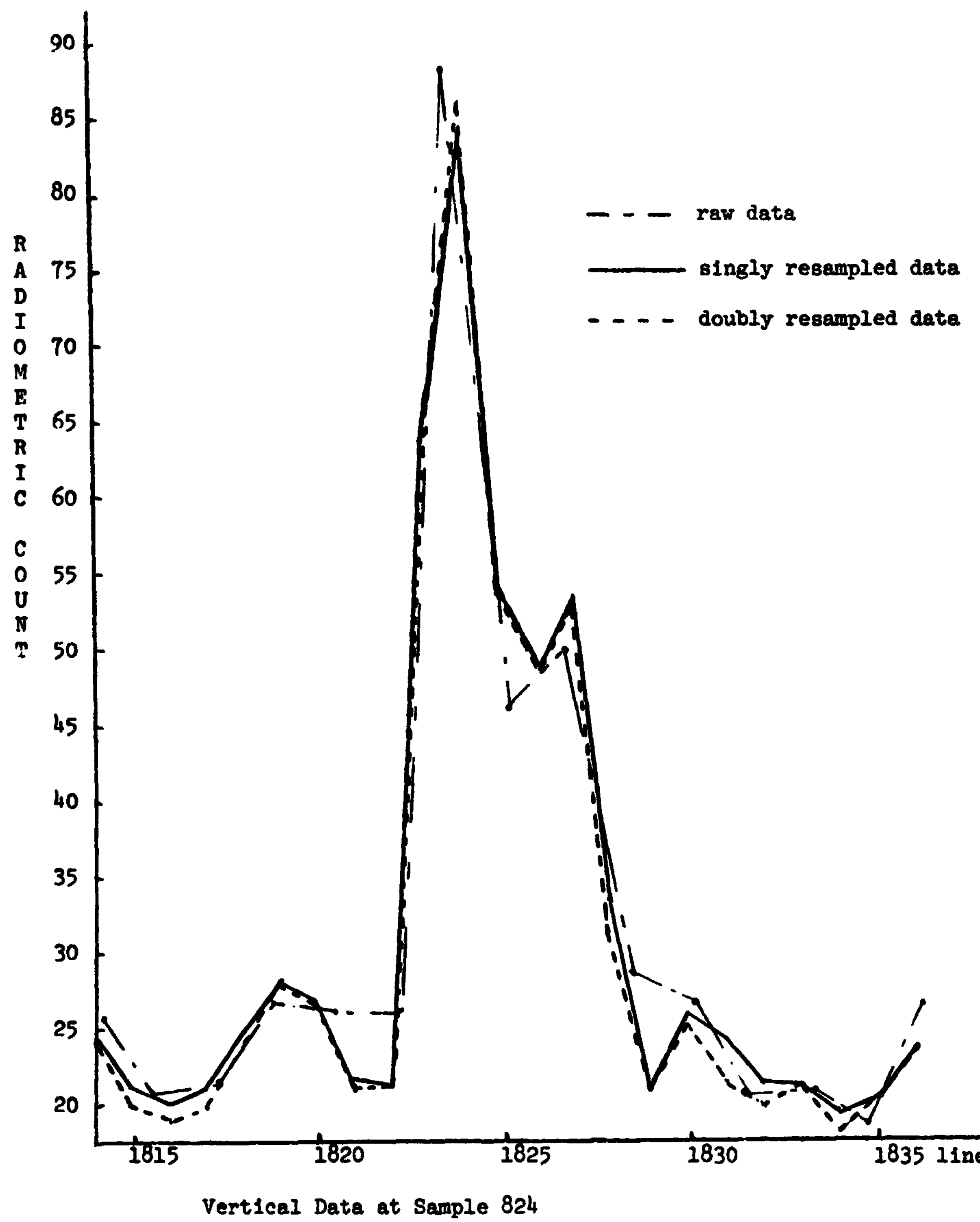

Figure 4-41. Edge Effects of Bi-resampling, Scene E-1080-15192, Dulles Airport Region

Section 5. Classification Results

This section discusses the results obtained in a comparison study of the two resampled Landsat data sets of scene B (Hand County, South Dakota) over the LACIE Intensive Study Site. The image comparison was based on three analysis applications in IBM's Earth Resources Labortory (ERL): classification, image differencing, and bivariate histograming.

The training and test fields used in classification and bivariate histogramming were checked against the ground truth data to identify the ground cover. The training fields were grouped into the following classes: pasture, grass, oats, corn, and spring wheat. In this discussion of classification, channels 1 to 4 refer to bands 4 to 7 of the singly resampled version of scene B, and channels 5 to 8 refer to bands 4 to 7 of the doubly resampled version.

Separate classification processing using the maximum liklihood method was performed on each of the two images for the defined test and training fields. Two classification summaries were generated for each image, one with a 0% threshold and one with a 1% threshold for the training and test fields. These 0% and 1% thresholds refer to the chi-squared test. Assuming the class statistics to be multivariate normal, the 1% threshold, for example, means that the probability of a sample belonging to a class having a quadratic form value greater than chi-squared(.01,4) is 0.01.

The areal proportion estimate of each ground cover category is computed as a function of the proportion of pixels assigned to the ground cover class. The 1% threshold results indicated that 5.4% of the pixels were unclassified for the singly resampled image and 5.5% of the pixels were unclassified for the doubly resampled image.

The areal proportion estimates from the classification summaries show that the two images correlate well with ground truth data.

AREAL PROPORTION ESTIMATES (%)

IMAGE	CORN	OATS	PAST/ GRASSES	SPRING WHEAT
Single Resampled				
0% thresh.	7.3%	6.8%	80.0%	5.1%
1% thresh.	6.8%	5.6%	77.3%	4.8%
Double Resampled				
0% thresh.	7.5%	6.7%	79.8%	5.8%
1% thresh.	7.1%	5.5%	76.2%	5.0%
Ground Truth Map	8.06%	6.47%	81.23%	4.24%

The results were derived from the classification of the ground truth test data.

The bivariate histograms of the input data, Figures 5-1 through 5-4, show the variations in the values assigned to a given pixel by the resampling procedures. For example, in Figure 5-2 it can be seen that the pixels which were assigned a value of 29 for channel 2 (band 5 in the singly resampled image) were assigned values ranging from 25 to 32 in channel 6 (band 5 in the doubly resampled image), and pixels which were assigned a value of 29 in channel 6 were assigned values ranging from 27 to 34 in channel 2. There are 36 unique symbols (*,1,2,...,9,A, B,C,...,Y,Z) used in the bivariate plot, with the later symbols in the sequence indicating a greater density than the earlier symbols. Inspection of the various bivariate plots shows that these high-density symbols are distributed along the diagonal of the plots, indicating that

the bulk of the pixels in the singly and doubly resampled images have the same value in both images.

When the input channels are differenced and the difference images displayed (Figures 5-5 to 5-8), no clear field boundaries or field structure is seen, which suggests that the pixels with different values in the two images are not related to the field structure.

With the particular training fields defined in this study, the single resampled image classification results were closer to the ground truth data for three of the four classes. However, these differences in the classification results are slight, and are within the accuracy limits of the classification algorithm. Therefore, the classification results indicate no clear preference for singly or doubly resampled data.

The bivariate histogram for the two classification maps (Figure 5-10), with channel one containing the singly resampled result and channel two containing the doubly resampled result, shows that approximately 27000 pixels, **out of a total of 30248, were classified** the same in the two images. These numbers can be derived from the symbols on the diagonal. Therefore, approximately 11% of the pixels were classified differently for the two images.

The classification difference map in Figure 5-9 shows the differing pixel ground cover assignments in the non-white areas. The white areas represent areas where the pixel values in the maps agreed. This map shows that the differences are scattered across the image, and do not appear to fall on field boundaries or within specific fields.

In conclusion, it can be said that:

- The positioning of the pixels which differ appears to be random and not associated with field boundaries for both the imagery

and the classification maps

- The classification results show no basis for concluding that one resampling procedure produces significantly less accurate classification results than the other.

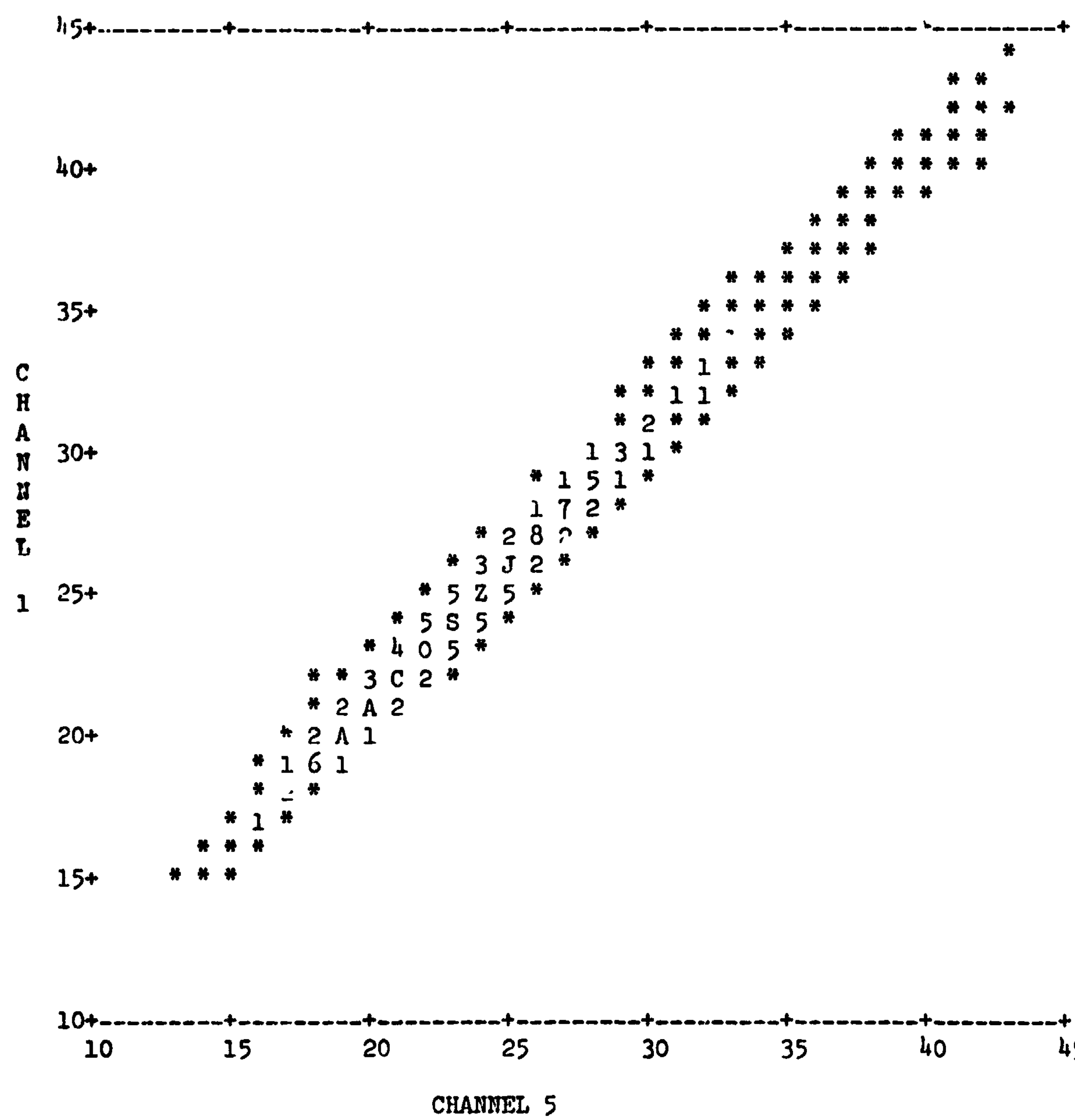

Figure 5-1. Channel 1 and 5 Bivariate Histogram

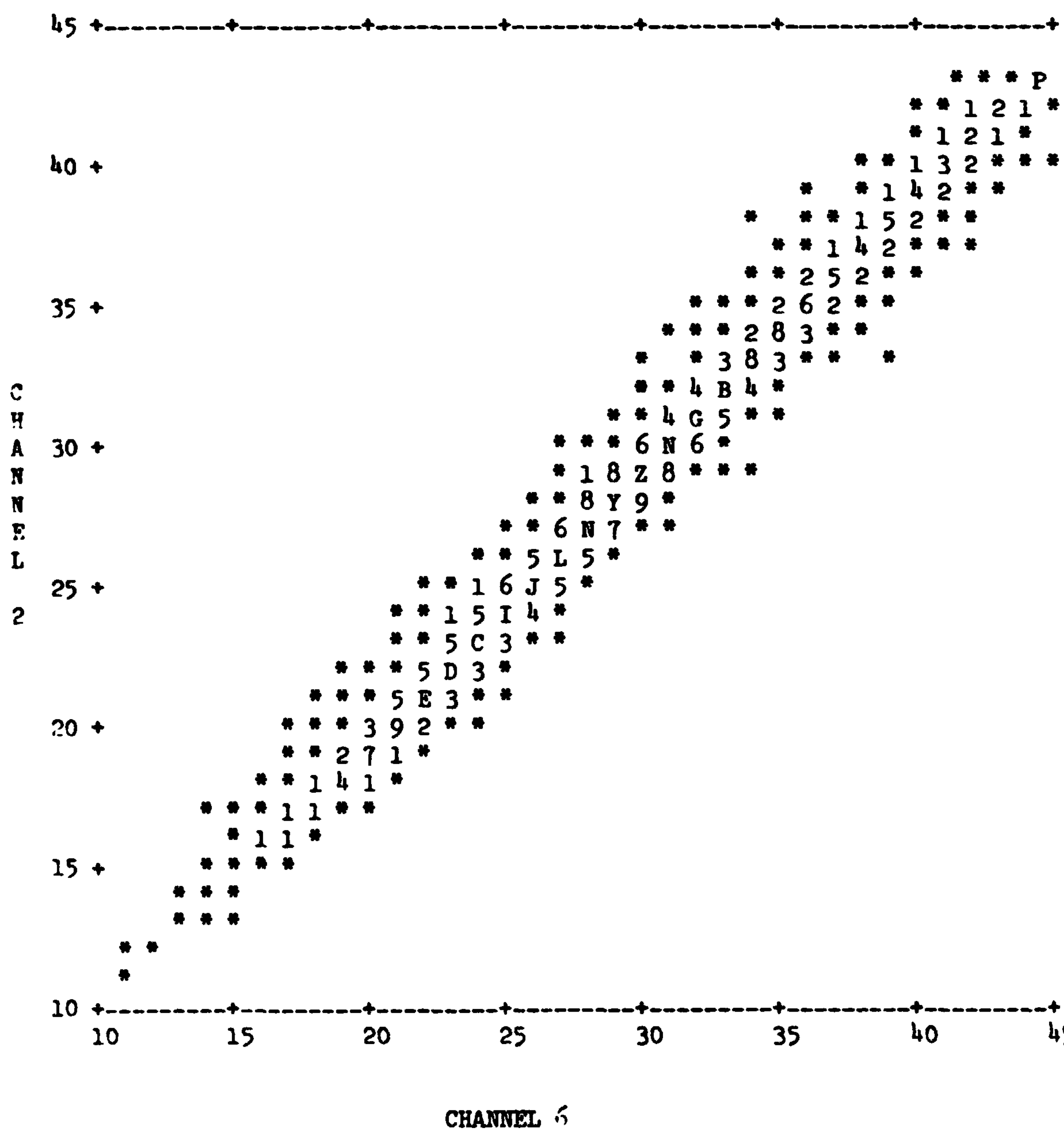

Figure 5-2. Channel 2 and 6 Bivariate Histogram

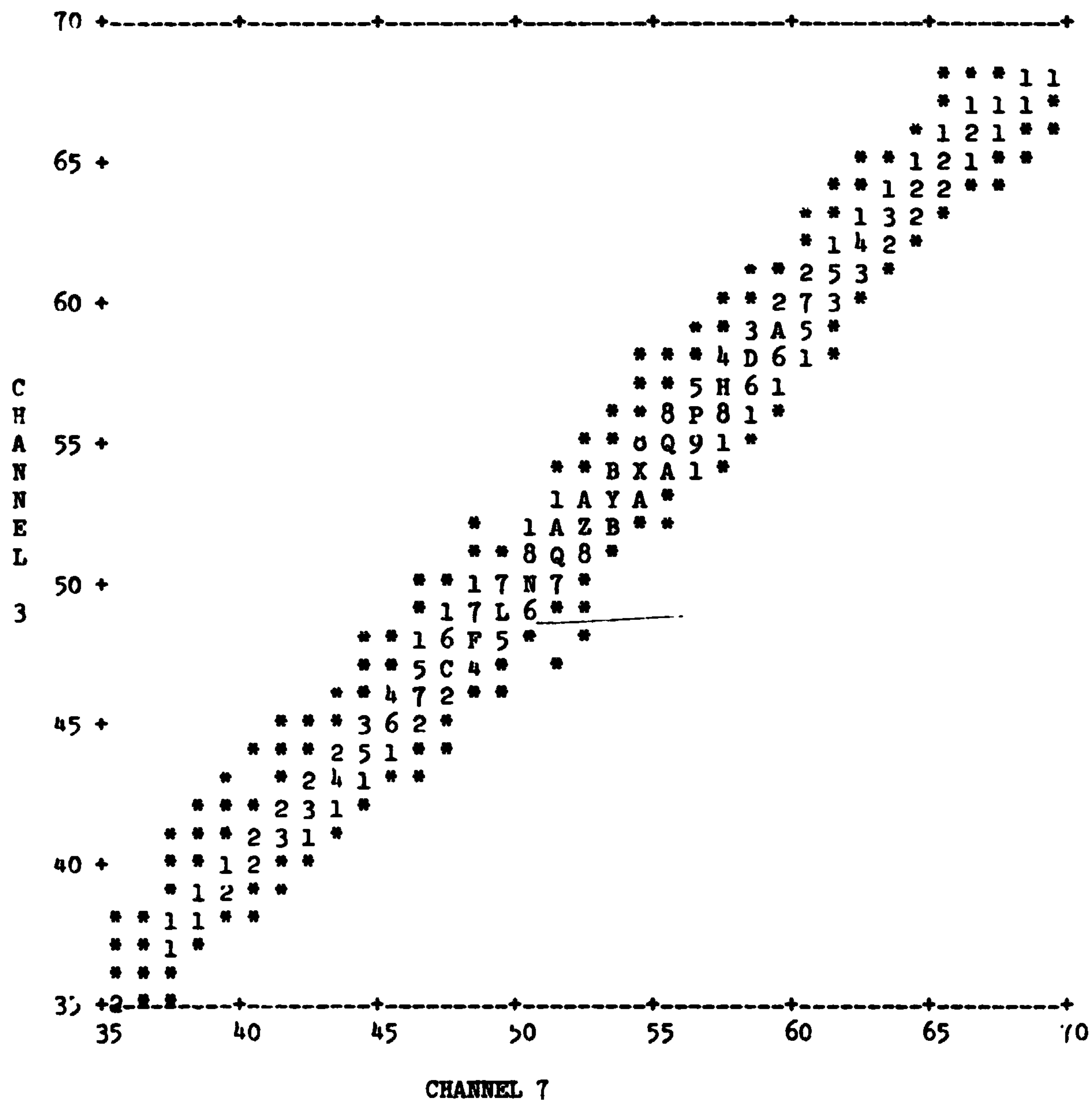

Figure 5-3. Channel 3 and 7 Bivariate Histogram

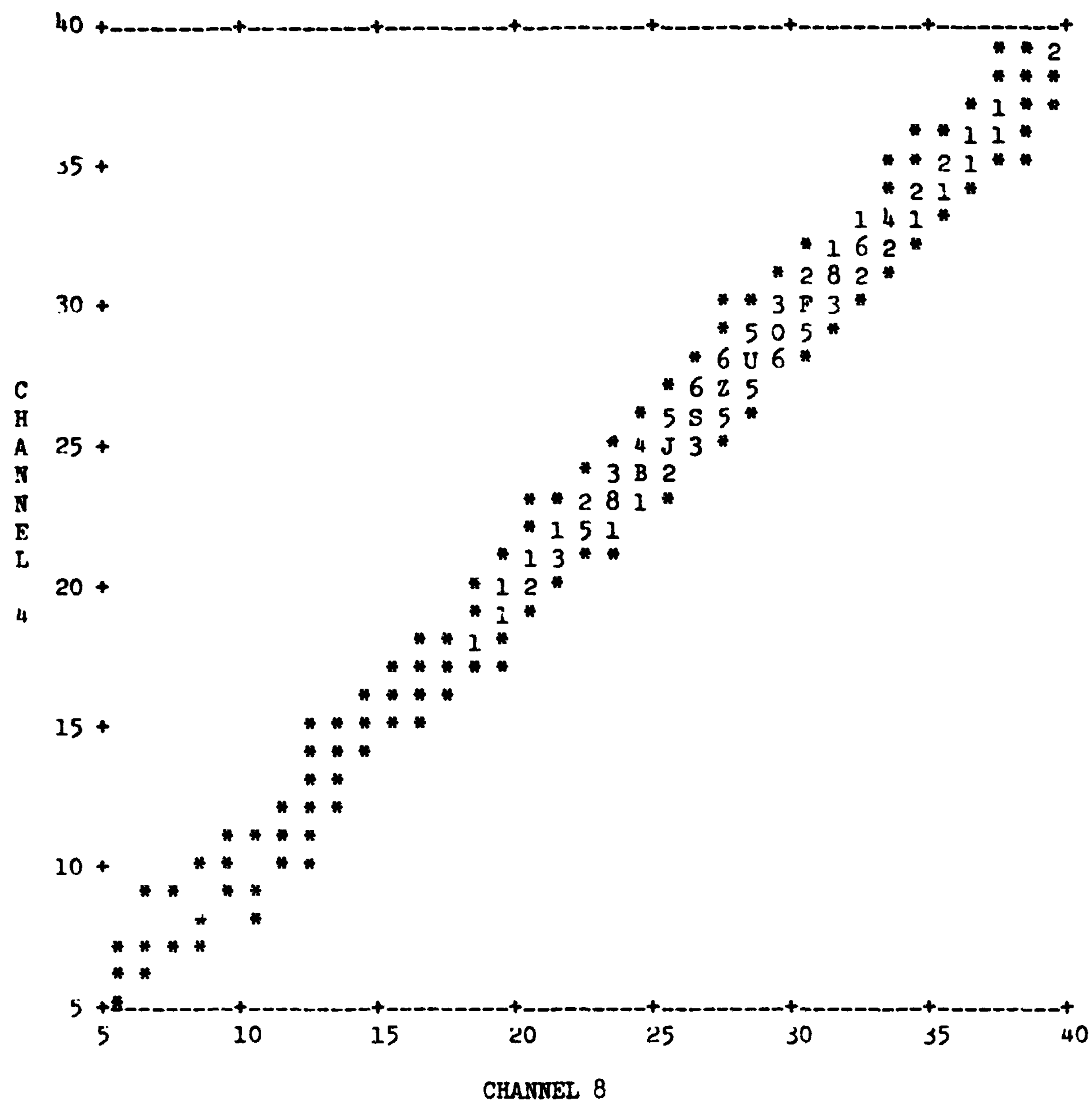

Figure 5-4. Channel 4 and 8 Bivariate Histogram

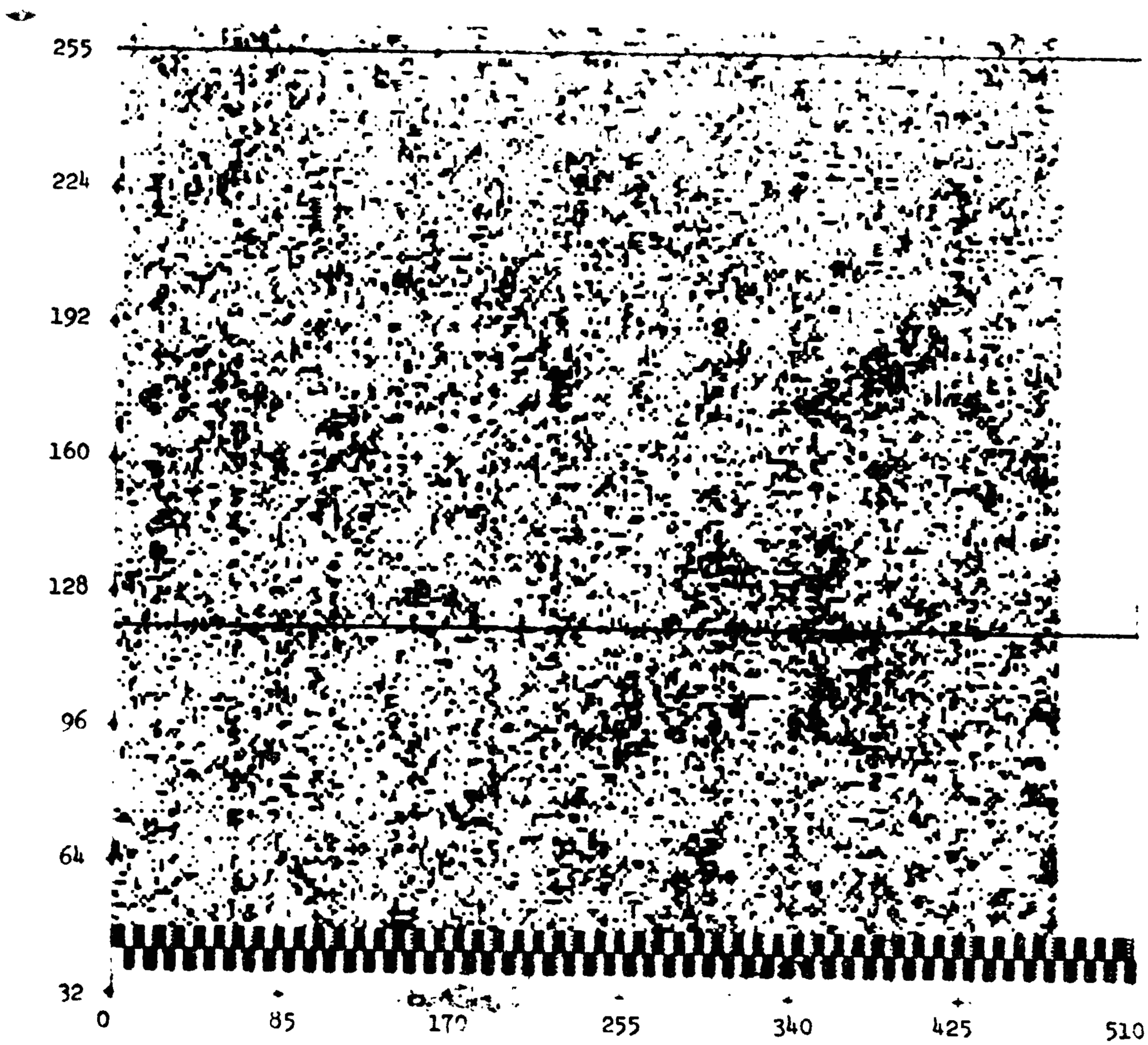

Figure 5-5. Pixel Differences, Channels 1 and 5

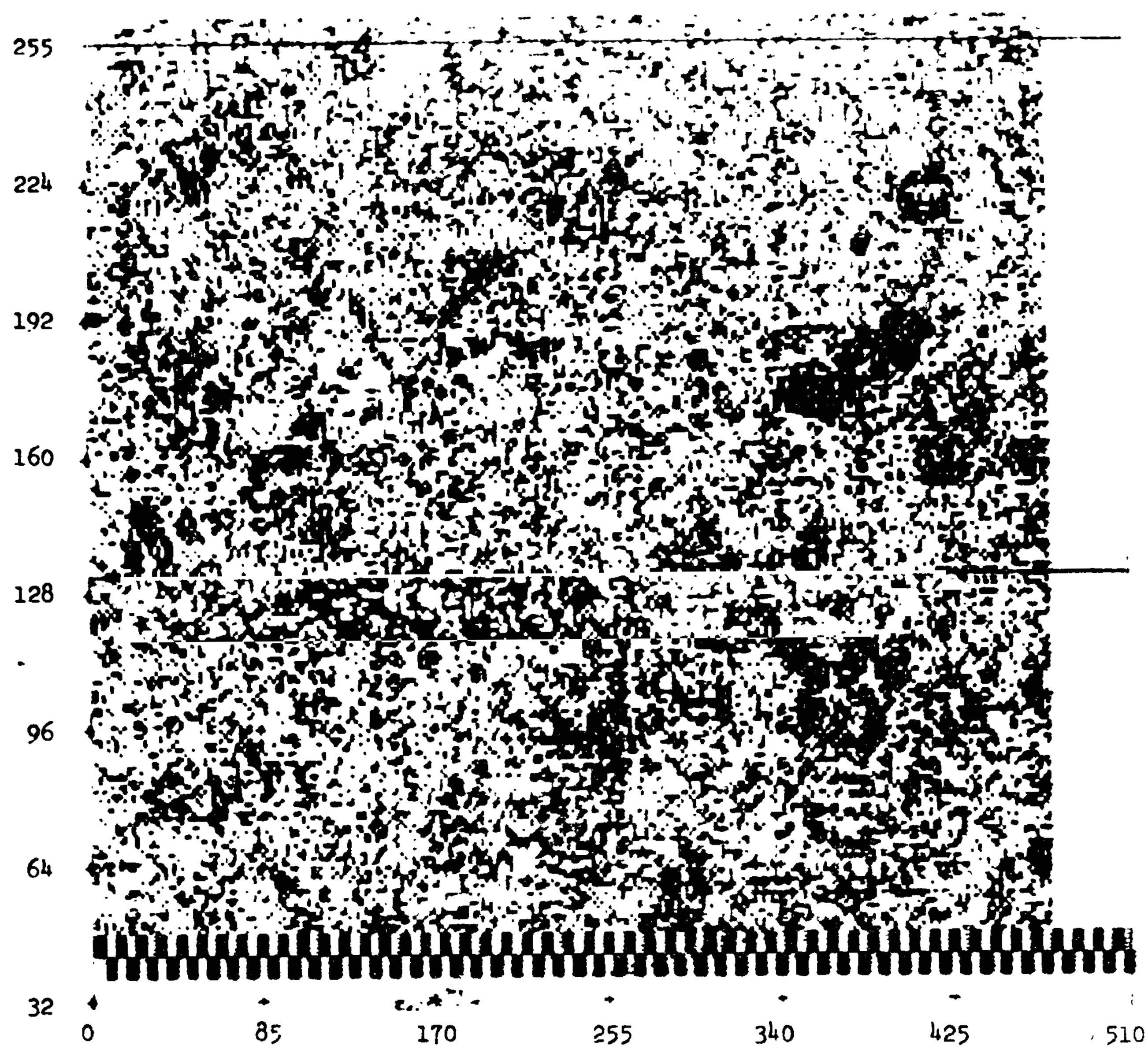

Figure 5-6. Pixel Differences, Channels 2 and 6

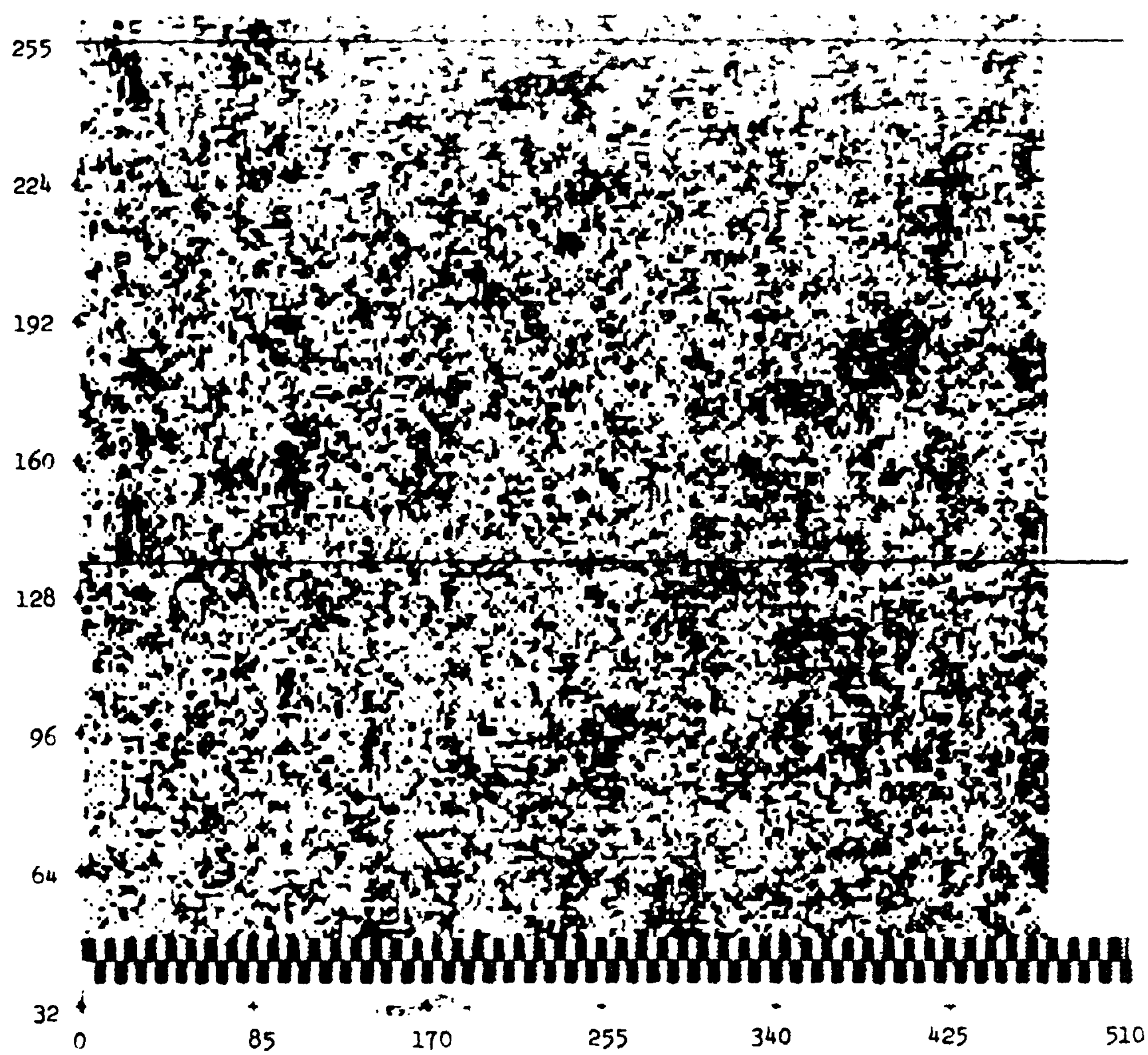

Figure 5-7. Pixel Differences, Channels 3 and 7

REPRODUCIBILITY OF THE
ORIGINAL PAGE IS POOR

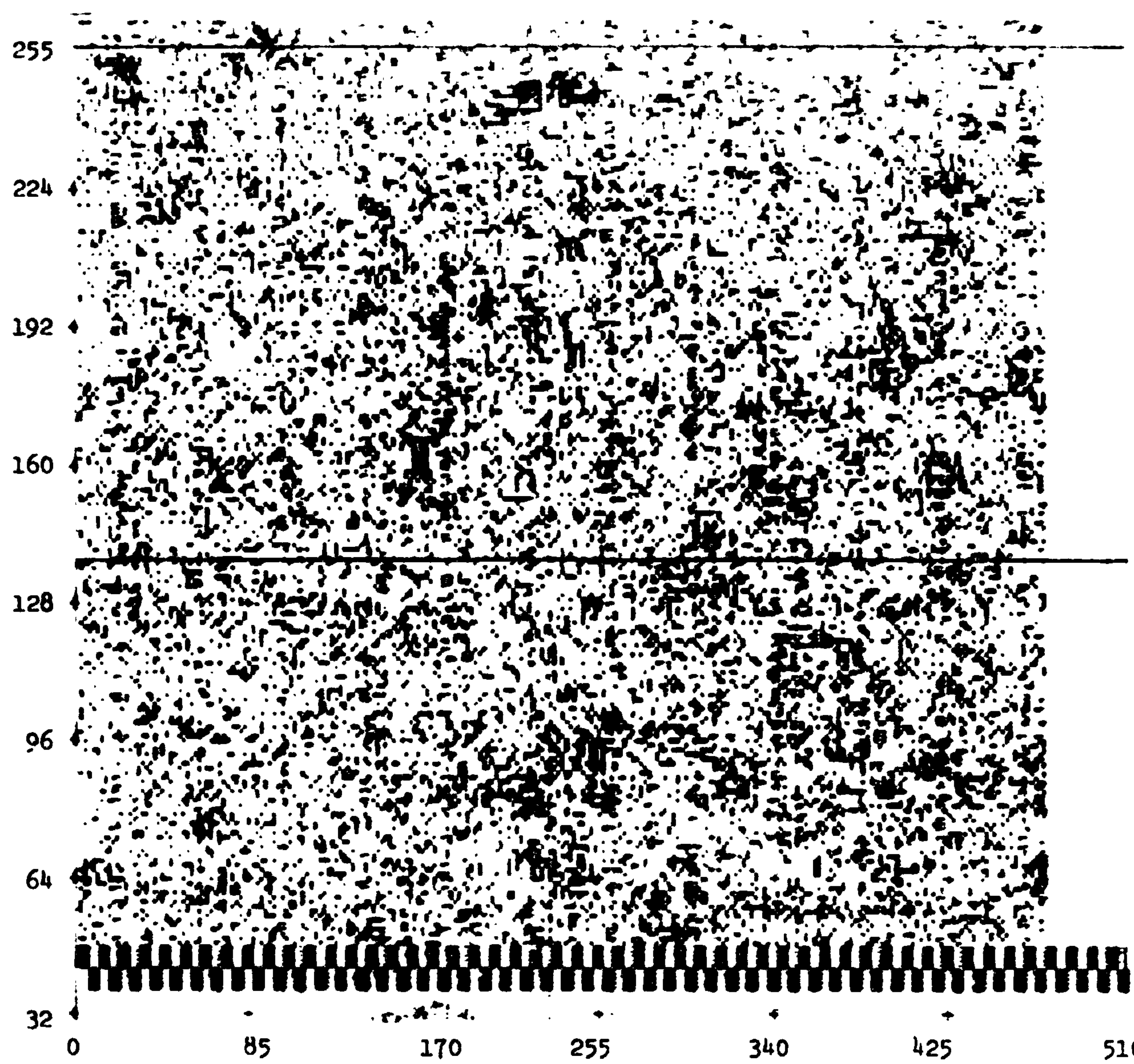

Figure 5-8. Pixel Differences, Channels 4 and 8

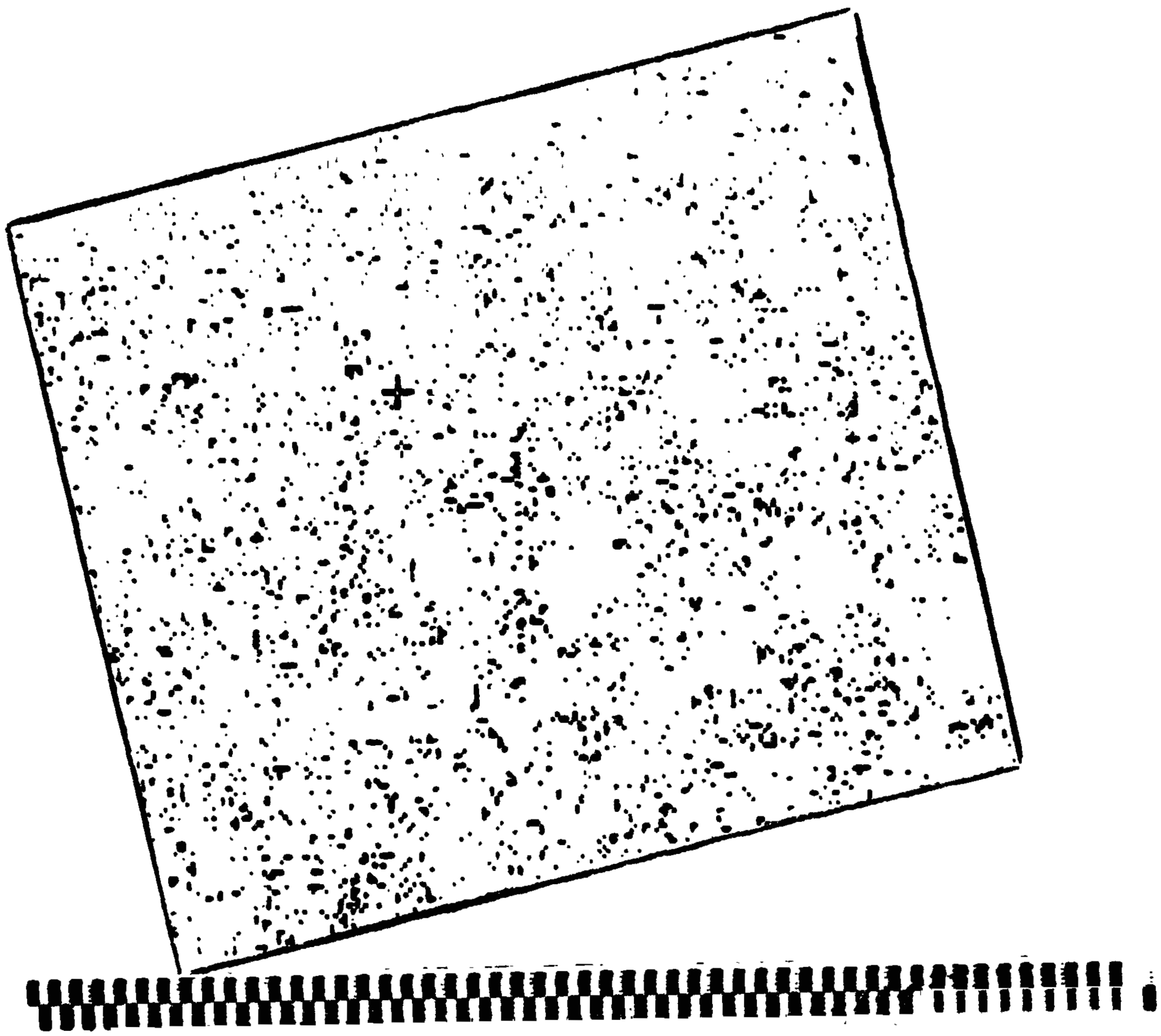

Figure 5-9. Classification Differences

```
   15 +----------+----------+----------+



C           *   *   3   *   Z
H  10 +
A
N           *       *   5   *
N
E
L           1       L   *   2

1   5 +
                5           *


            3   *   1   *   *

    0 +----------+----------+----------+
      0          5          10         15

                 CHANNEL 2
```

Figure 5-10. Class Map Bivariate Histogram

APPENDIX

1. Equations for projecting to the Lambert Conformal Conic Space

The equations mapping points on the earth's surface expressed in geodetic latitude and longitude to the Lambert Conformal Conic (LCC) projection are presented here.

A spheroidal earth model is assumed with semimajor and semiminor axes

$$a = 6378165$$

$$b = 6356783$$

Basic parameters of the ellipse are the eccentricity, e, defined by

$$e = \frac{1}{a}\sqrt{a^2 + b^2}$$

and the principal radius of normal curvature, N, at latitude ϕ, defined by

$$N(\phi) = \frac{a}{\sqrt{1 - e^2 \sin^2\phi}}$$

Let ϕ_1 and ϕ_2 denote the two standard parallels of the projection. Let $\phi_0 = (\phi_1 + \phi_2)/2$ and λ_0 denote the latitude and longitude, respectively, of the origin in the LCC space. The mapping functions will be expressed in terms of the functions

$$\ell = \ell(\phi_1, \phi_2) = \frac{\ln\cos\phi_1 - \ln\cos\phi_2 + \ln N_1 - \ln N_2}{\ln\tan(Z_1/2) - \ln\tan(Z_2/2)}$$

where $N_i = N(\phi_i)$, $Z_i = Z(\phi_i)$

$$\tan(Z(\phi)/2) = \cot(\pi/4 + \phi/2)\left[\frac{1 + e \sin\phi}{1 - e \sin\phi}\right]^{e/2}$$

and

$$K = K(\phi_1,\phi_2) = \frac{N_1 \cos\phi_1}{\ell\,(\tan(Z_1/2))}$$

The mapping equations are

$$x(\phi,\lambda) = r \sin\ell(\lambda-\lambda_0)$$

$$y(\phi,\lambda) = r_0 - r \cos\ell(\lambda-\lambda_0)$$

where

$$r = r(\phi,\phi_1,\phi_2) = K \tan^{\ell}(Z(\phi)/2)$$

and

$$r_0 = r(\phi_0,\phi_1,\phi_2)$$

Refer to Figure A-1 for the geometric interpretation of these relationships.

2. Equations for mapping points from the LCC projection to geodetic latitude and longitude in the northern latitudes.

The equation for longitude, λ, is straightforward.

$$\lambda = \lambda_0 + \frac{1}{\ell}\tan^{-1}\left(\frac{x}{r_0-y}\right)$$

For latitude, it is necessary to solve

$$\left(\frac{K}{r}\right)^{1/\ell} = \tan(\pi/4 + \phi/2)\left[\frac{1 - e\sin\phi}{1 + e\sin\phi}\right]^{e/2} = f(\phi)$$

for ϕ. This equation does not have a closed form solution. Therefore, an iterative procedure (Newton-Raphson Method) is used.

Initially, ϕ_N is set to a latitude corresponding to a spherical earth and then the Newton-Raphson Method is applied to the parameter

$$F(\phi_N) = \frac{f(\phi)}{f(\phi_N)}$$

where

$$f(\phi_N) = \tan(\pi/4 + \phi_N/2) \left[\frac{1 - e \sin\phi_N}{1 + e \sin\phi_N} \right]^{e/2}$$

In this method, the latitude is updated according to

$$\phi_{N+1} = \phi_N - F(\phi_N)/F'(\phi_N)$$

It is clear that finding a zero for the function F is equivalent to ϕ_N converging to ϕ.

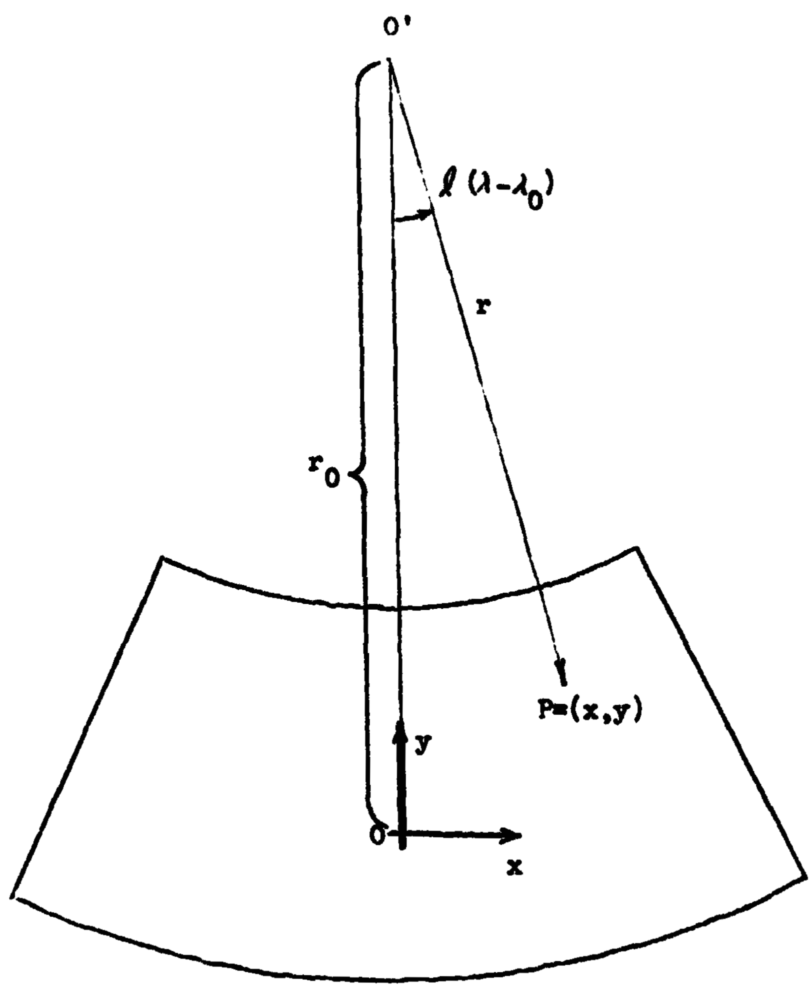

$x = r \sin(\lambda-\lambda_0)$

$y = r_0 - r \cos(\lambda-\lambda_0)$

O' = cone apex

O = origin of Lambert Conformal Conic space

Figure A-1. Geometry of Lambert Conformal Conic Projection

Figure 3-1 Feature Location, Cluster Region, and High, Low, and Medium Frequency Regions of Scene 1080

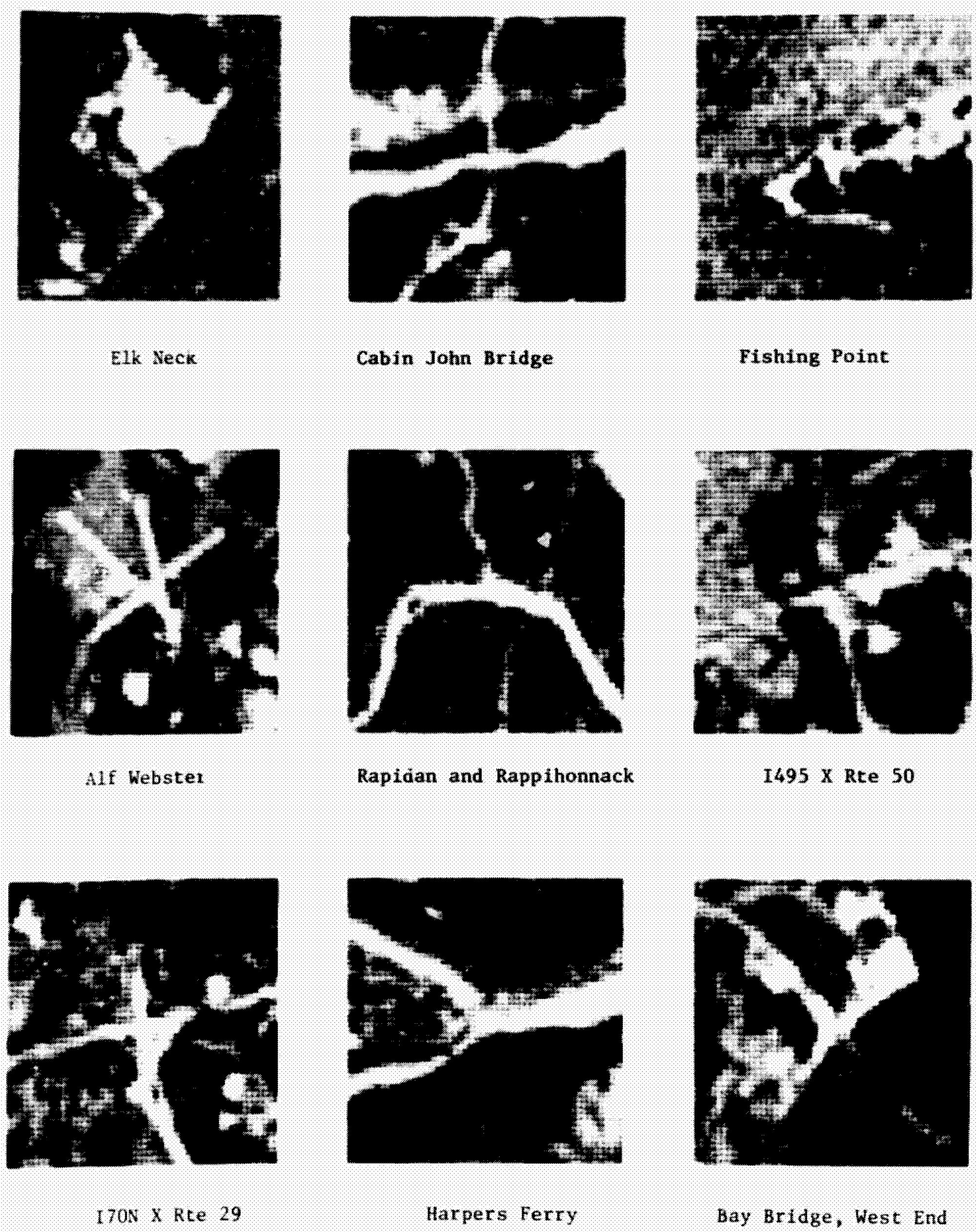

Figure 3-2 Nine Features from the Single Resampled Imagery, Scene 1080

Elk Neck

Cabin John Bridge

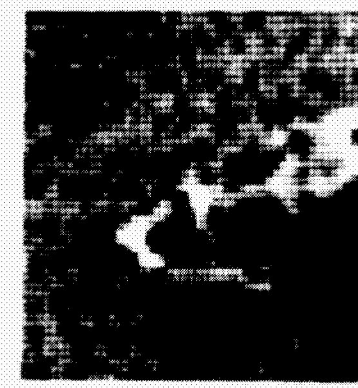

Fishing Point

Alf Webster

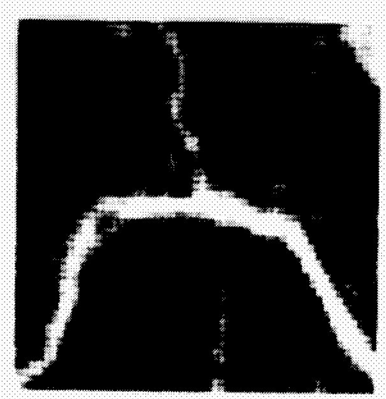

Rapidan and Rappihonnack

I495 X Rte 50

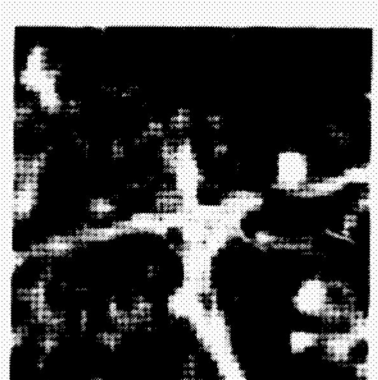

I70N X Rte 29

Harpers Ferry

Bay Bridge, West End

Figure 3-3 Nine Features from the Bi-Resampled Imagery,
Scene 1080

PROGRAM: GEOM
RESAMPLER: GEOMCCSD
SCENE 1080 BAND 5 LAMBERT CONFORMAL CONIC PROJECTION

Figure 4-1 Scene 1080, Single-Resampled Imagery

Figure 4-2 Scene 1080, Bi-Resampled Imagery

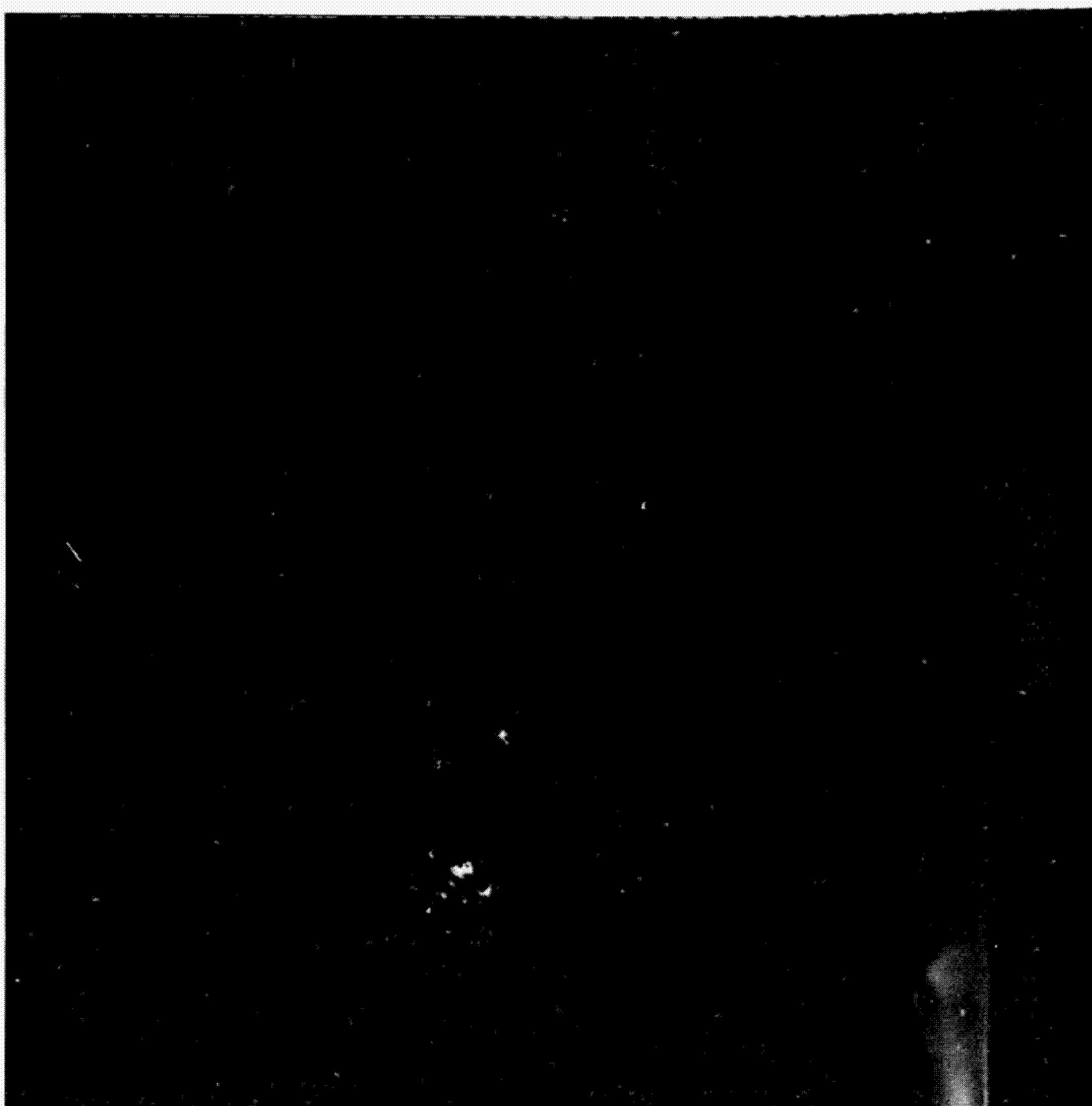

SCENE 1080 BAND 5 LAMBERT CONFORMAL CONIC PROJECTION
LCC SINGLY RESAMPLED IMAGE - LCC BI-RESAMPLED IMAGE

DIFFERENCE IMAGE

Figure 4-3 Scene 1080, Difference Imagery (Exaggerated)